CHARACTERISATION OF THE FUNCTIONAL ROLE OF OCTN1 IN THE PATHOGENESIS OF COPD

by

Caoimhe Geraldine Clerkin, B.A. Pg.Cert.

A dissertation submitted for the degree of Doctor of Philosophy

at the

University of Dublin, Trinity College

This research was conducted in the School of Pharmacy and Pharmaceutical Sciences, Trinity College, Dublin 2, Ireland

Under the direction and supervision of

Dr. rer. nat. Carsten Ehrhardt

2017

Trinity College Dublin
Coláiste na Tríonóide, Baile Átha Cliath
The University of Dublin

For the big woman,
You are my inspiration and my anchor.

Declaration

I declare that this thesis has not been submitted as an exercise for a degree at this or any other university and it is entirely my own work.

I agree to deposit this thesis in the University's open access institutional repository or allow the library to do so on my behalf, subject to Irish Copyright Legislation and Trinity College Library conditions of use and acknowledgement.

_____

Caoimhe G. Clerkin

Summary

The organic cation transporter (OCTN1) has been reported to play a role in the pathogenesis and development of inflammatory diseases. However, this association remains conflicting. Without fully elucidating the physiological function of OCTN1, the link between the transporter and these diseases will never be understood.

For the first time this research has identified the functional role of OCTN1, through the uptake and transport of Ergothioneine (ET) in the bronchial epithelial cell line, NCI-H441. Three novel single nucleotide polymorphisms (SNPs) of the gene responsible for the coding of OCTN1 i.e. *SLC22A4* in the cell line NCI-H441 were identified. However, the functional impact of these mutations on the functional activity of OCTN1 is not yet fully understood. Furthermore, the transport of ET, the physiological substrate of OCNT1, was determined to be pH and temperature dependent. The antioxidant potential of ET was confirmed by counteracting reactive oxygen species (ROS) production intracellularly. It is suggested that ET carries out its cytoprotective properties by stabilising the intracellular pH.

Once characterisation of OCTN1 *in vitro* was completed it was important to investigate its expression in patients suffering from Chronic Obstructive Pulmonary Disease (COPD). Bronchial epithelial samples were isolated and *SLC22A4* was quantified by quantitative reverse transcriptase polymerase chain reaction (qRT-PCR). It was identified that risk factors such as age, weight and cigarette smoking, upregulated the expression of the gene. Further, upregulation of the gene also occurred with reduced lung capacity, a key determinant of the pathogenesis and severity of COPD. This research for the first time has identified a significant association of OCTN1 function with COPD in the Irish population.

As previously mentioned, OCTN1 is responsible for the uptake of ET. ET was confirmed to behave as an antioxidant, but its mechanism of action has never been fully elucidated. We identified structural changes that occur to ET once exposed to oxidative stressors, such as

cigarette smoke extract (CSE). It was identified that ET is converted to hercynine (EH) and ergothioneine sulfonic acid (ESO_3H). However, *in vitro,* only ESO_3H was detected in a concentration dependent manner. The remaining presence of ET suggests an alternative mechanism of action. ET was identified to undergo phase II metabolism by reacting with 1-chloro-2,4-dinitrobenzene (CDNB), to form dinitrophenyl-ergothioneine (DNP-ET). DNP-ET formation was identified to be catalysed by glutathione s-transferase (GST). However, there is some suggestion that alternative enzymes may play a role in this formation. The conjugate, DNP-ET was further identified to be effluxed from the cell by multi-drug resistant related protein (MRP) transporters. Hence, ET behaves in a similar way to glutathione (GSH) by carrying out its antioxidant properties.

Finally, NCI-H441 was investigated to behave as a suitable model for *in vitro* analysis of transporters and channels in human alveolar epithelial primary cells (hAEpCs). For the majority of genes investigated, no change in the expression of ATP-Binding cassette (ABC) and Solute carriers (SLC) transporters occurred upon culturing under air-interface culture (AIC) or liquid covered culture (LCC) conditions. However, a markedly different expression in the majority of transporters did occur when comparing the expression of NCI-H441 with hAEpCs, but also during transdifferentiation of hAEpCs from alveolar type II (ATII) to an alveolar type I-like (ATI-like) phenotype. This may be as a result of NCI-H441 representing bronchial epithelium and not alveolar epithelium. Nevertheless, NCI-H441 does not represent the true phenotype of hAEpCs and so the need for a suitable *in vitro* model is still required.

Collectively, these results have determined the functional role of OCTN1 in bronchial epithelium and have confirmed an association of an upregulation of OCTN1 and COPD in the Irish population.

Contents

Chapter 1

Introduction

Parts of this chapter have been published in:

S Nickel, CG Clerkin, MA Selo, C Ehrhardt, Transport mechanisms at the pulmonary mucosa: implications for drug delivery, *Expert Opin Drug Deliv*, 13, (5), 2016, p667-690

1.1 Chronic Obstructive Pulmonary Disease

Chronic Obstructive Pulmonary Disease (COPD) affects 329 million people worldwide (*8*). Each year, 2.5 million people die from this disease, a similar mortality to HIV/AIDs (*8*, *9*). In Ireland, 440,000 people suffer from COPD, with over 180,000 patients having moderate to severe form of the disease (*10*). With the Irish death rate over twice the EU average and the highest in West Europe (*11*), it is evident that a need for new treatments and methods of prevention are required for COPD.

Misdiagnosis of COPD is a common occurrence in patients. In reality, patients diagnosed often have simple deconditioning less common lung conditions. Similarly, many patients are not diagnosed until the disorder is advanced and interventions become less effective. Regardless, COPD sufferers usually present with an ongoing cough that produces a lot of mucus, shortness of breath, wheezing or whistling when breathing and chest tightness. Based on these signs and symptoms, diagnosis depends on pulmonary function tests (PFTs), which measure the total volume of air inhaled and exhaled out of the lung, typically spirometry, a chest x-ray may also be requested to provide information on any constriction of the airways and finally, arterial blood gas tests may also reveal if oxygen therapy is required to counteract the acidic nature of high concentrations of carbon dioxide. Patients are also asked to provide information on their lifestyle.

Pollution remains the largest environmental cause of disease and death in the world today, responsible for an estimated 9 million premature deaths. The Lancet Commission reported that air pollution was the greatest risk factor compared to water, occupational, soil, chemical and metal pollution (*12*). This is reasoned by inhaled toxins such as carbon monoxide, methane, asbestos for example in the air, capable of infiltrating deep within the bifurcates of the lung. And as a result, people are present with lung diseases such as COPD and lung

cancer more frequently than cardiovascular diseases such as ischaemic heart disease or ischaemic haemorrage stroke (*13*).

1.1.1 How cigarette smoke leads to the development of COPD

COPD is a progressive obstructive lung disorder symptomised by chronic airflow limitation and an inability to breathe out fully (*14*). However, cigarette smoke remaining the major aetiological factor for its development and progression. Irritants like smoke activate lung epithelial cells to release chemotactic factors. However, the exact mechanism still requires further evaluation.

Cigarette smoke contains a complex mixture of variable components that orchestrate chronic lung inflammation and destructive lung remodelling. One major component of cigarette smoke is free radicals with an estimation of 10^{15} free radicals per puff (*15*). A radical can be defined as a highly reactive atom or group of atoms with one unpaired electron. Radicals are detected during the burning of a cigarette, within the tar of a cigarette and the aqueous extract of a cigarette (*16*).

When a cigarette is ignited, the components are burned in excess oxygen known as combustion. The result is the formation of oxygen or carbon radicals that are highly reactive that they react with each other and so are short lived. Their estimated life time is fractions of a second and so, do not have sufficient time to reach the deep bifurcates of the lung (*15*).

The principal radical found in the tar of cigarettes is the conjugated quinone (Q), semi-quinone ($QH^{\cdot}$) and hydroquinone (QH_2) (*16*). These radicals stem from melanin, a by-product of the oxidation of tyrosine to dihydroxyphenylalanine (DOPA). Q, $QH^{\cdot}$ and QH_2 exist in equilibrium as illustrated in Scheme 1.1, and so can act as an oxidising or reducing agent (*17-19*). Acting as a reducing agent, this group of compounds may alter the oxy-radical

concentrations in the lung (*16*), by reducing molecular oxygen (O_2) to superoxide ($\cdot O_2^-$). This will eventually lead to the production of hydrogen peroxide (H_2O_2) (Scheme 1.2).

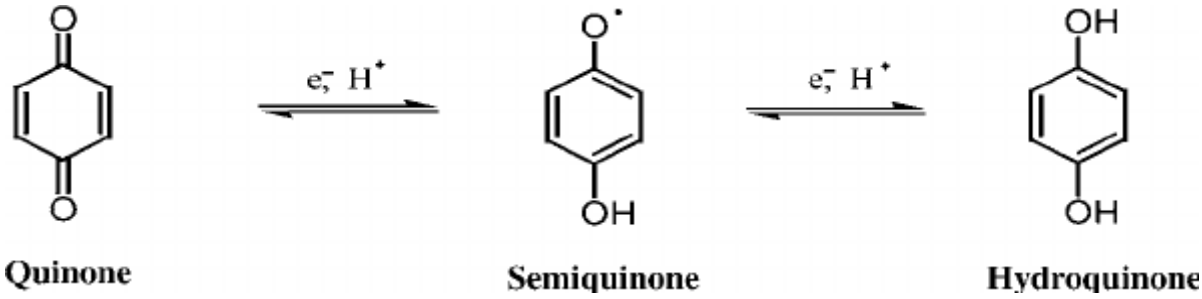

Scheme 1.1: Illustration of quinone, semi-quinone and hydroquinone in equilibrium balance with each other (*20*).

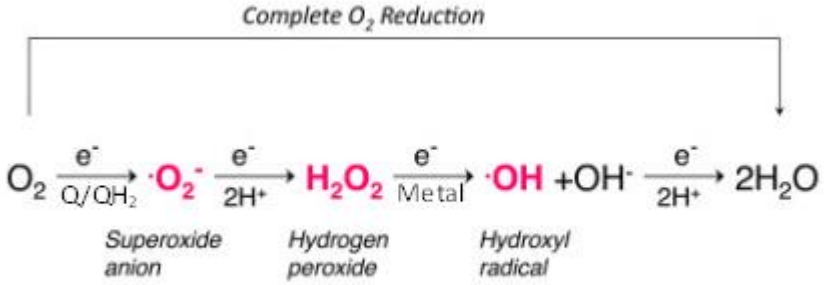

Scheme 1.2: The complete reduction of molecular oxygen. The production of reactive oxygen species by single electron additions (e^-) facilitated by quinone (Q), and hydroquinone (QH_2) and/or metals. This scheme is adapted from Bartz *et al. (21).*

Hydrogen peroxide can be further reduced to the hydroxyl radical in the presence of a transition metal such as iron (Fe) (Scheme 1.2). Through the reduction of H_2O_2, iron becomes itself oxidised from Fe^{2+} to Fe^{3+}, by process of the Fenton reaction. Interestingly, O_2^* and tar can later reduce Fe^{3+} to Fe^{2+} (*15*), allowing it to become widely available for further reductions of H_2O_2 as in Scheme 1.3. Further, as high as 42 μg of iron has been quantified per cigarette (*22*).

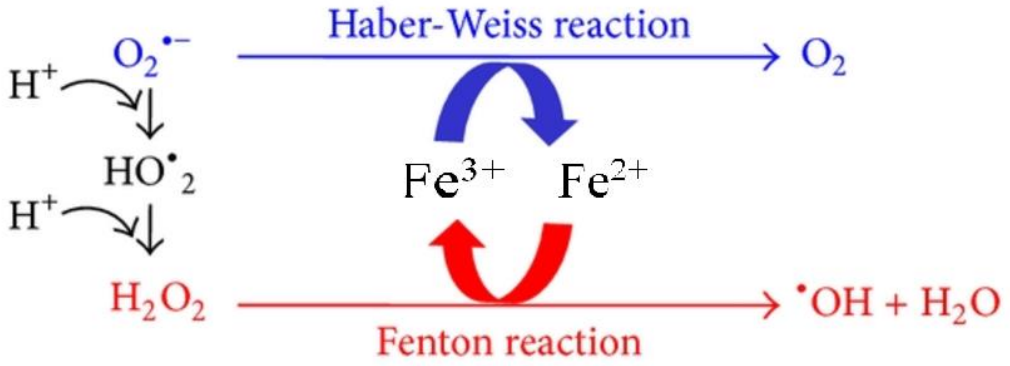

Scheme 1.3: Oxidation and reduction of iron by hydrogen peroxide (H_2O_2) and superoxide ($O_2^{\cdot-}$) respectively (*23*).

Radicals found in the gaseous phase have longer lifetimes (10^{-1} sec) than those radicals (10^{-9} sec) previously discussed, with their lifetimes in parenthesis (*24*). Detection of these radicals at high concentrations was carried out by electron spin resonance spin trap (ESPR) (*25*). It can therefore be concluded that gaseous radicals are constantly formed and destroyed. The radicals produced by the gaseous phase are small oxygen and carbon centred with higher reactivity than others. In each cigarette, there are high levels of nitric oxide (NO) detected, which react with molecular oxygen (O_2) to form nitrogen dioxide (NO_2) (Equation 1.1). NO_2 is more potent to the lung epithelium that NO and is detected as high as 300 ppm in smoke compared to 1 ppm in smog (*15*). When reacted with isoprene, an alkyl free radical forms (Equation 1.2) that can later combine with O_2 yielding a peroxyl radical as illustrated by Equation 1.3. This peroxyl radical can now react with more NO to form the alkoxyl radical to further the production of NO_2 (Equation 1.4), giving rise to a viscous chain cycle of oxidants. These oxidants are capable of attacking proteins, lipids and nucleic acids and may be responsible for the progression of many diseases. Although the human body is equipped with various mechanisms of defence such as antioxidant enzymes like superoxide dismutase or

antioxidants themselves, an imbalance between the levels of oxidants and anti-oxidant gene products results (*26*). This is known as oxidative stress.

$$NO + \tfrac{1}{2} O_2 \longrightarrow NO_2 \qquad \text{Equation 1.1}$$

NO_2 + 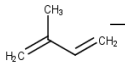 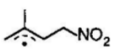 ($R^{\cdot}$) Equation 1.2

$$R^{\cdot} + O_2 \longrightarrow ROO^{\cdot} \qquad \text{Equation 1.3}$$

$$ROO^{\cdot} + NO \longrightarrow RO^{\cdot} + NO_2 \qquad \text{Equation 1.4}$$

Another key feature of COPD is emphysema, the damage and enlargement of the air sacs causing breathlessness. Emphysema can be explained by the inhibition of an Alpha 1-antitrypsin Protease Inhibitor (A1PI) (*15, 16*). A1PI is a serum anti-protease that controls 90% of the anti-elastase activity (*16*). By inhibition of this enzyme, an unchecked activity of neutrophil elastase results, causing emphysematous lesions and eventual loss of activity (*15*). However, this is not as a result of a direct inhibition of the enzyme but the result of the formation of an inactive form, containing an oxidised methionine residue (*16*). Inhibition can be protected by the enzyme catalase, however, superoxide dismutase (SOD) and hydroxyl radical scavengers are too reactive to reduce the methionine residue and are deemed unsuitable (*16*). Inactivation of A1PI can occur by oxidants stimulated by phagocytes and smoke. Peroxynitrite/peroxynitrate formation as illustrated in Equation 1.4 can cause fast inactivation of A1PI that lasts only a few seconds. However, protection of A1PI by catalase, results in a slower inactivation, thereby prolonging the duration of A1PI activation and thus preventing damage to the air sacs (*15*)

1.1.2 Patient Symptoms of COPD

COPD may affect those who have never smoked, however, cigarette smoke is the major risk factor, featuring in 85% of patients (*27*). Research has shown that smoking cessation is the

most important preventive step for COPD with an improvement in lung function in mild-moderate COPD sufferers (*28*). However, despite great preventive efforts for smoking cessation, the prevalence and mortality of COPD continues to rise.

Once cigarette smoke triggers the release of chemotactic factors from the lung epithelium, an inflammatory immune response leading to elastin degradation, emphysema, mucus hypersecretion and small airway fibrosis, results (*29, 30*). Consequently, these physiological changes cause air to become trapped within the alveoli and/or physically restrict air from being inhaled or exhaled, instigating great difficulty in breathing (Figure 1.1).

Although cigarette smoke is the major risk factor for the development of COPD, only a small minority of people develop clinically relevant diseases. Therefore, genetic differences are most likely explanations for an increased susceptibility in patients to COPD.

Currently, the only proven genetic risk factor for COPD is alpha 1-antitrypsin, which accounts for 1-5% of patients (*31*). Recently, smokers with the homozygous Z allele for alpha 1-antitrypsin had increasing variability in lung function compared to non-smokers or ex-smokers of the condition (*32, 33*). These findings suggest that a co-existing genetic factor is present, which increases the susceptibility to cigarette smoke and hence the development of COPD (*34*). And so, new novel and innovative steps must be taken to explore this problem.

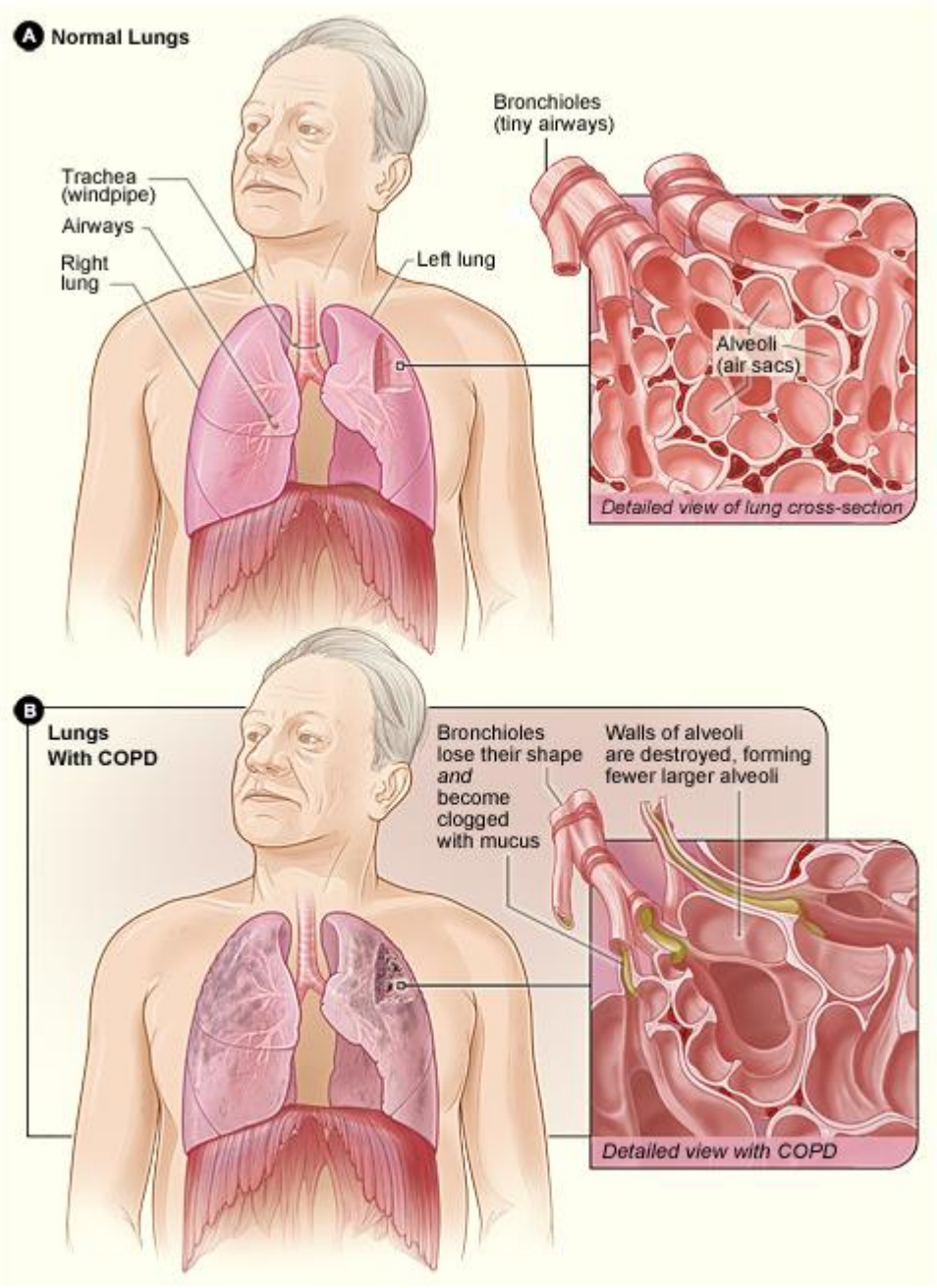

Figure 1.1: Illustrates the location of the airways in the body. The image displays a detailed cross-section of the bronchioles and alveoli of healthy individuals in comparison to those suffering from COPD. Blocked bronchioles from mucus and inflammation can be observed with the alveoli displaying an enlarged and damaged structure in figure B (*3*).

1.2 Drug Transporters

Drug transporters belong to two main transporter families: the solute carriers (SLC) and the ATP binding cassette (ABC). These transporters can either facilitate transmembrane translocation or further enhance barrier function by extruding their relevant substrates (*35*). Biological membrane barriers that obstruct the accessibility for drugs to intracellular targets, deeper tissue layers or into the pulmonary systemic circulation, nevertheless, were rarely considered in pulmonary drug delivery.

ABC transporters are a superfamily of membrane proteins that can transport a wide variety of substrates across biological membranes in an energy-dependent manner. The ABC genes in the human genome are divided into eight subfamilies based on amino acid sequence similarities and phylogeny, which have been characterised by genome sequencing (*36*). Many of these transporters act as drug efflux pumps and so the expression of ABC transporters in the lung suggests that they are pivotal in the protection against endogenous or exogenous toxic compounds. ABC transporters such as P-glycoprotein (P-gp), multidrug resistance-related protein 1-8 (MRP1-8), and breast cancer resistance protein (BCRP) are highly expressed in lung tissue.

SLC series of transporters comprises to date a total of 52 subfamilies and almost 400 genes and will be the main focus of this research. SLC transporters are either facilitative transporters, meaning they allow passage of membrane impermeable solutes with an electrochemical gradient or they are secondary active transporters which use existing electrochemical gradients of one solute as the driving force for the transport of a second solute against its electrochemical gradient (*37*). The different members of this huge group of transporters are involved in the most diverse biological processes, such as nutrient supply, metal-ion transport or peptide transport, pathogen defence, or embryonal development, just to

mention a few, while the physiological function of many of these proteins to date still remains obscure (*37-39*).

1.2.1 Organic Cation/Carnitine Transporters

Organic cation transporters (OCT1-3) and the novel organic cation transporters (OCTN1, 2) belong to the *SLC22* gene-family of organic cation/anion/zwitterion solute carriers, which comprise more than 20 members (*37-39*). OCT/Ns mediated, bi-directional transport is either membrane potential sensitive (OCT) or pH-dependent (OCTN). Physiological substrates of OCT/N include acetylcholine (ACh) - the most potent physiological broncho-constrictor, nutrients, hormones like prostaglandin E_2 (PGE_2), neurotransmitters (e.g. dopamine), antioxidants such as L-ergothioneine (ET) and a number of molecules e.g. [^{14}C]-tetraethylammonium (TEA) (*37, 39, 40*). The OCT/N transporters have been detected in a great variety of tissues such as in liver, intestine, kidney, brain, blood-brain barrier, heart and also in the lung (*38, 40*). In the airway, one physiological role of OCTs is non-neuronal ACh transport, thus they play a possible role in asthma (*41-44*). A recent study also identified OCTN1 as an ACh transporter (*45*), but an involvement in airway ACh release still needs to be shown. Since a great variety of pulmonary administered drugs, e.g. β_2-adrenergic agonists or anti-muscarinics for the treatment of asthma and COPD are either cations or bases, the relevance of OCT/Ns for drug absorption in the lung have been hypothesised in the last decade.

1.2.2 Organic Cation Novel Transporter 1, OCTN1

The organic cation transporter number 1 (OCTN1) was first cloned in 1997 (*46*) and was discovered as a physiological transporter of ET by Gründemann *et al.* (*47*). Although OCTN1 has been described as a transporter of multispecific organic cations like TEA, carnitine, ACh (*46, 48*), ET is the key substrate of OCTN1, being transported >100 more efficiently than

TEA (*49*). In addition, cells lacking OCTN1, by blockage or inactivation with inhibitors like cimetidine, procainamide, pyrilamine, quinidine, quinine, verapamil, or alternatively by knock down OCTN1 ($OCTN1^{-/-}$), did not accumulate ET to high levels demonstrating a specific role of OCTN1 in the uptake of ET (*49-51*).

OCTN1 is a product of the gene *SLC22A4* (solute carrier family 22, member 4) and is found on chromosome 5q31. Interestingly this gene is found in close proximity to functioning genes of the inflammatory response. Further, it is abundantly expressed in macrophages and monocytes (*46-48, 52*) and so correlates with data collected about ET and its antioxidant role in human respiratory epithelial cells exposed to oxidative stress and hence inflammation.

1.2.2.1 OCTN1 Tissue Distribution

Unlike other OCTs and organic anion transporters (OATs), OCTN1 is ubiquitously detected in all tissue types, suggesting a role in the disposition and excretion of xenobiotics (*53*). OCTN1 was originally cloned from human foetal kidney (*46*) and found to have highest expression in this organ along with bone marrow. Tamai *et al.* also detected moderate expression in human skeletal muscle, lung and placenta with low expression detected in the small intestines, heart, spleen and uterus. No expression of OCTN1 was detected in adult human liver (*46*). Mouse *Octn1* shares 84% amino acid homology to human OCTN1 (hOCTN1), which allows for comparisons to be made between the gene of *in vivo* models to that of human models at a cellular level by reverse transcriptase polymerase chain reaction (qRT-PCR) and Western blotting (WB) for gene and protein expression, respectively. The gene transcript and protein of OCTN1 was also identified in a broad range of tissues withhighest detection of OCTN1 detected in the kidney and lowest detection in the heart (*54*). Although the gene transcript of OCTN1, *Slc22a4* was detected in the skeletal muscle of mice, no such protein expression was detected. Similar to humans, the mRNA and protein in mouse liver was undetectable (*55*). In contrast, rat OCTN1 was highly detected in hepatic and

kidney tissue, with moderate expression in skin, intestine and lung and lowest expression in testis, brain and thymus tissues (*53*). In all three species, OCTN1 was in highest abundance in the kidney (*55*) with localisation of the protein to the cortex-medulla junction of rats, where efflux occurs (*56*). Tamai *et al.* further identified the uptake of TEA from renal epithelial suggesting OCTN1 to behave as an antiport system. Both Tamai and Yabuuchi determined OCTN1 to be localised to the apical membrane of human kidney tissue (*46, 57*).

1.2.2.2 OCTN1 Expression in the Human Lung

OCTN1 has been detected in rat, mouse and human lung tissue with moderate expression (*48, 54, 58*). A number of reports also detail the presence of mRNA in normal human nasal epithelia and polyps (*59*). In human airway epithelia of human trachea and parenchyma, mRNA and protein were detected by qRT-PCR and immunofluorescence (IF), respectively (*60*). By IF, OCTN1 protein was predominantly localised to the apical portion of epithelial cells of human trachea with lower levels detectable in the alveolar epithelia (*60*). Slitt *et al.* found the tissue distribution of *Octn1* by qRT-PCR in rats to be similar to that of humans (*53*). Moderate expression was detected in the lungs with localisation of the protein occuring to the apical membranes (*46, 57*). Similarly, OCTN1 was found in mice but with lower mRNA expression compared to human and rat tissue (*54, 58*).

OCTN1 expression has also been confirmed in human cell lines of lung epithelial both on gene and protein level. By PCR, OCTN1 mRNA was detected in the bronchial epithelial cell line BEAS-2B (*51, 61*) with Salomon *et al.* detecting the protein in the alveolar epithelial cell line A549 with predominant subcellular localisation confirmed by confocal microscopy (*50*).

Although a sizeable number of studies have been conducted, results on the expression, localisation and activity of OCTN1 in lung tissue and relevant *in vitro* models remain in parts contradictory, with many open questions - the most important one being their role in pulmonary pharmacokinetics of inhaled compounds -still needing to be clarified.

1.3 Ergothioneine

A method to control oxidative stress is through homeostasis, a complex process in which a physiological redox balance is maintained. Cells are equipped with various antioxidants, like SOD, catalase, glutathione peroxidase (GP_x), glutathione (GSH), to help eliminate excess reactive oxygen species (ROS) and consequently their effects. Similarly, we can enrich our bodies with antioxidants through diets rich in vitamins and minerals, like fruit and vegetables, to help prevent the effects of cellular and tissue damage.

GSH is an important antioxidant in many species. However, during oxidative stress the thiol group present within glutathione becomes oxidised forming the thione (Figure 1.2a) and consequently, compromises the antioxidant potential of this amino acid. Zeng *et al.* demonstrated that GSH levels were down regulated in the sputum and plasma of COPD patients (*62*), leading to an increased imbalance between oxidants and antioxidants in the airway. Similar data was established for superoxide dismutase (SOD) and glutathione peroxidase (GP_x) in the same study (*62*).

In 1909, an analogue of GSH known as ET was first discovered. ET was dissimilar from GSH as it is synthesised only by a few organisms: actinobacteria, cyanobacteria and non-yeast fungi (*63*). However, ET was found to accumulate to higher concentrations than that of GSH, in tissues, exposed to oxidative stress (*64*, *65*). With the elucidation of ET's structure, it is evident that ET is an adaptive antioxidant, i.e. ET once oxidised, can be rapidly reduced due to the presence of the tautomeric ring (Figure 1.2b).

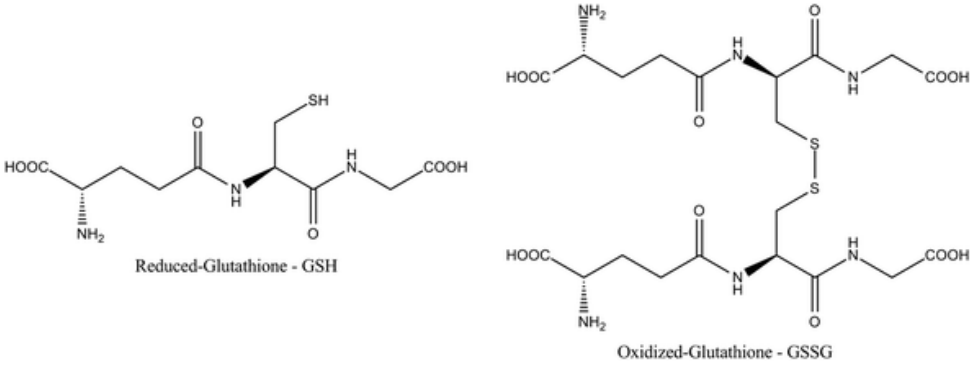

Figure 1.2a: Reduced and oxidised forms of glutathione (*6*).

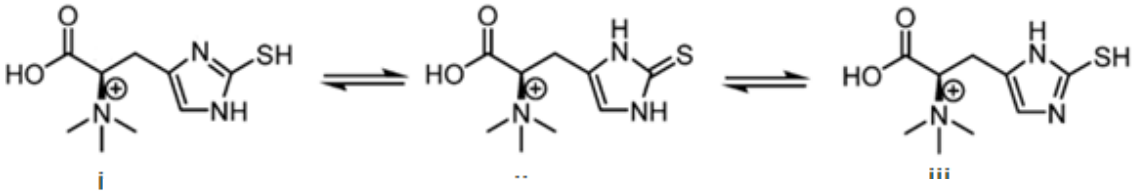

Figure 1.2b: Tautomeric equilibrium of ergothioneine isomers in which the thione (ii) form is the predominate state at physiological pH (*5*).

The exact mechanism of action of ET remains nebulous. However, ET has been shown to provide protection against p38 MAPK and Akt activation through inhibition of phosphorylation, which is critical for the activation of NF-κB, a transcription factor for pro-inflammatory cytokine release from epithelial cells (*66*). Pretreatment of A549 cells demonstrated the complete inhibition of interleukin-8 (IL-8) release and its transcriptional activation mediated through NF-κB (*64)***.** Similarly, inhibition of tumour necrosis factor-alpha (TNF-α) release from macrophages has been detected upon treatment with ET (*67*) and finally, ET treatment demonstrated an anti-inflammatory role in interleukin 1 beta (IL-1β) and interferon insufflated rats (*68*).

Therefore, ET treatment could be effective in the progression of COPD (*67*)

1.3.1 The Role of OCTN1 *in vivo*

As a result of the toxic presence of oxidants, the immune system is stimulated to release cytokines from cells (e.g. macrophages, dendritic cells, mast cells) (*69*). Activation of macrophages is the predominant secretor of these small proteins, even though the mechanistic pathway remains unclear (*70, 71*). Yang *et al.* previously determined that pro-inflammatory cytokines, i.e. TNF-α, IL-1β, interferon-gamma (IFN-γ), increased both intra and extracellular ROS production in a time/concentration manner, initiating a vicious chain cycle. It has been established, that release of cytokines is prevented or completely inhibited when mice are administered ET. One such cytokine, TNF-α is a potent pro-inflammatory mediator, which is tightly linked to the persistence of inflammation, characteristic of COPD (*72*). IL-1β, a mediator for inflammation and apoptosis, was also found to be released at significantly lower concentration when incubated with ET (*67*).

A recent collaboration with Brigham Young University (Provo, UT), has allowed for the further investigation of the protective role of *Octn1* in whole mouse lung. Their initial studies investigated the effect of second hand smoke (SHS) on the lung structure of wildtype and *Octn1* silenced mice for 90 days, with results displayed by Figure 1.3. Their controls were mice exposed to room air (RA). After the mice were sacrificed, histology of the mouse lung was performed. By qualitative analysis, a simplification of the lung structure was identified and confirmed by an increase in chord length. No such significant increase in chord length occurred in mice, where the transporter was present.

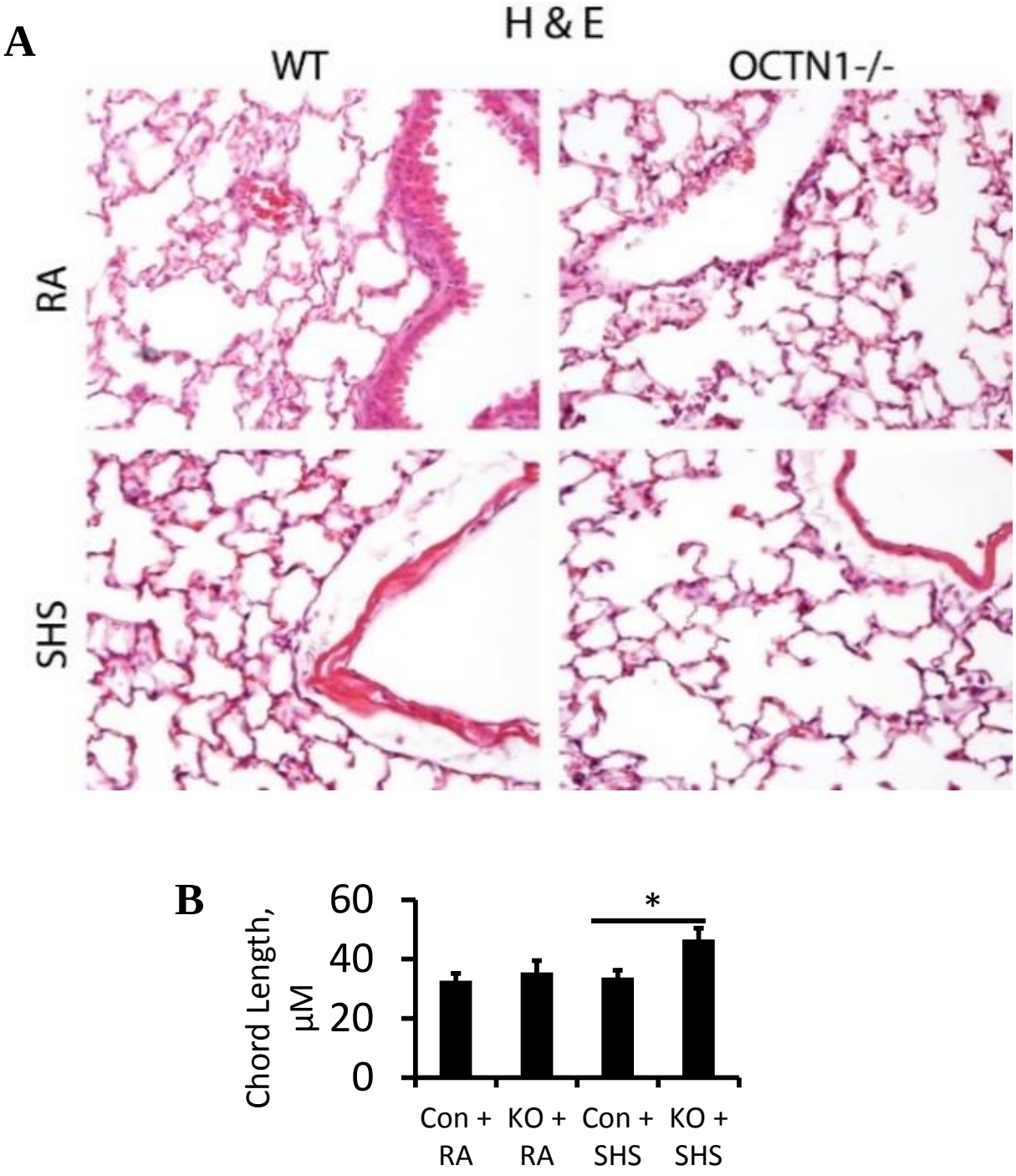

Figure 1.3: Histology of wildtype (WT) and silenced *Octn1* (*Octn1*$^{-/-}$) mouse lung exposed to room air (RA) and second-hand smoke (SHS). **A,B)** Illustrates a qualitative and quantitative simplification of lung tissue in *Ocnt1*$^{-/-}$ mice when exposed to SHS, respectively. Graphs represent mean ± SD (*n*=3).

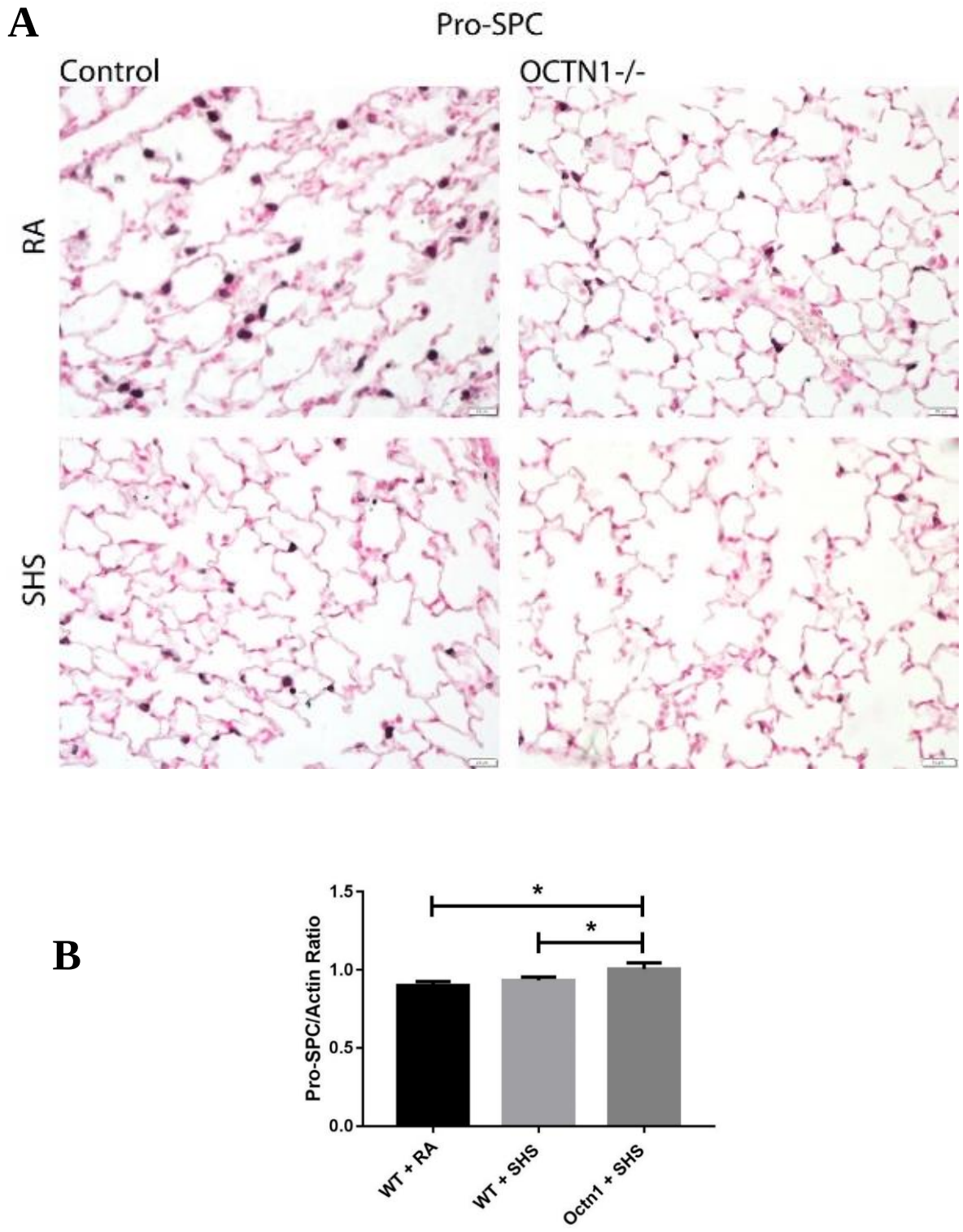

Figure 1.4: Histology of wildtype (WT) and silenced *Octn1* (*Ocnt1*$^{-/-}$) mouse lung exposed to room air (RA) and second-hand smoke (SHS). **A,B)** Identifies a depletion of AT-II cells in knockout *Octn1* mice exposed to SHS by staining for Pro-SPC, a protein secreted by AT-II cells. Graphs represent mean ± SD (n=3), P<0.05.

Alveolar type II (ATII) and alveolar type I (ATI) cells cover 5% and 95%, respectively, of the alveolar epithelium, cellular damage was studied by staining for ATII cells with Pro-SP-C. Their research identified a significant decline in the level of actin present in the lung tissue and as a result when calculating pro-SPC/Actin ratio an increase is observed (Figure 1.4). This is representative to a decline in the number of ATII cells, in the presence of SHS, when the transporter was silenced. Hence, there is a strong suggestion that OCTN1 plays a protective role against cigarette smoke exposure.

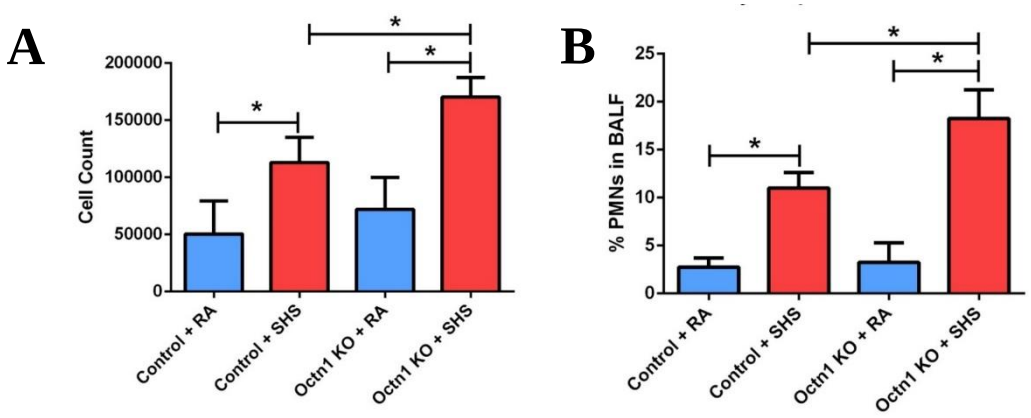

Figure 1.5: Octn1 protects against inflammation. **A)** Increase in total cell count occurs in *Octn1* knockout mice exposed to SHS. **B)** Increase in polymorphonuclear leukocytes was seen in *Octn1* silenced mice exposed to SHS. Graphs represent means ± SD (n =3), P<0.05.

Further investigation was carried out to identify the degree of protection by OCTN1 during cell damage. Total cell counts were performed in broncho-alveolar lavage fluid (BALF), as a marker for inflammation. As predicted, a significant increase in cell number occurred when mice (both wildtype and knockout) were exposed to SHS. This rise in number was further enhanced when *Octn1* was silenced. This study further investigated the release of pro-inflammatory leukocytes, specifically, polymorphonuclear (PMN) cells, to which a similar

trend occurred. A strikingly significant increase in the number of PMNs occurred in mice exposed to SHS when *Octn1* is depleted. These data are illustrated in Figure 1.5.

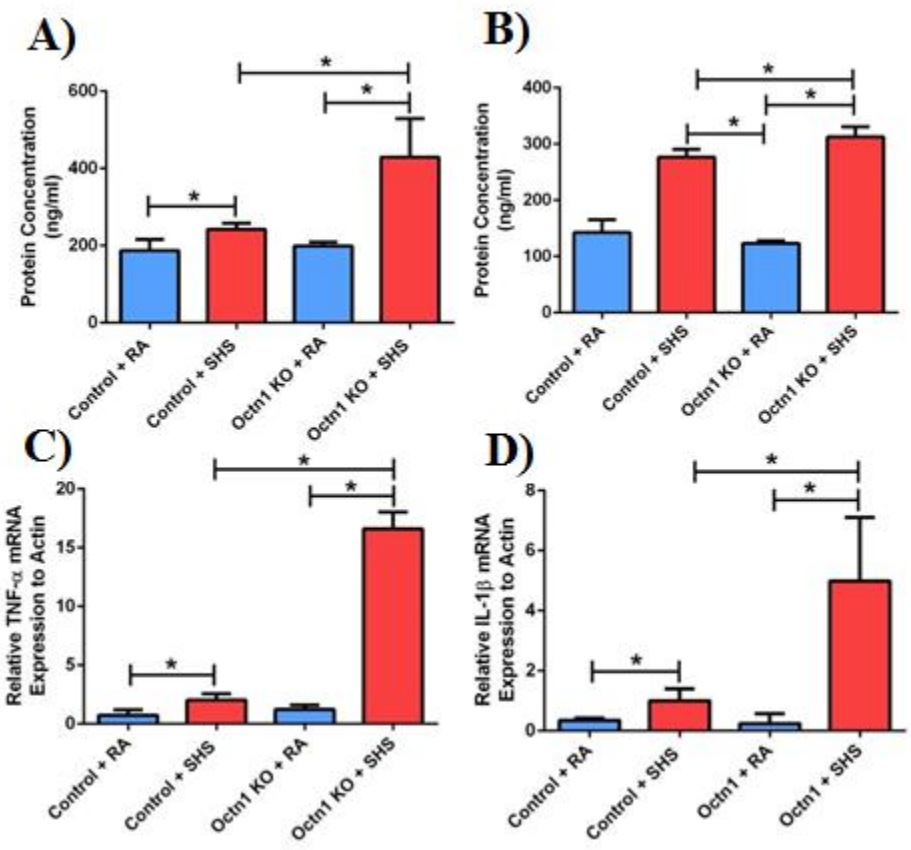

Figure 1.6: Octn1 protects against the release and expression of pro-inflammatory mediators. **A)** Increase in TNFα release occurs in OCTN1 silenced mice exposed to SHS. **B)** Increase in IL-1β occurs in OCTN1 silenced mice exposed to SHS. **C, D)** Increase in TNFα and IL-1β also occurred, respectively, in the total cell matrix. Graphs represent means ± SD (n = 3), P<0.05.

As displayed by Figure 1.6, Reynolds *et al.* also examined pro-inflammatory mediators; TNF-α and IL-1β. Their expression was studied in the total lung of wildtype and knockout mice, exposed to SHS. Their findings were similar to findings of Rahman *et al.* When the transporter, *Octn1* was silenced, the expression of both mediators is significantly increased compared to all other groups.

In summary, there is a strong suggestion indicating that *Octn1* does play a protective role *in vivo* and when absent or dysfunctional, may further increase and contribute to chronic inflammation, typical of COPD.

1.4 Expression of OCTN1 in NCI-H441, primary cells and mouse lung tissue

Together with colleagues from Brigham Young University, our research group has also successfully identified the presence of OCTN1 by Confocal Laser Scanning Microscopy (CLSM) in cell types: NCI-H441, AT-II and ATI-like primary cells, and lung tissue specimens from wildtype mice exposed to room air (RA) as shown in Figure 1.7. This was similar to findings previously established by Salomon *et al.* (*73*).

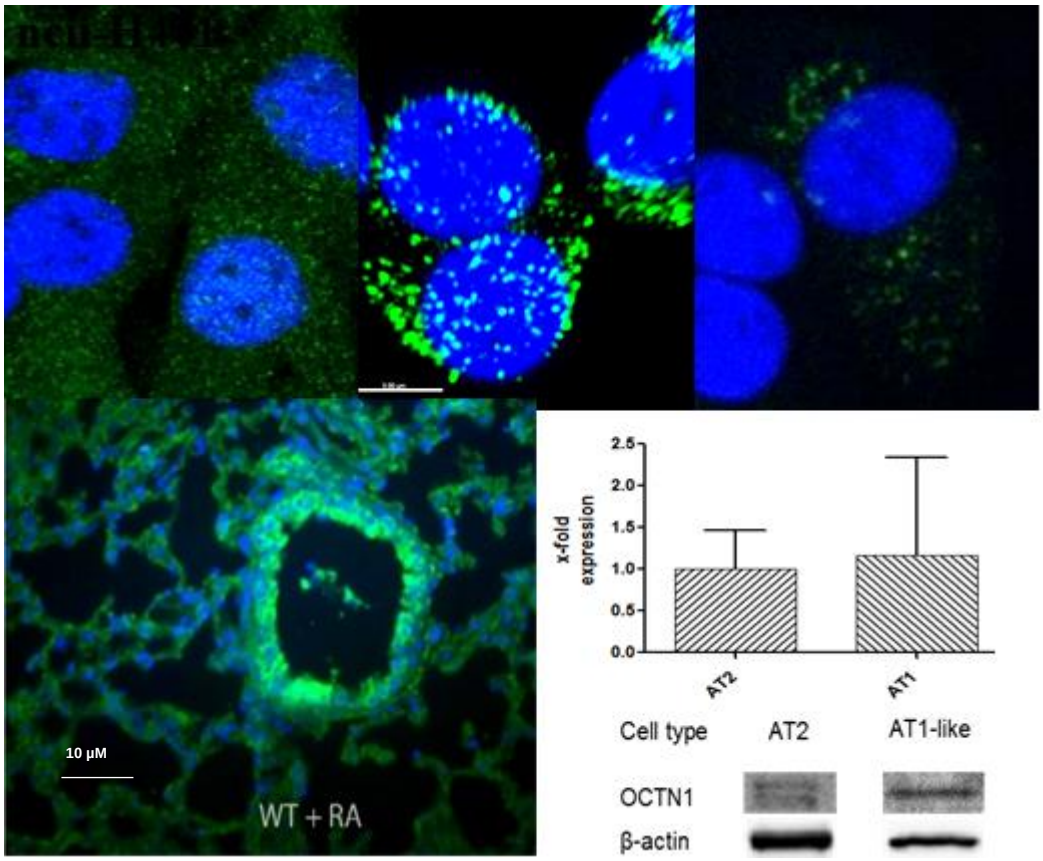

Figure 1.7: Immunolabelling of OCTN1 in NCI-H441, human alveolar epithelial cells (hAEpC) AT-II and hAEpC ATI-like differentiated cells. Monolayers were grown on Transwell filters. **B)** Immunolabelling of *Octn1* in whole mouse lung**.** Staining for OCTN1 (green) is shown by confocal laser scanning microscopy. Nuclei were counterstained with DAPI. Bar 500 µm. **C)** Gene expression of OCTN1 by qRT-PCR in AT-II and ATI-like differentiated human alveolar epithelial cells.

Finally, expression of OCTN1 has more recently been quantified by our research group in the presence and/or absence of CSE and ET. Upon incubation with CSE a slight increase in the expression of the transporter, both at gene and protein level is observed (Figure 1.8). No such change is seen when cells are exposed to ET.

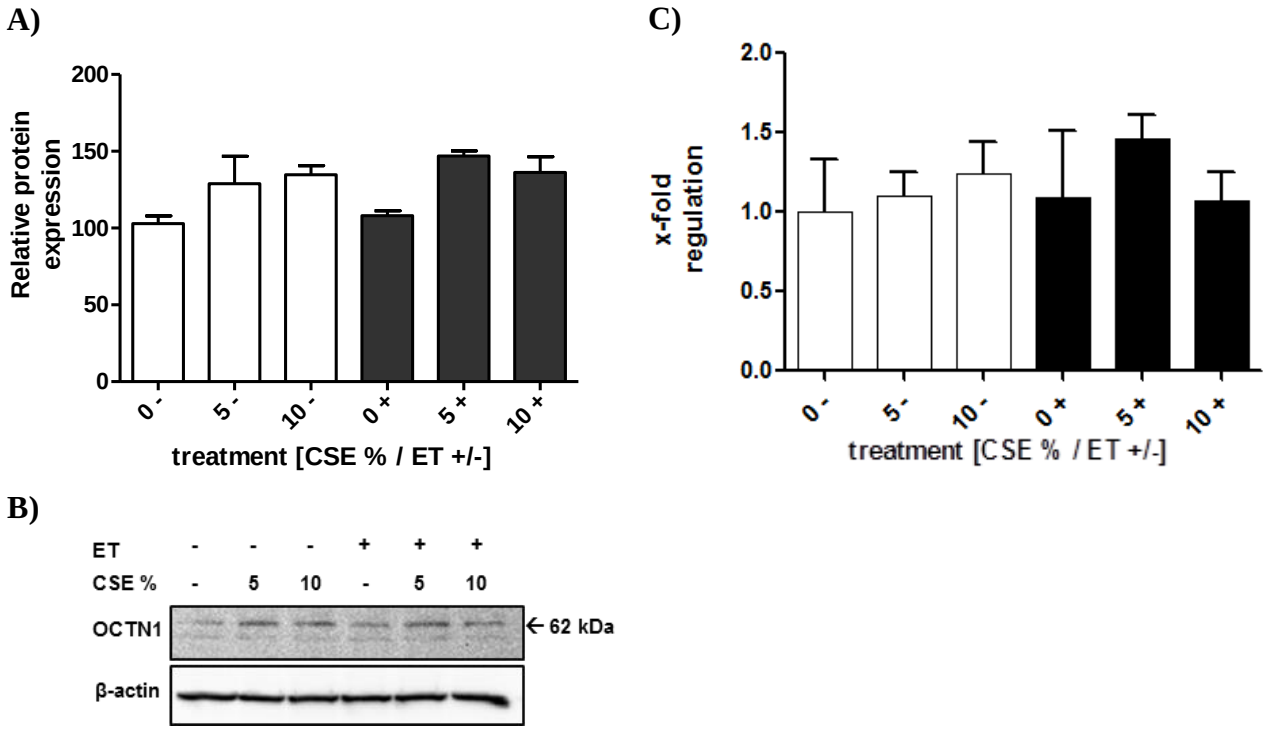

Figure 1.8: A,B) Western blot analysis of OCTN1 in NCI-H441 cells exposed to various conditions of CSE and ET **C)** Relative gene expression profile of OCTN1 in NCI-H441 cells exposed to various conditions of CSE and ET. Graph represents means ± SEM (*n* = 3).

1.5 Aims of the Thesis

To date, OCTN1 has been identified as a key player in the protection of lung tissue SHS *in vivo.* However, a need for greater understanding of the functional role of the transporter OCTN1 and the molecular mechanism of its specific substrate ET is required. Elucidating the activity of OCTN1 and ET will be discussed in this thesis and may be the basis for a novel therapy of COPD.

The aims of this research will be to:

1. To investigate the functional activity of OCTN1 in the cell line NCI-H441. SNPs associated with the transporter in the cell line NCI-H441 will be highlighted. Uptake and transport studies of OCTN1 in NCI-H441 cells and hAEpCs will be performed to determine the localisation of OCTN1 in bronchiolar epithelium. Further, confirm the protective role of OCTN1 against oxidative stress in the cell.
2. To characterise the expression of the gene *SLC22A4* responsible for the coding of OCTN1 in the bronchiolar epithelium of patients with COPD by RT-PCR.
3. To elucidate the mechanism of xenobiotic detoxification by action of ET under oxidative stress, ET, and its oxidative products will be studied when exposed to CSE. Further, it will be imperative to investigate whether ET can participate in phase II metabolism similar to GSH. Therefore, ET and CDNB reactions will be investigated *in vitro* and whether GST and MRPs play a role in its formation and efflux, respectively.
4. To provide a suitable *in vitro* model for the analysis of drug transporters and channels. The cell line NCI-H441 will be investigated for the expression of 23 ABC, 56 SLC, 8 SLCO transporters and 3 AQP channels under air interface culture (AIC) and liquid covered culture (LCC) conditions to determine whether the expression detected represents the true expression of human alveolar epithelial cells.

Chapter 2

The functional activity of OCTN1 in distal lung epithelial cells, NCI-H441

Abstract

Evidence surrounding OCTN1 in the lung epithelium and its functional role is limited. Through its entire charaterisation, the potential importance of OCTN1 and its protective impact on inflammatory diseases maybe revealed. Here, two novel SNPs were identified to be associated with the transporter in the cell line, NCI-H441. OCTN1 activity was examined through uptake and transport experiments of its specific substrate ET, revealing a high affinity of ET for OCTN1 in lung epithelium, data correlating to previous studies published in liver cells. It is suggested that the transporter might have an apical localisation in epithelium, identified by the preferential apical-to-basolateral transport of ET. It is further hypothesised that the protective properties of OCTN1 may be through the uptake of ET and its ability to counteract the toxic production of ROS and through the stabilisation of the intracellular pH. These data support previous findings that OCTN1 may play a protective role in the cell and tissue of the lung.

2.1 Introduction

In tissues, the organic cation transporter, OCTN1 has been identified to be responsible for cellular transport of L-ergothioneine (ET) (*47*), and has been found to share protective properties against the toxic effects of second hand smoke (SHS). Despite the considerable amount of work done on this transporter, the real physiological function of OCTN1, as well as its conceivable role in human disease remains unclear. This could be due to the lack of data collected based on its expression under certain conditions of oxidative stress and/or, reliable methods for the measurement of its specific substrate in biological specimens.

An association between single nucleotide polymorphisms (SNP) of the gene *SLC22A4*, is reported to result in an increase susceptibility to chronic inflammation (*74*). One example of such a SNP is rs1050152, encoding the Leu503Phe variant (c1672C>T), which is responsible for altered substrate specificity, specifically ET (*75, 76*). Other mutations include Gly462Glu (1385C>G), resulting in the complete loss of transport of the ammonium cation tetraethylammonium (TEA) and an example of a synonymous substitution being Thr306Ile (917C>T), yielding no difference in functionality (*77*). Studying SNPs of the transporter will reveal mutations in the gene that may result in an increase susceptibility of developing COPD.

Past methods of quantifying ET have included coupling ET to a fluorophore, which is then detected by UV (*78, 79*) but this lacks the sensitivity required for accurately quantifying ET in cells. In recent years, the sensitivity and accuracy has improved with the development of hydrophilic interaction liquid chromatography tandem mass LC-MS/MS proposed by Wang *et al.* However, it was necessary to use radiolabelled ET as an internal standard for this technique to ensure quantification of ET at µM concentrations (*80*). Therefore, here we propose a new rapid and sensitive method to detect non-labelled ET, in the nM range, in NCI

H441 cells by water deproteinisation treatment followed by fast high-performance liquid chromatography separation and mass tandem detection. Through its quantification the uptake and transport capabilities of OCTN1 *in vitro* will be determined to help determine the functional role of the transporter.

Research previously carried out by our lab investigated the expression of OCTN1 by Western blot under air interface culture (AIC) conditions and liquid covered culture (LCC) conditions of NCI-H441 cells as shown in Figure 2.1. Although statistically, no significant difference was detectable, there was evidence for a slight increase in expression of the transporter when incubated under AIC conditions. This is the first investigation to determine the expression of OCTN1 under culture conditions and could further support the hypothesis that OCTN1 plays a crucial role in the uptake of ET into epithelial cells.

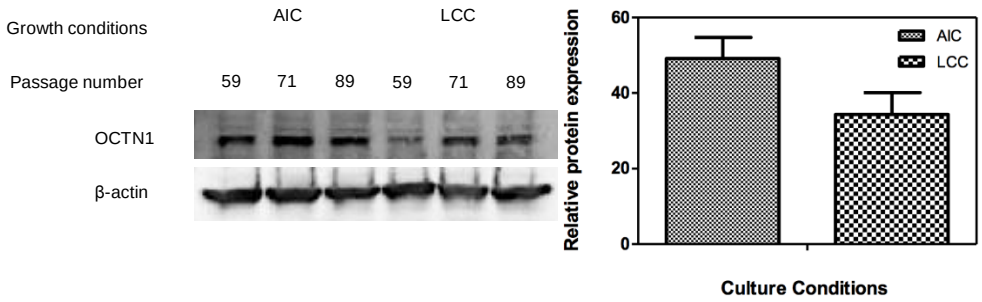

Figure 2.1: Western blot analysis of OCTN1 in NCI-H441 cells cultured under AIC (A) and LCC (B) conditions. OCTN1 protein expression is determined to be slightly higher under AIC conditions compared to LCC conditions. Graphs represent means ± SEM, (n = 3).

ET is an unusual naturally occurring histidine derived amino thiol (*81*), which is exclusively synthesised by fungi and bacteria and is widely distributed in both plants and animals (*82*). Different physiological functions have been suggested for ET including the role as an antioxidant (*79*). ET is highly water soluble and appears to prevent carbonylation of water soluble proteins resembling the actions of glutathione (GSH) (*83*). However, ET

concentrations are frequently higher than those of GSH suggesting that it may be the principle antioxidant in these tissues. In contrast, GSH is often rendered to be close to depletion in the face of oxidative stress (*79*). Therefore, it has been reported that ET is somewhat more active than GSH or vitamin C (*79*) with cells frequently exposed to oxidative stress, accumulating ET in the millimolar range (*84*). Together with the data collected based on the functionality of OCTN1, we can elucidate a potential mechanism for the protective properties of ET and hence OCTN1.

2.2 Materials and Methods

2.2.1 Cell culture

Cell Maintenance of immortalised cell line

Human bronchiolar epithelium NCI-H441 (American Type Culture Collection, HTB-174, Teddington UK) were cultured at 37°C in 5% CO_2 atmosphere in Gibco RPMI-1640 medium (Biosciences, Dun Laoghaire, Ireland) supplemented with 5% foetal bovine serum (FBS), 1% sodium pyruvate, 1% penicillin streptomycin (all from Sigma Aldrich). Passages 55-85 were used for these studies. NCI-H441 cells were routinely cultured in 75 cm^2 growth area tissue culture flasks (Greiner BioOne, Frickenhausen, Germany) and passaged when approximately 80% confluency. NCI-H441 cells were seeded at a density of 75,000 cells/cm^2 on well plates (Greiner). Twenty-four hours prior to experimentation cells were serum starved to reduce proliferation. On the day of the experiment, cells were washed twice with warm, Krebs-Ringer Buffer (KRB) composed of 15 mM HEPES, 116.4 mM NaCl, 5.4 mM KCl, 0.78 mM NaH_2PO_4, 25 mM $NaHCO_3$, 1.8 mM $CaCl_2$, 0.81 mM $MgSO_4$ and 5.55 mM glucose, pH 7.4.

Cell Maintenance of primary epithelial cells

Human alveolar type II epithelial (ATII) cells were obtained from the Helmholtz Institute for Pharmaceutical Research, Saarland University (Saarbrücken, Germany). They were isolated from non-tumour lung tissue obtained from patients undergoing lung surgery according to a protocol modified from Demling *et al.* (*85*). The use of human material was approved by Saarland State Medical Board (Saarbrücken, Germany).

Purified ATII cells were either used directly for protein and RNA isolation or cultured at a density of 200,000 cells/cm^2 in a humidified atmosphere at 37°C and 5% CO_2 using small airways growth medium (SAGM; Lonza, Verviers, Belgium) supplemented with 1% FBS, 100 U/ml penicillin and 100 μg/ml streptomycin (Sigma-Aldrich) on surfaces coated

overnight with 25 µg/cm^2 rat-tail collagen type I (Sigma-Aldrich) and 5µg/cm2 fibronectin (BD Bioscicences, Oxford, U.K.).

The cells were kept in culture for at least 7 days to transdifferentiation into an alveolar type I-like (ATI-like) phenotype.

Transduction of NCI-H441 cells with OCTN1 shRNA lentiviral particles.

This was carried out by Dr. Sabrina Nickel

NCI-H441 cells at passage 60 were used to generate the knock-down cell line. Ahead of the lentiviral transduction, optimal concentrations of the cationic transduction enhancer polybrene (2.5 µg/ml, Santa Cruz Biotechnology, Dallas, TX) and minimal lethal dose (2 µg/ml) of the selection reagent puromycin dihydrochloride (Santa Cruz Biotechnology) were determined using Alamar Blue (BioSciences Ltd, Dun Laoghaire) cytotoxicity assay. NCI-H441 cells were seeded in a 12 well plate at a density of 100,000 cells/cm^2 in RPMI culture medium (5% FBS, 1% sodium pyruvate, 1% penicillin-streptomycin) one day prior to transfection. Monolayers of 50-70 % confluency were used for viral transduction the following day. The culture medium was removed and replaced by transduction medium (RPMI, 5% FBS, 1% sodium pyruvate, 1% penicillin-streptomycin, 2.5 µg/ml polybrene). Lentiviral particles were thawed at room temperature and the cells were transfected with 2x10^4 Infectious Units (IFU) of the *OCTN1* shRNA lentiviral particles (Santa Cruz Biotechnology) per well. One well was additionally transduced with scrambled shRNA lentiviral particles to create a control cell line. The cells were incubated for 24 h with the viral particles before the transduction medium was removed and replaced with culture medium. Following an additional 24 h incubation period, NCI-H441 cells were split at a 1:3 ration, seeded in culture medium onto six well plates and allowed to attach over-night. Subsequently, the culture medium was replaced by selection medium (RPMI, 5% FBS, 1%

sodium pyruvate, 1% penicillin-streptomycin, 2 µg/ml puromycin HCl). The selection medium was replaced every two to three days until resistant colonies could be observed. Colonies were picked and expanded in selection medium for another 3 weeks to ensure complete removal of non-transfected cells.

Cigarette smoke extract

Two Kentucky 2RF4 reference research cigarettes were ignited and the gaseous component bubbled through 20 ml of medium to yield 100% cigarette smoke extract (CSE) for 1.5 min. Two filters from unused Kentucky reference research cigarettes were bubbled through 20 ml medium to act as a control. All medium was sterilised by filtration before use.

2.2.2 Sequencing of OCTN1 in the cell line NCI-H441

DNA isolation from NCI-H441 cells

Genomic DNA was isolated from the immortalised cell line using Blood and Cell Culture DNA mini kit (Qiagen). Isolation occurred following the products specifications.

Quantification of DNA

DNA was quantified using a NanoDrop ND-1000 spectrophotometer (Fischer Scientific Ireland Ltd, Dublin, Ireland) and ND-1000 software. The optical surfaces of the instrument were cleaned with RNA free wipes and it was initialised using nuclease free water. The NanoDrop was then blanked using the elution solution. Each sample is measured by loading 1 µl onto the lower optical platform and lowering the arm gently. The surfaces were wiped clean between each measurement. The DNA concentration was automatically calculated by the software from the absorbance at 260 nm and given as ng/µl. Purity of the sample was primarily assessed by the 260/280 ratio, which was again automatically calculated by the software and should be approximately 1.8. A further measure of purity was the 260/230 ratio,

which should be approximately 2-2.2. These ratios serve as a rule of thumb for purity assessment. All samples were diluted to 1 µl/10 µl with nuclease free water.

***SLC22A4* primer selection**

BLAST, NCBI allowed the determination of the exonic fragments within *SLC22A4* genome and allowed for the prediction of the amino acid sequence as displayed in Figure 2.2. Based on this primers were designed for the *SLC22A4* exonic fragments. The USCS genome browser was used to view the exons before selecting the primers. Once the selected region was found the sequence was submitted into the online program; primer3 plus. After submission primer3 plus returned a list of appropriate primer pair options to choose from. Suitable primers were chosen based on the different characteristics of the sequence; primer length, GC content, GC clamp, annealing temperature, target region. The chosen primer was then inserted into the online oligoDT calculator to test possible sequence hairpin loops or primer dimer formation. Primer Blast on NCBI was then used to determine if the primer target sequence is found in many genes to ensure amplification of only the targeted sequence. Selected primers were named accordingly and ordered.

PCR and sequence analysis

Exonic fragments of the gene *SLC22A4,* which codes for OCTN1 were generated using the primer sequences shown in Table 2.1. Amplification was performed using 12.5 µl Taqman Master Mix (Qiagen), 1.25 µl of forward and reverse primer for the specific exon (Sigma) and finally a concentration of 50 ng/µl of DNA, made up to 25 µl with nuclease free water. PCR conditions were pre-denaturation at 95°C for 5 min, followed by 35 cycles of denaturation at 95°C for 1 min, annealing for 1 min and extension at 72°C for 1 min and then a final extension at 72°C for 10 min. Annealing temperatures for the individual exons are summarised in Table 2.1.

Table 2.1: Primer sequence and PCR conditions used for the analysis of *SLC22A4* gene encoding OCTN1 and obtained from NCBI. Reference sequence is NT_003334772.5

Exon Amplified	Forward primer (5' to 3')	Reverse primer (3' to 5')	Amplified Region	Annealing Temperature	Fragment Weight (bp)
1	GCCCCAGCTACAAGACACTG	CCGCTGCTGGAAGTATGAAC	34045247_34045853	55	607
2	CGTGCTAATATTCCCTCAGAGC	CTGAGGGTCCTCCCTTTCTCT	34062783_34063083	60	301
3	TCTGCATTGATGCCTGACTC	CCCTCCCAAGACACATATATCC	34064236_34064597	53	362
4	AATGCCTTTCCCCTTTTCTAAG	ATCAGGCTCCAGGTGTGTTC	34072773_34073133	56	361
5	TTCATTCCTGAATCTCCCCGATGG	CTCCACAGAATCAATATCACTGCT	34077910_34078213	55	304
6	TATTGCCTCCAATCACCAGAC	CCCAGTCGTTGTCATAATGTTC	34082320_34082649	53	330
7	TGACCATCATAAAATTTTAGAGCG	GACTCAGAAGCAGCCTAGTCAA	3400085359_34085707	55	349
8	CCACTGAAGCAAAAAGGACAAT	CTGGGAGAGGAGAGGTGAACT	340863434_34086838	55	405
9	CCAACTTCACAAAATGATGCTC	CCCAGCCAACAATATGCTTTAT	34091191_34091546	59	356
10	GTCAATTTGGATGGAGCATTTT	AGTCCATTTCAGTGGGAACAAC	34094391_34094625	55	235

Purification of PCR products

Purification was performed using the Qiaquick gel extraction kit (Qiagen) following the manufacturers specifications.

Sequencing of *SLC22A4* exons

The PCR products were sequenced by Eurofins Genomics (Ebersberg, Germany) in a 5'→3' direction.

2.2.3 Quantification of ET intracellularly by LC-MS/MS

Apparatus and chromatographic conditions

Chromatographic separation consisted of an Accela high pressure liquid chromatography (HPLC) system equipped with a LTQ Orbitrap Discover Mass Spectrometer detector. Sample separation was performed at a fixed flow rate of 940 µl/min with the eluent delivered gradiently with a column temperature of 25°C. Separation was investigated on a Waters T3 HSSC18 (150 mm x 2.1 mm, 1.8 µm) and a Kinetix HSSC18 (100 mm x 4.6 mm, 2.6 µm) with a mobile phase of A) water (Sigma Aldrich, Dublin, Ireland) and 0.1% formic acid

(Sigma Aldrich) and B) acetonitrile (Sigma Aldrich) and 0.1% formic acid or A) water and 0.1% acetic acid (Sigma Aldrich) and B) acetonitrile and 0.1% acetic acid, where all solvents were of HPLC grade. Samples were held in the auto sampler and the amount injected was 12 µl. Column eluents were detected by Tandem Mass Spectrometry (MS/MS) at a retention time of around 2.67 min.

Full accurate high resolution mass scans were carried out under positive electrospray ionisation (ESI). Several parameters were optimised to achieve efficient detection sensitivity. ET (Tetrahedron, Romainville, France) was first nebulised with nitrogen gas and introduced to the detector at 520°C. From the product ion spectra, the following signals will be chosen for selected reaction monitoring (SRM) (molecule of interest, *m/z* parent, *m/z* fragment), and magnitude of voltage: ET, 230, 186 and 16 V. Sample analyte content will be calculated from the analyte response ratio and the slope of the calibration curve, obtained by weighted linear regression.

Calibration curve

For LC-MS/MS analysis, calibration standards of ET were prepared by serial dilution of the stock solution (50 mM) with high purity water. This was prepared and analysed for each experiment.

Method validation

The validation of the current method was tested according to the Bioanalytical Method Guidelines of the US Food and Drug Administration and the International Conference of Harmonisation (ICH) (*86, 87*). Linearity, precision and accuracy, sensitivity and selectivity, and stability were determined according to these guidelines. Calibration curves determined linearity by demonstrating an increase in concentration with a corresponding increase in peak area. The limit of detection (LOD) was determined by investigating the lowest concentration of ET registered by the LC-MS/MS and distinguished from zero concentrations by ensuring the signal to noise ratio is 3:1 as identified by the ICH. The limit of quantification (LOQ) was determined by quantifying results that had a large degree of confidence and were registering a signal to noise ratio of 10:1 to that of a blank solution as highlighted by the ICH. The LOD and LOQ were 3 nM and 5 nM, respectively. Curves were constructed daily within the concentration range of 5 nM to 100 µM. Precision and accuracy were calculated intra- and interdaily with a variety of concentrations (Equation 2.1 and 2.2, respectively) (*80*). Finally, matrix effect (Equation 2.3) (*80*) and stability of ET was tested under a range of conditions, i.e. -20°C, 2-8°C, 21°C and 95°C.

$$\% \text{ Precision} = \frac{\text{SD}}{\text{Mean calculated concentration}} \text{ x } 100 \qquad \text{Equation 2.1}$$

$$\% \text{ Accuracy} = \frac{\text{Calculated mean}}{\text{Nominal}} \text{x } 100 \qquad \text{Equation 2.2}$$

$$\% \text{ Matrix Effect} = \frac{\text{peak area obtained after media extraction}}{\text{peak area obtained in neat solution}} \qquad \text{Equation 2.3}$$

2.2.4 Uptake studies

The validated LC-MS/MS method was applied to an *in vitro* study of ET in distal lung epithelial cells, NCI-H441.

Uptake studies were carried out using NCI-H441 monolayers seeded on 6-well plates.

Uptake of ET was investigated at different concentrations, temperatures and pH values. Time dependency of ET was also measured by incubating the cells with various concentrations of ET and measuring the uptake at different time points (0-60 min). Concentration dependence was studied from 0-50 μM ET at 37°C and 4°C for 0-30 min. Uptake experiments were also performed in buffers of varying pH values (i.e. 5.6-8.4).

To initiate uptake of ET by OCTN1, cells were incubated with a range of ET concentrations. For concentration dependency of organic cation uptake into cell monolayers, cells were incubated with ET (0-50 μM) for 30 min to identify maximal uptake of ET. For time course analysis, cells were incubated with 50 μM ET for 0-7 days at various intervals.

Uptake experiments were stopped by washing the cell monolayer three times with ice-cold buffer. Cells were detached from the plate using 0.5 ml of 100% trypsin. The resulting solution was centrifuged at 12,000x*g* for 10 min before adding 1 ml of water to lyse the cells. The solution was briefly sonicated and the resulting solution centrifuged at 17,000x*g* for 5 min. The supernatant was removed and filtered prior to analysis by LC-MS/MS.

2.2.5 Kinetic analysis for uptake studies

Michaelis Menten constant (K_m) and maximum uptake rates (V_{max}) of ET can be calculated from the Michalis Menten Model where the uptake rate is plotted against substrate concentration ([S]). (Figure 2.2a). However, with this plot, V_{max} is hard to estimate as the rate still increases. Therefore, a direct linear plot known as the Eadie Hofstee plot may be used, which is a powerful non-parametric statistical method that assumes all errors are either too high or too low (Figure 2.2b). This is calculated by fitting the υ against $V/[S]_0$ giving

intercepts at V_{max} and V_{max}/K_m where $\upsilon = \frac{Vmax\ X\ (S)}{[Km+(S)]}$ and (S) was [ET]. This analysis was performed by utilising the online software ic50.tk.

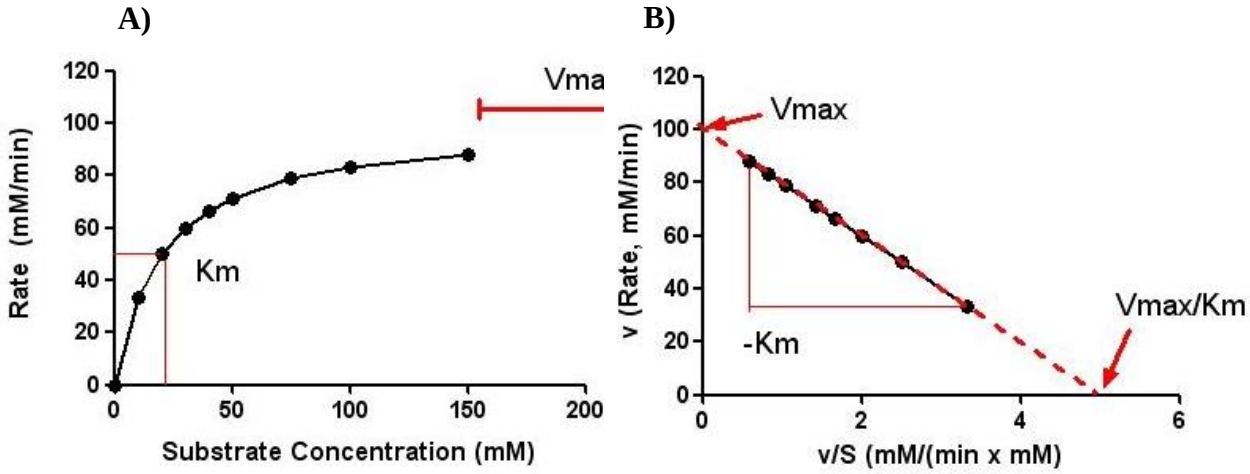

Figure 2.2: A) Michaelis Menten plot where uptake rate is plotted against substrate concentration giving rise to a hyperbolic curve. B) Eadie Hofstee plot where $\frac{Vmax\ X\ (S)}{[Km+(S)]}$ is plotted against $V/[S]_0$ to give a direct linear plot.

2.2.6 Transport studies

NCI-H441 and human alveolar primary epithelial cells were grown on Transwell Clear filters (12 mm diameter with 0.4 µm pore size, and 6.5 mm diameter with 0.4 µm pore size, respectively) for at least 8 days with medium supplemented with 10 µM dexamethasone and 1X concentration of Insulin Transferrin Selenium (ITS) (Transepithelial Electrical Resistance (TEER)>350 ohm×cm^2) (*88*). Before transport of ET was initiated, cells were washed once with pre-warmed fresh KRB, before incubation with KRB for 1 h at 37°C. For the actual transport, the buffer was replaced with 0.51 ml donor solution (ET) in the apical chamber and 1.5 ml KRB in the basolateral chamber. This was to behave as a model for apical-to-basolateral (AB) transport studies. In comparison, 1.51 ml donor solution was placed in the basolateral chambers with 0.5 ml KRB in the apical chamber to study basolateral-to-apical (BA) transport. The initial donor concentrations were determined by sampling 10 µl of the

donor solution. The cells were kept at 37°C with 200 µl samples taken from the receiver compartment every 15 min. To keep sink conditions, an equal amount of fresh KRB was returned to the receiver compartments. TEER values were recorded before and after the experiment to access cell integrity.

The utilised equation to calculate the apparent permeability coefficient (P_{app}) is the following:

$$P_{app} = (\frac{\Delta Q}{\Delta t})/(A.C_0) \quad \text{Equation 2.5}$$

Where ΔQ was the change in quantity of the compound over a designated period of time (Δt), A was the nominal surface area of the cell layers (1.13 cm^2) and C_0 was the initial concentration of the drug in the donor fluid and used in this study

Bioelectric measurements

The time of the cellular layers reaching confluence was determined by measuring TEER as a function of days in culture. TEER was measured daily with an epithelial volt-ohm meter equipped with STX-2 electrodes (WPI, Berlin, Germany) and corrected for the background value contributed by the Transwell Clear insert and medium.

2.2.7 Cytotoxicity of CSE and ET

NCI-H441 cells were seeded in a 96-well plate (Greiner). On the day of seeding cells were incubated with 250 µM ET. A day prior to experimentation, cells were serum starved and incubated with a range of CSE concentrations. Cells were then incubated with 1X concentration Alamar Blue (BioSciences Ltd) for 4 h in the dark. Thirty min prior to the end of incubation 3 wells of cells were incubated with 1% Triton X-100 (VWR International), to act as a negative control. After the 4 h incubation, cells were measured using FLUOstar Optima spectrophotometer and Optima software at an excitation of 570 nm and an emission of 585 nm. The fluorescence recorded is directly proportional to the number of viable cells as only viable cells can reduce reazurin to resorufin. The percentage cell survival was calculated

by (F_T-F_n)100 where F_T is the fluorescence of the treated wells and F_n the fluorescence of the negative controls.

2.2.8 Contribution of CSE and ET towards oxidative stress response

The ROS assay was employed to investigate the production of ROS when incubating with ET. On the day of seeding cells were incubated with 250 µM ET. A day prior to experimentation, cells were serum starved and incubated with a range of CSE concentrations. NCI-H441 cells were incubated with 2, 7 dichlorofluorescein diacetate (H_2DCFDA) for 30 min in the dark at 37°C. Negative controls are treated with 1% Triton X-100 for 20 min. After incubation, the plate is read using FLUOstar Optima spectrophotometer and Optima software at an excitation of 485 nm and an emission of 535 nm. H_2DCFDA-AM is taken into the cell, where it is deacetylated by cellular esterases to be later oxidised by the presence of ROS generating a highly fluorescent compound, DCF. The fluorescence detected is related to the level of ROS present within the cells and so ROS production is calculated by (F_T-F_n) where F_T is the fluorescence of the treated wells and F_n the fluorescence of the negative controls.

2.2.9 Contribution of CSE and ET towards intracellular pH

H441 cells were seeded on a 96-well plate at 75,000 cells/cm^2 and grown to about 80% confluency. On the day of seeding, cells were incubated with 250 µM ET. A day prior to experimentation, cells were serum starved and incubated with a range of CSE concentrations. Cells were washed once with live cell imaging solution buffer (LCIS, BioSciences). A 1X solution of cell dye was prepared by adding 10 µl of pHrodo™ Green AM and 100 µl of Powerload™ concentrate to 10 ml of LCIS. One-hundred microlitres of the resulting solution was added to the cells and allowed to incubate for 30 min at 37°C, protected from light. After incubation, the cells were washed with LCIS buffer. A calibration curve was calculated by

incubating cells with a 10 μM final concentration of nigericin and valinomycin in the respective pH buffer (i.e. 4.5, 5.5, 6.5 and 7.5). Fluorescence was then quantified by using FLUOstar Optima spectrophotometer and Optima software at an excitation of 509 nm and an emission of 533 nm.

2.2.10 Assessment of cell motility in response to ET and CSE

To assess the motility rates of NCI-H441 cells in response to ET, cells were seeded in a 12-well plate (Greiner) and grown to confluency. A day prior to experiment, the cells were serum starved and incubated with or without 5% CSE. The cells were then scratched with a 200 μl pipette tip. The scratch was washed twice with KRB and replaced with fresh serum free medium supplemented with a range of ET concentrations or CSE as required. The wound areas were monitored and photographed by phase contrast microscopy and measured using Olympus Cell^A Image Acquisition Software.

2.2.11 Statistical analysis

All experiments were carried out at least in triplicate using cells from at least three different passages (n = 3-9). Results were expressed as means ± S.D. and were compared using one-way analysis of variance (ANOVA), followed by the Bonferroni *post hoc* test, with $P<0.05$ considered as significant.

2.3 Results

2.3.1 Sequencing of *SLC22A4* in NCI-H441

Sequence analysis of the 10 coding exons of *SLC22A4* from the cell line NCI-H441 were identified by DNA sequencing and resulted in the identification of 3 genetic variatants. Variants on exon 1 and 10 were novel.

Table 2.2: Summary of *SLC22A4* variations detected in NCI-H441 cells.

Location	dbSNP (NCBI)	SNP	Amino Acid Change	Detected in cell line
Exon 1	**Novel**	**5672C>G**	**L75V**	**Yes**
Exon 1		188G>A	R63H	No
Exon 1		225C>T	R75R	No
Exon 1		248G>C	R83P	No
Exon 2		400C>A	L134M	No
Exon 2	rs11568511	465C>T	L155L	No
Exon 3		475G>A	V159M	No
Exon 3		494A>G	D165G	No
Exon		615G>A	M205I	No
Exon 4		774G>C	M258I	No
Exon 4		819G>A	L273L	No
Exon 5	rs272893	917T>C	I306T	No
Exon 5	**rs750523509**	**1083T>C**	**F313L**	**Yes**
Exon 6		1031T>A	M344L	No
Exon 7	rs272879	1182C>G	T394T	No
Exon 8	rs12777	1413C>G	G471G	No
Exon 9		1445G>A	G482A	No
Exon 9		1460T>C	M487T	No
Exon 9		1499T>A	I500A	No
Exon 9	rs1050152	1507C>T	L503F	No
Exon 9		1531G>A	G462E	No
Exon 10	**Novel**	**1232A>T**	**F528T**	**Yes**

2.3.2 Analysis of the functional activity of OCTN1

2.3.2.1 Uptake of ET into NCI-H441 cells

The active component of OCTN1 was investigated by temperature dependency studies at 37°C and 4°C for 30 min (Figure 2.3). At 4°C, a negligible concentration of ET was quantified in the cell, in comparison to that measured at 37°C. The active component of OCTN1 was then analysed to reveal a K_m and V_{max} values of 10.30 ± 6.96 µM and 0.39 ± 0.1 µ0omol/mg protein, respectively.

To investigate time dependency studies, NCI-H441 cells were incubated with 50 µM ET for 0-30 min (Figure 2.4). A linear dependency occurred within 1 min of commencement of the experiment. Cells then appeared to be completely saturated after 5 min, i.e. 0.4 ± 0.03µM/mg protein.

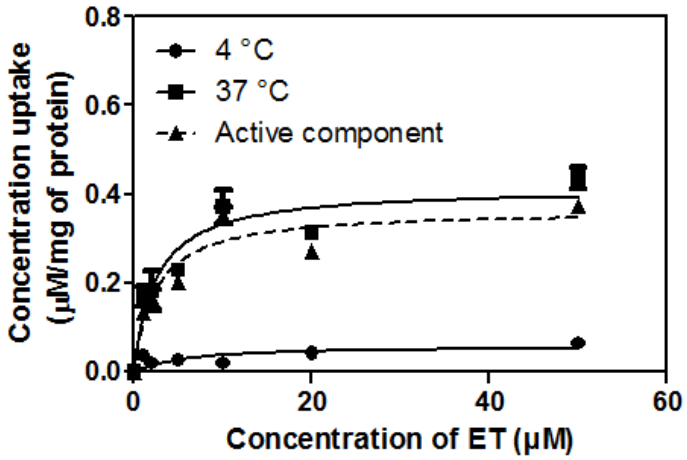

Figure 2.3: The active component of ET was revealed by quantifying the difference in uptake of ET (0-50 µM) at 37 ºC and 4 ºC for 30 min. This study confirmed that OCTN1 is temperature dependent at a physiological temperature and pH. Graph represent mean ± SEM, (*n* = 3-6).

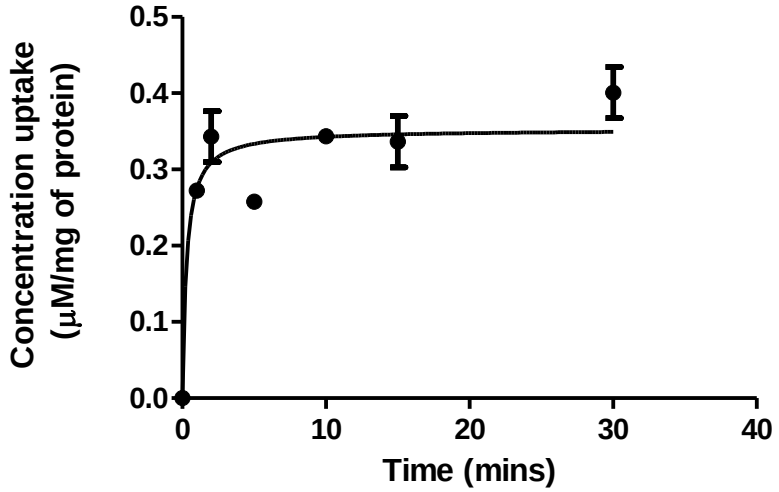

Figure 2.4: OCTN1 is time dependent as illustrated with 50 µM ET in NCI-H441 cells at 37 ºC and pH of 7.4. Cells quickly accumulated ET within 1 min of incubation before reaching their maximum concentration at 5 min, indicated by the graph plateauing at this time point. Graph represent mean ± SEM, (*n* = 3).

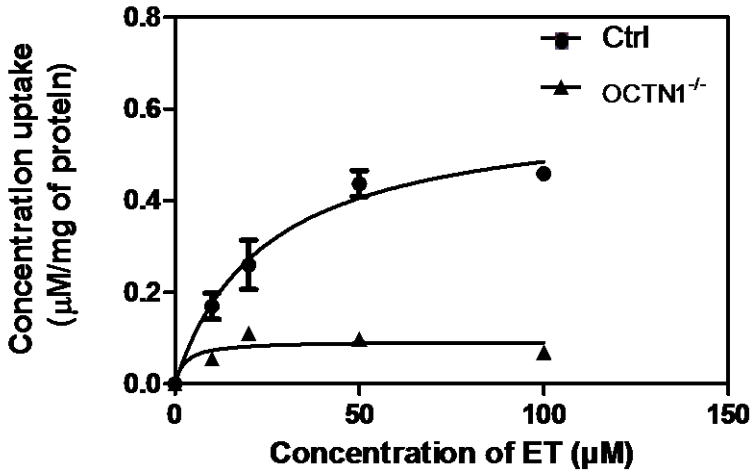

Figure 2.5: The uptake of ET (5 nM – 100 µM)by OCTN1 in wildtype and OCTN1$^{-/-}$ NCI-H441 cells. These data confirm OCTN1 to be responsible for the uptake of ET. Graph represent mean ± SEM, (n = 6).

NCI-H441 cell silenced of OCTN1 were chosen to confirm the uptake of ET by OCTN1 and not another transporter or passive diffusion. As a result, the uptake of ET in OCTN1 knock-down cells, rendered a significant lower accumulation of the substrate (Figure 2.5). Kinetic analysis was performed by online software (ic50.tk). The uptake of ET into NCI-H441 was a saturable process, with the kinetic parameters estimated to be K_m = 23.39 ± 5.26 µM and V_{max} = 0.59 ± 0.05 µM/mg protein when concentrations of 0-100 µM ET were investigated.

Further, OCTN1 has been reported to be a dependent proton/organic cation antiporter at pH 7.6 (*57*). Therefore, ET uptake was studied at various pH values. When the pH in the transport medium became increasingly acidic (<5.9), OCTN1 mediated transport of ET decreased to about 25% of those at neutral pH. In comparison when the pH of the transport medium became increasingly more basic (pH > 7.7), the uptake of ET was around 50% of that at neutral pH (Figure 2.6).

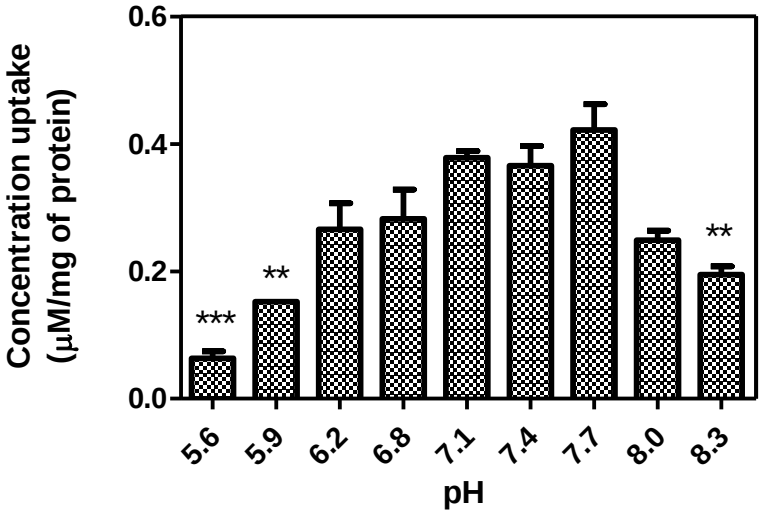

Figure 2.6: OCTN1 is pH dependent as identified through the uptake of 50 µM ET at various pH, ranging from 5.6-8.3. Graph represent means ± SEM, (n = 6), ***P*<0.01, ****P*<0.005, where statistical analysis is comparing all data to pH 7.4

2.3.2.2 Transport of ET by OCTN1

Resistance values

NCI-H441 monolayers could form polarised, electrically tight monolayers, reaching peak TEER values of 1056 ± 121 Ω×cm^2 for NCI-H441. TEER was significantly lower when cultured at an air-liquid interface. For NCI-H441 cells there was a clear peak in monolayer resistance at day 4, but no such peak was obtained for the primary cells until day 8. Primary cells cultured under AIC generated electrically tight cell layers (Figure 2.7). This observation has been previously well documented (*73*).

A) **B)**

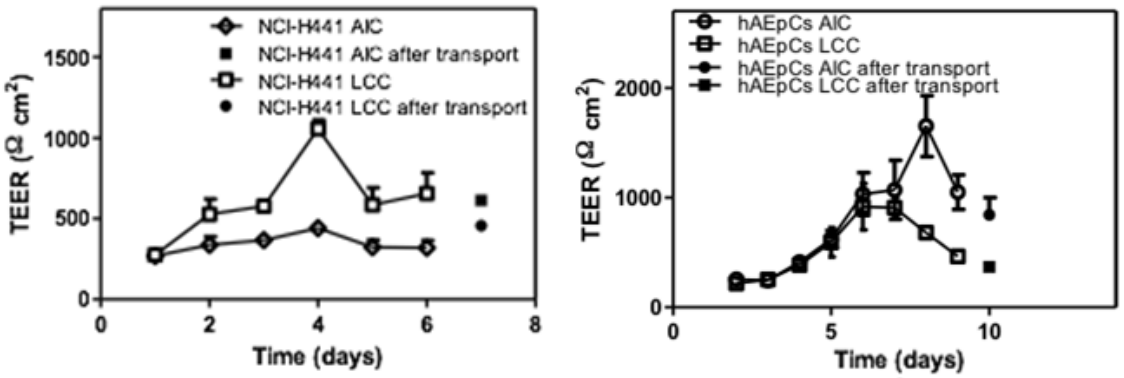

Figure 2.7: Time course of TEER development in **A)** NCI-H441 and **B)** hAEpC monolayers. Cells were seeded on Transwell Clear filter inserts (12 mm diameter with 0.4 µm pore insert, 6.5 mm diameter with 0.4 µm pore size, respectively) and grown under liquid-covered culture (LCC) or under air-interfaced culture (AIC) conditions from day 1. Each data point represents means ± SD, n = (3 – 9).

The bidirectional transport of ET across NCI-H441 bronchiolar and ATI-like epithelial cell monolayers were grown under air-interfaced (AIC) and liquid covered conditions (LCC), 6 and 9 days after seeding, respectively for NCI-H441 and ATI-like cells. At a donor concentration of 50 µM, the P_{app} from apical-to-basolateral (AB) was 8.00 ± 1.00 $\times 10^{-6}$ and 3.73 ± 0.50 $\times 10^{-6}$ cm$\times$s^{-1} for AIC and LCC, respectively in NCI-H441 cells. In comparison, the P_{app} for basolateral-to-apical (BA) transport was 10.0 ± 0.38 $\times 10^{-6}$ and 3.76 ± 0.96 $\times 10^{-6}$ cm$\times$s^{-1} for AIC and LCC, respectively (Table 2.3). Across primary cell monolayers, at a donor concentration of 50 µM, the P_{app} in the AB direction was 0.71 ± 0.24 $\times 10^{-6}$ and 0.12± 0.14 $\times 10^{-6}$ cm$\times$s^{-1} for AIC and LCC, respectively. In comparison, the P_{app} in the BA direction was 0.58 ± 0.13$\times 10^{-6}$ and 0.63 ± 0.89 $\times 10^{-6}$ cm.s^{-1} for AIC and LCC, respectively.

Table 2.3: Permeability of 50 µM ET across NCI-H441 and primary alveolar epithelium cell monolayers at 37°C for 90 min. Cells were cultured for 6 and 9 days for NCI-H441 and primary alveolar epithelium cells, respectively, on Transwell Clear inserts under air and liquid covered culture conditions. Data are represented as means ± SEM, n = 3 - 9.

	P_{app} ($\times 10^{-6}$ cm$\times$s^{-1})			
	AIC		**LCC**	
Cell type	**AB**	**BA**	**AB**	**BA**
NCI-H441	8.00 ± 1.00	10 ± 0.38	3.73 ± 0.50	3.76 ± 0.96
ATI-like cells	0.71 ± 0.24	0.58 ± 0.13	0.12 ± 0.14	0.63 ± 0.89

After 90 min of ET transport, primary and NCI-H441 cells were lysed and their intracellular ET content determined by LC-MS/MS (Figure 2.8). The uptake of ET into NCI-H441 cells in a AB direction was 0.06 ± 0.01 µM/mg protein and 0.02 ± 0.00 µM/mg protein, for AIC and LCC, respectively. In comparison, the uptake of ET in a BA direction in hAEpCs was 0.05 ± 0.01 µM/mg protein and 0.02 ± 0.01 µM/mg protein, for AIC and LCC, respectively.

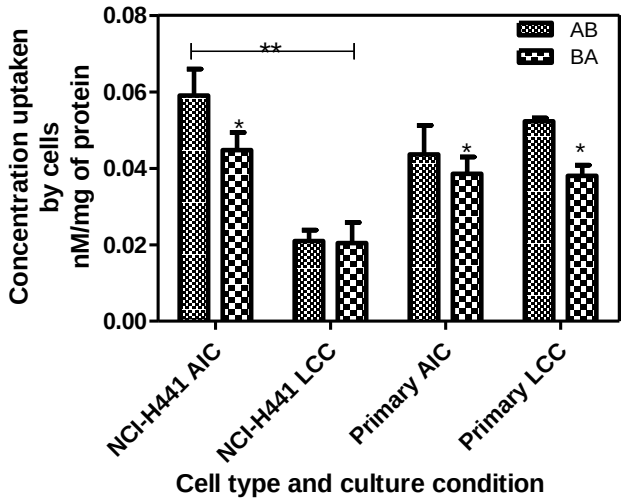

Figure 2.8: Concentration of ET uptake by OCTN1 in NCI-H441 cells and primary human alveolar epithelial cells seeded on Transwell Clear inserts and grown under AIC (A) and LCC (B) conditions for at least 6-10 days. Cells were lysed after transport studies and the intracellular accumulation of ET was quantified in NCI-H441 and primary alveolar epithelial cells. Graph shows that uptake of ET is preferential from an apical to basolateral direction in NCI-H441 cells cultured under AIC conditions and hAEpCS under both AIC and LCC conditions. Graphs represent means ± SEM, (n = 6), *P <0.05.

This study was also performed in primary alveolar epithelial cells, which yielded an uptake of 0.04 ± 0.01 µM/mg protein and 0.05 ± 0.00 µM/mg protein, for AIC and LCC, respectively. When the BA directional study was performed, an accumulation of 0.04 ± 0.01 µM/mg protein and 0.04 ± 0.00 µM/mg protein, for AIC and LCC, respectively, resulted. Regardless of cell type and cell conditions, a significantly higher uptake from to the apical side resulted ($^{*}P<0.05$).

2.3.3 The Cytoprotective Properties of ET

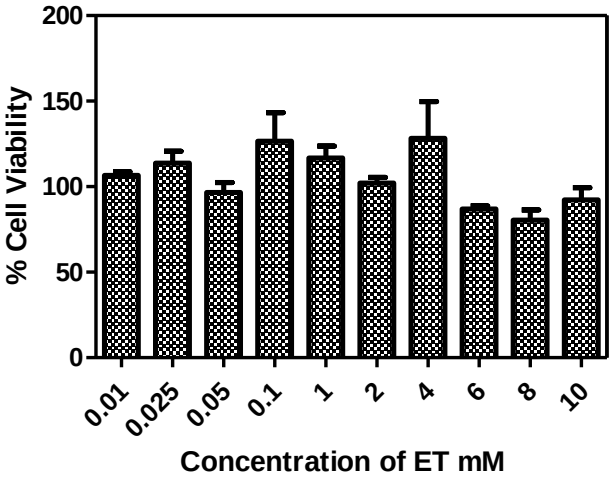

Figure 2.9: Uptake of high mM concentrations of ET was determined to have no effect on cell viability of NCI-H441 cells. Graph represents means ± SEM, (n = 6).

Cell viability of NCI-H441 cells was investigated upon exposure to mM concentrations of ET. No change in cell viability occurred upon incubation, indicating that ET does not affect cell viability but remains unchanged (Figure 2.9).

NCI-H441 cells were also incubated with 250 µM ET from day of seeding and a range of CSE concentrations incubated 24 h prior to experimentation, respectively (Figure 2.10). Cell viability was investigated and as predicted, increasing CSE concentrations causes a decline in

cell viability, by up to 50%. Upon incubation with ET from day of seeding however, a significant increase in cell viability is observed ($^{*}P < 0.05$).

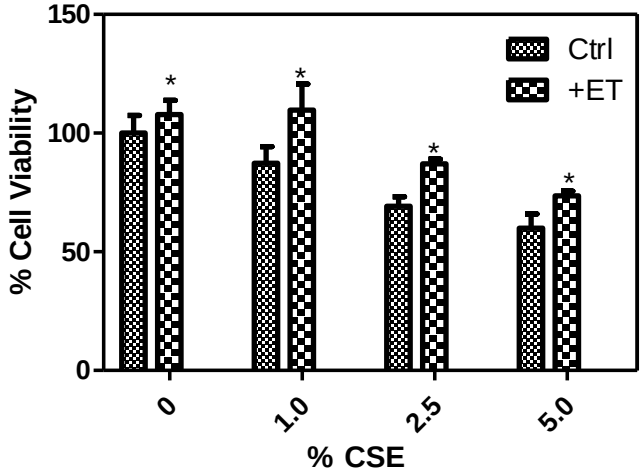

Figure 2.10: Incubation of 250 μM ET improves cell viability when incubated with various concentrations of CSE. Cell viability was assessed by Alamar Blue assay. Results are expressed as means ± SEM, (n = 9), *P<0.05

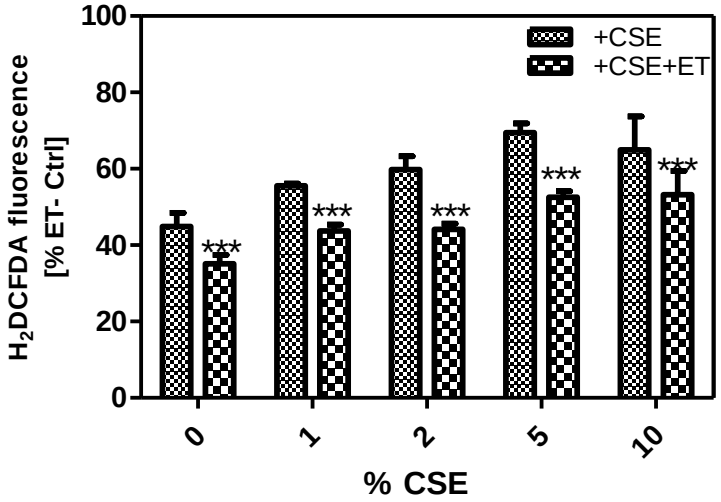

Figure 2.11: ET (250 μM) is counteractive against the production of reactive oxygen species (ROS) in the presence of CSE. ROS production was assessed by utilising dichlorofluorescein diacetate (DCFDA).Results are expressed as means ± SEM, (n = 9), ***P<0.001.

The production of ROS was also monitored in the presence and absence of CSE and ET (Figure 2.11). In a similar way, CSE lead to the increased development of intracellular ROS by up to 50%. A significant decrease in the production of ROS occurs upon incubating with ET (***$P < 0.001$).

The intracellular change in pH was also monitored over time. Within 15 min of incubating with ET, intracellular pH plateaued (Figure 2.12).

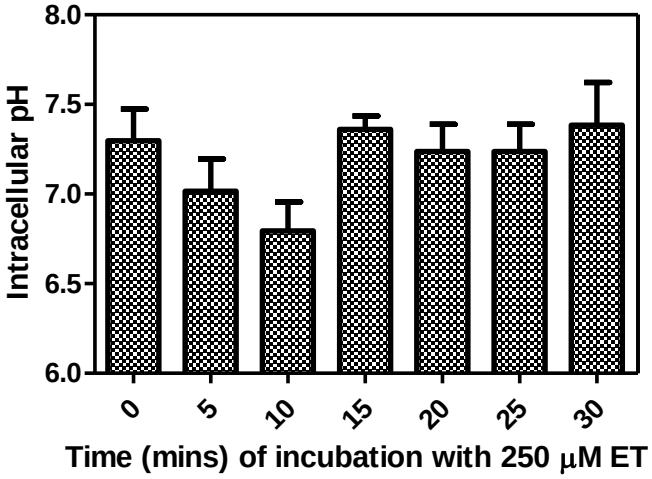

Figure 2.12: ET (250 μM) incubated changes the intracellular pH of NCI-H441 cells over time (0-30 min) , determined by use of pHrodo green dye. Graphs represent means ± SEM, (n = 6).

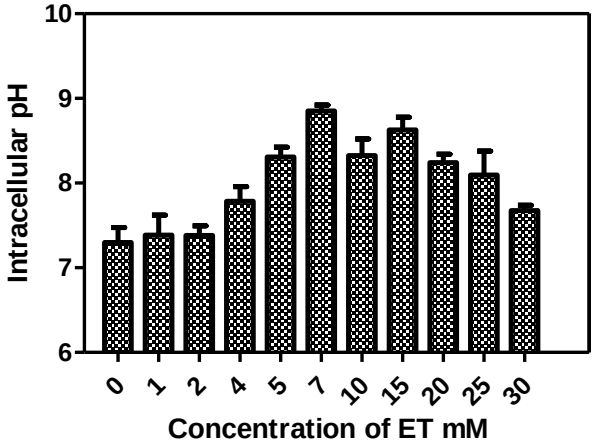

Figure 2.13: Change in intracellular pH upon incubating with a range of ET concentrations for 30 min determined by using pHrodo green dye. Graphs represent means ± SEM, (n = 6).

Upon incubating with a range of concentrations of ET, the pH gradually became basic at an ET concentration of 7 mM with higher concentrations of ET resulting in a decline of intracellular pH returning to a homoeostatic condition (Figure 2.13).

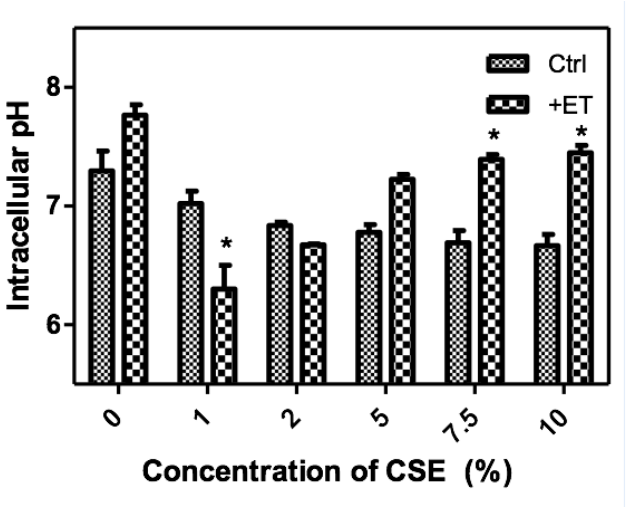

Figure 2.14: Role of ET on the intracellular pH was investigated when cells were incubated with CSE (0-10%) to determine the antioxidant potential of 250 µM ET against CSE. These data identify that incubation with ET returns the intracellular pH to baseline when incubated with CSE. Results are expressed as means ± SEM, (n = 6), *P<0.01

Further, the intracellular pH was also monitored in the presence of CSE with/without ET (Figure 2.14). Not surprisingly, the acidity of the cytosol increases with incubation of CSE. However, in the presence of ET, the acidic nature of CSE is counteracted by returning the pH to normal physiological conditions (*P<0.05)

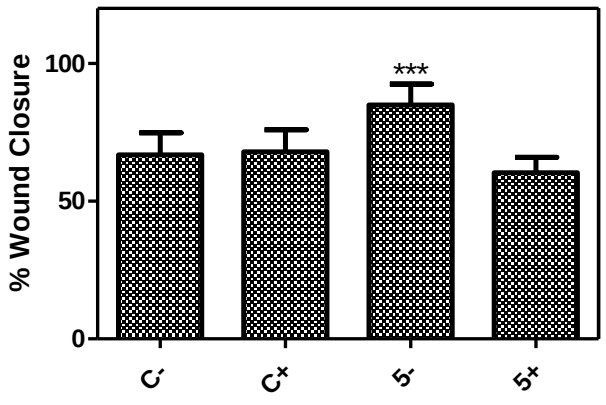

Figure 2.15: Effect of CSE on cell migration when incubated with or without ET (250 µM) after 24 h where C-: cells with no treatment, C+; cells treated with 250 µM ET, 5-; cells incubated with 5% CSE and 5+ cells incubated with 5% CSE and 250 µM ET.. Results are expressed as means ± SEM, (n = 9), ***P<0.001.

Finally, cell migration was investigated in the presence or absence of CSE and/or ET with complete wound closure occurring after 12-16 h making it unlikely that cell proliferation is occurring (Figure 2.15). No change in migration rate was observed upon treatment with ET. However, incubation with CSE caused an increase in migration rate. To determine if ET could counteract the increase in migration caused by CSE, cells were treated with both ET and CSE. A consequential decrease in cell migration occurred, corresponding to the migration rate of cells not exposed to CSE or ET.

2.4 Discussion

Sequencing of SLC22A4 in NCI-H441 cells

Literature has reported several single nucleotide polymorphisms that code for the incorrect translation of L503F (c1672t), G462E (g1531a) and T306I (c1063t), and are associated with inflammatory diseases such as Crohn's Disease, Irritable Bowel Disease, Rheumatoid Arthritis, Ulcerative Colitis, Colorectal Cancer (*47, 75-77, 89-92*). However, only the mutation L503F has been detected in the cell line NCI-H441 to date and is illustrated by Figure 2.17 (*7*). DNA from the cell line, NCI-H441, was amplified with primers specific to the individual coding exonic fragments, which were purified and sent for sequencing. Two novel mutations were detected, which to date have not been reported. Future studies should examine the functional activity, if any, of these mutations.

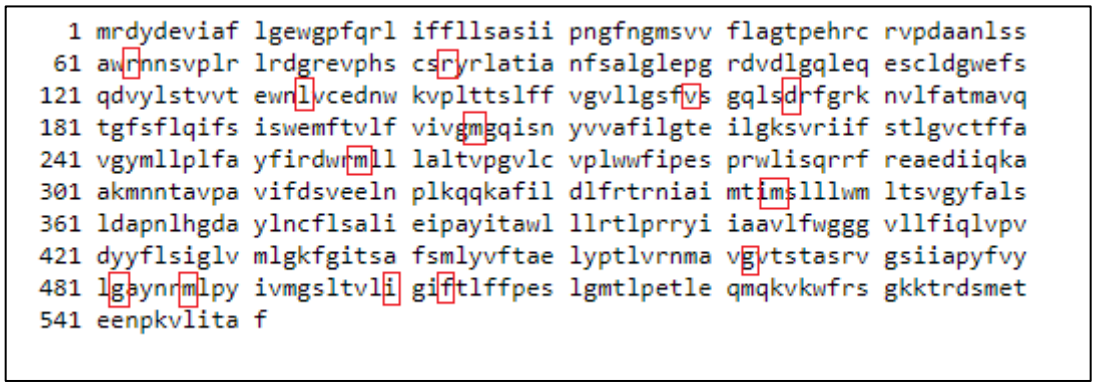

Figure 2.16: Amino acid sequence of hOCTN1 with all known single nucleotide polymorphisms highlighted.

Quantification of ET by LC-MS/MS for the characterisation of OCTN1

The transport activity of OCTN1 has previously been investigated in rat, mouse and human species. However, limited data is collected on the uptake of ET by OCTN1 as previous methods of the substrates' detection and quantification was performed by fluorescence, and

UV. These methods lack sensitivity when detecting ET and prevent accurate quantification of ET. Radiolabelled ET is also available with increased sensitivity in its detection. However, due to its unstable nature radiolabelled ET is not suitable for quantification. Only recently, the utilisation of liquid chromatography tandem mass spectrometry (LC-MS/MS) has been implemented.

Our studies have identified the active functional activity of OCTN1 in NCI-H441 revealing a K_m value of 10.30 ± 6.96 µM and a Vmax of. 0.39 ± 0.10 nmol/mg of protein. The Michaelis constant for ET uptake by the active component of OCTN1 is not reported in the literature.

Tamai *et al.* investigated mouse constructs of OCTN1 in HEK-293 cells, where they showed that uptake of TEA increased linearly for up to 10 min at which time the cells reached a point of saturation (*54*). When human OCTN1 (hOCTN1) was cloned in HEK-293 cells, uptake of TEA increased linearly for up to 5 min, after which a steady state was obtained (*46*). Our studies focused on the uptake of ET in the human distal lung cell line NCI-H441, where cells appeared to be fully saturated within 5 min of incubation with ET.

ET was quantified in NCI-H441 cells to reveal a high affinity of OCTN1 for ET (K_m = 23.39 ± 5.26 µM). These findings are similar with Gründemann *et al.* who previously quantified ET, in hOCTN1 overexpressing HEK-293 cells (K_m: 21 µmol/l), and later determined OCTN1 to have low affinity for compounds of related structure such as hercynine (EH, K_m: 1.4 mmol/l) (*52, 54, 56*). As a control for the experiment, silenced OCTN1 NCI-H441 cells were incubated with ET, and uptake experiments performed. Negligible concentrations of ET occurred in the cell, establishing that ET does not passively diffuse across the cell membrane. A Michaelis constant of 6.48 µM was obtained suggesting little amount of substrate is required for saturation of OCTN1. Gründemann *et al.* similarly investigated the uptake of ET in mock transfected HEK-293 cells and found a negligible uptake of the substrate (*47*).

The extracellular pH is an important factor to explore when investigating COPD. Patients who present with the condition, typically suffer from restrictive inhalation of oxygen and an exhalation of carbon dioxide. As a result, levels of carbon dioxide increase in the alveoli, consequently causing the pH to become more acidic. Through investigation of OCTN1, when exposed to various pH, might reveal further insight into its activity in the lung during typical hypoxic conditions of COPD patients. Previously, rat cDNA was transfected in human pigmented retinal epithelial cells (HPRE) and the uptake of TEA investigated (*56*). It was determined that the uptake of the substrate was influenced by extracellular pH. As pH changed from 6.5-8.0, uptake of TEA increased. However, as pH became acidic a reduction in uptake resulted. Our studies are in parallel with findings of Tamai *et al.* and Maegawa *et al.*(*54, 93*), where an optimal uptake at pH 7.7.occured. A significant reduction greater than pH 8.0 occurred, which could be due to initiation of cell death. Therefore, it can be concluded that OCTN1 is pH dependent and at pH 7.7, OCTN1 reaches its optimal activity.

TEER development

TEER measurements are an indicator for cell integrity by calculating the transepithelial polarity. Previous studies have demonstrated the presence of junctional proteins such as ZO-1, E-cadherin, claudin-3 to be present in the cell line NCI-H441, with confirming high TEER (around 500-1000 $\Omega \times cm^2$) (*73, 94*) indicative of a polarised cell monolayer. The bidirectional transepithelial permeability of ET across NCI-H441 cell monolayers was measured in cells grown under air-interfaced (AIC) and liquid covered culture (LCC) conditions. In Calu-3 cells, TEER values were calculated to be 3 times higher when cultured under LCC compared to AIC (*95*). However, bronchiolar epithelial cells 16HBE14o- and CFBE41o- reached TEER values of <250 $\Omega \times cm^2$ (*88, 96, 97*). Our investigation utilised the bronchiolar cell line NCI-H441 and hAEpCs. In all cell types, TEER values were able to reach values >1000 $\Omega \times cm^2$. This is in line to values detected by Salomon *et al.* (*73*). A significant decrease in TEER

values were calculated for AIC conditions compared to LCC in both cell types. Similar to previous findings where TEER values were determined to be 3 times lower in AIC than LCC in Calu-3 cultured cells (*95*).

Transport activity of OCTN1

To further explore the proposal of apical localisation of OCTN1, transport studies of ET in absorptive and secretive direction were performed.

The permeability coefficient P_{app} was calculated in all transport studies. From this analysis, it was identified that in NCI-H441 cells and hAEpCs, P_{app} values were statistically higher for both AB and BA under AIC than LCC grown cells. This correlates to previous studies which investigated the paracellular transport of fluorescein, whereby they concluded that a leakiness in the integrity of the cell membrane may be occurring under AIC conditions in the cell line NCI-H441 (*73*).

Further, ET transport across NCI-H441 cells showed slightly but not significant secretory direction (BA). In hAEpCs, a slight increase is observed in a BA direction only under AIC conditions. These findings are similar with findings of Salomon *et al.* where the uptake of TEA in NCI-H441 was investigated to reveal a net secretion of TEA (*73*). In comparison, hAEpCs under LCC conditions, a preference for BA transport is observed. However, only one patient was isolated for hAEpCs and so further analysis should be performed on a greater sample of primary cells.

After the bidirectional transport of ET was performed, intracellular concentration of ET was investigated. A significantly higher accumulation of ET occurred in NCI-H441 cells when cultured under AIC conditions. Little research has been done to date on the expression of OCTN1 under these culture conditions with only Horvath *et al.* confirming expression of the transport under AIC to be identical to freshly isolated lung epithelium (*60*), with no comparison made to OCTN1 expression under LCC conditions. Data carried out by our

research group investigated the expression of OCTN1 under AIC and LCC conditions by Western blot, and revealed a slightly higher expression of the transporter in NCI-H441 cells, which could explain the higher uptake of ET under AIC conditions. Regardless, this could also be due to leakiness in cellular membrane as demonstrated by the uptake of fluorescein (*73*). Therefore, a need for further investigation into the expression of OCTN1 under AIC and LCC is required.

When absorption and secretory transport of ET was investigated a significant increase in the uptake of ET from AB was determined under AIC conditions, which favours the expression of OCTN1 to the apical membrane of the cell. No such significant difference was observed under LCC conditions. These data compare to conclusions established by Horvath *et al.* who detected expression of the protein on the apical membrane of bronchial epithelia by immunofluorescence (*60*). However, uptake is still occurring from BA, which could suggest that expression of the transporter is present on the basolateral membrane to a lower extent. Alternatively, from the P_{app} data collected, paracellular transport of ET could be occurring to returning the substrate to the apical side for uptake. A study carried out by Busche *et al.* investigated the permeability properties of apical and basolateral membranes in intestinal epithelium. It was revealed that permeability was significantly lower in apical membranes than basolateral membranes (*98*)**.** These data were supported by regulation of internal pH with absorptive treatment of small chain fatty acids having a minor change to intracellular pH but a pronounced effect to intracellular pH when treated in a BA direction (*98*). They concluded that the apical membranes provide a significant barrier to diffusion of molecules (*98*). From the transport data obtained in this study, a preference for ET uptake in an AB direction is indicated, suggesting that OCTN1 is localised to the apical membranes. However, with the lack of a suitable antibody for OCTN1, confocal and immunostaining remain inconclusive for the determination of OCTN1 localisation.

The molecular actions of ET in NCI-H441 cells

The effect of high concentration of ET incubation on lung epithelial cells in the presence of CSE was investigated. Cell viability remained unaffected by mM concentrations of ET. Similar to findings by Aruoma *et al*. who incubated human neuronal hybridoma cells with up to 5 mM concentrations of ET and found no change in cell viability (*99*)**.**

Cytoprotective properties of ET

The cytotoxic effects of CSE is widely studied in primary human small airway epithelial cells, transformed human cells (A549, NCI-H1299, NCI-H441), and rodent cells (murine, MLE15 and rat L2). A range of CSE (0.2%-10%) was explored for 24 h at 37°C. At 5% CSE, cell viability was 70% (NCI-H1299), 61% (A549), 39% (NCI-H441), 30% (L2) and 17% (MLE15) with cell type in parenthesis. In all cases necrosis occurred (*100*)**.** Although the mechanism of cell death is not explored in this research, it was calculated that 50% cell death resulted, when incubated with 5% CSE. The role of the antioxidant ET on cell viability was investigated as it has previously been reported to protect against apoptosis (*84, 101*). A subsequent significant increase in cell viability against the cytotoxic effects of CSE resulted suggesting ET to protect against apoptosis and necrosis.

Contribution of ET to the production of ROS

CSE contains a plethora of oxidising species (*102*). These species are capable of entering deep within the lung to cause oxidative damage to DNA, lipids membranes, proteins etc. (*16*). A study performed on A549 cells in the presence of CSE for 4 h, caused a dose dependent increase in intracellular levels of ROS (*103*)**.** Our studies correlate to these findings by identifying a significant increase of 50% in the levels of ROS when incubated with up to 5% CSE. ET is well documented as a powerful free radical scavenger and so, the antioxidant potential of ET against CSE generating ROS, was investigated and found to significantly supress ROS production. This is comparable with a study performed on human brain

microvascular endothelial cells, where ET significantly reduced ROS induced by pyrogallol, xanthine oxidase and high glucose concentrations (*104*). And so, there is striking evidence to suggest that ET protects against cell death by reducing the level of ROS *in vitro.*

The effect of ET on intracellular pH

The effect of ET on the intracellular pH was also investigated. Within 15 min of incubation, the cell reaches a steady state of pH, i.e. 7.4 ± 0.24. However, upon incubating with various concentrations of ET, the acidity/basicity varies. This is puzzling as no corresponding decrease in cell viability occurred. Therefore, if time permitted it could be of worth to investigate the effect of ET on markers of apoptosis or necrosis for example. Incubation of ET appears to stabilise the intracellular pH upon incubating with 5% CSE.

Therefore, a plausible method of protection against CSE by ET could be through the reduction of ROS and the neutralising effect on the intracellular pH.

ET's role in cell migration.

An increase rate in cell migration has been established in COPD sufferers by utilising the cell line, A549, and subjected to serum isolated from COPD patients (*105*). However, much debate circulates whether CSE is responsible for this change.

Studies performed in human bronchial smooth muscle cells and mesenchymal cells have suggested that CSE causes a reduction in cell migration (*106*). In comparison, a study performed in vascular smooth muscle cells stimulated a promotion in the migration rate (*107-109*). Our studies investigated the effect of 5% CSE in NCI-H441 cells and quantified an increase in cell migration.

The human lung carcinoma NCI-H460 was incubated with hydrogen peroxide and a decrease in cell migration resulted, which was counteracted upon addition of catalase, a free radical scavenger (*110*). In comparison, ROS has been found to be directly involved in the activation of Src (*111*). Src is an important regulator of cellular processes such as cytoskeletal

organisation, cell-cell contact and cell matrix adhesions. Upon activation of Src initiation of epithelial mesenchymal transition can occur leading to an increased capacity for migration.

The contribution of pH to cell migration in human primary keratinocytes and fibroblasts, revealed a deceleration in cell migration in acidic or alkaline environments (*112*). The exact mechanism of action of CSE remains unknown and further efforts are required to elucidate this role, which is beyond the scope of this research.

Regardless, upon incubation with the antioxidant ET, cell migration returned to the baseline. It could be explained that neutralising ROS by ET, prevents the activation of Src and hence prevents accelerated cell migration. Further investigation is required to confirm this hypothesis.

2.5 Conclusions

The aims of this research was to identify the functional activity of OCTN1 in the cell line NCI-H441.Two novel SNPs associated with OCTN1 in the cell line were detected. However, their impact on OCTN1 function and/or activity remains unknown. Our findings confirm OCTN1 to be temperature and pH dependent. Activity of OCTN1 in lung epithelium was determined by uptake and transport studies and were confirmed to be similar to data already collected for OCTN1 in liver cells. There is a suggestion for localisation of the transporter on the apical membrane, however, further evidence is required to confirm this. Following findings previously established by Reynolds *et al.*, we can hypothesise that OCTN1 carries out its protective properties via the uptake of ET and its counteractive ability against ROS through the stabilisation of intracellular pH.

Chapter 3

Characterisation of OCTN1 in patients with COPD

Abstract

The association between OCTN1 and inflammatory lung diseases remains unclear. This study aims to quantify *SLC22A4* gene expression in the bronchial epithelium of patients with COPD and healthy controls undergoing bronchoscopy. Non-smokers were removed from this analysis as it is believed that these patients may be biased to alpha-1-anti trypsin. An increase in the expression of *SLC22A4* in elderly patients with COPD was observed ($P = 0.19$). No difference in expression was determined between the two genders. Patients suffering from COPD had an increased expression of *SLC22A4*, with this increase exacerbated in those who were cachectic or obese ($P = 0.07$). Current smokers, and those who smoke/smoked greater than 21 pack years, expressed higher levels of mRNA ($P = 0.06$). Finally, a significant increase in expression was observed in patients with low lung capacity. Therefore, OCTN1 expression is associated with the pathogenesis of COPD and may be linked to its development.

3.1 Introduction

Membrane transporters are key determinants in drug uptake, metabolism and elimination, which in unison play a protective role in the cell. OCTN1 encoded by the gene *SLC22A4*, is responsible for the uptake of ET, a potent antioxidant (*47*).

SLC22A4 and its association with inflammatory diseases is investigated as the loci of *SLC22A4* at 5q31.1 lies immediately adjacent to a locus linked to Crohn's Disease (CD). However, controversial reports have been published favouring and disfavouring an association with *SLC22A4* and inflammatory diseases. The SNP rs1050152 (1672C-T) responsible for the missense of L503F on exon 9 has been associated with an increase susceptibility to CD in German, Swedish, Hungarian and Chinese Han populations (*113-116*). Similarly, L503F has also been associated with an increase risk in development of Tuberculosis in Japanese (*117*) and Inflammatory Bowel Disease (IBD) in Scandinavian populations (*118*). This association of L503F with IBD was also confirmed in Western populations (*119*). However the same study concluded that no such association may occur in Chinese (*119*). Further, it was reported that L503F is not a risk factor in Hungarians suffering from IBD, CD and Ulcerative Colitis (*120*), with a study performed in the Flemish population suggesting that the SNP did not change the susceptibility to CD but simply altered the phenotypic expression of the disease (*121*).

The causative role of L503F for an increase susceptibility to CD in Scottish individuals was investigated by Nobel *et al.* (*122*). However, no definitive conclusion was presented. Toh *et al.* identified 8 additional SNPs in Chinese and Indian populations of Singapore (*77*). Here, the impact of these SNPs on the function of hOCTN1 in transfected HEK293 cells was investigated. By utilising secondary protein structure software TOPO2, the transporter function was predicted. It was determined that the SNPs, R63H, R83P, G482D and I500N resulted in an impairment of transporter activity. The SNPs R63H and R83P are located in the

N-glycosylation site of the large extracellular loop and therefore responsible for the regulation of plasma membrane orientation. G482D is located in the small loop between transmembrane 11-12 and I500N in addition to L503F detected in the 12th transmembrane loop.

To date reports have determined the localisation of OCTN1 within lung tissue, with highest expression in the central lung and lower expression in the peripheral lung (*60, 123*). Their results indicated that no change in expression was detected in either central or peripheral lung of severe COPD patients in comparison to healthy controls (*123*). However, it was also determined that an increase in the expression of OCTN1 in cells of the lung of patients suffering from severe COPD (*123*)**.** Hence, data surrounding the expression of OCTN1 with regards to its localisation in the lung and the severity of COPD remain conflicting. Therefore, a collaboration with the University Medical Center Groningen has investigated the expression of *SLC22A4* in COPD patients compared to non-COPD patients in nasal, bronchial and lung epithelium. It was determined that no difference in expression of the gene occurred in nasal epithelium, whereas a significant decreased expression occurred in bronchial epithelium and a significant increased expression in lung parenchyma of patients with mild and moderate COPD. Further, the University Medical Centre further identified rs1050152, the SNP coding for L503F, as an expression quantitation loci for *SLC22A4 (*Refer to abstract of this thesis). Although, the causative role of this SNP remains nebulous Tahara *et al.* did report no change in the activity of the protein when expressing the 503F haplotype (*124*), with Peleketova *et al.* reporting a decrease in the levels of carnitine uptake of fibroblastic cells expressing 503F than 503L (*125*). No reports have yet been made to support this finding with regards to expression of *SLC22A4.*

COPD patients exhibit an irreversible expiratory airflow limitation and so diagnosis is established by pulmonary functional tests (PFTs), which measures the forced expiratory

volume (FEV_1) and the forced volume capacity (FVC) of an individual. The Global Initiative for Obstructive Lung Disease (GOLD) classifies the severity of COPD based on these two parameters and are illustrated in Table 3.1.

Table 3.1: GOLD standard criteria for the severity of COPD (*2*).

Stage	**Severity**	**FEV_1/FVC**	**FEV_1 %**
1	Mild	<0.7	≥80
2	Moderate	<0.7	50-79
3	Severe	<0.7	30-49
4	Very Severe	<0.7	<29

Many age associated changes occur in the respiratory system, resulting in decrease FEV_1 and FVC (*126*, *127*). And so, it was important to investigate if age was directly responsible for an emphysema phenotype. Senescence accelerated mice (SAM) were utilised as models for a study by Fukuchi *et al.* in which they demonstrated an enlargement in the alveoli of senile mice, without any wall destruction, a characteristic of emphysema (*128*). This contributed to the observed decrease in FEV_1/FVC. Upon incubation of tobacco smoke, both alveolar enlargement and wall destruction resulted. These findings suggested that age only increases the susceptibility of the lung to external insult and therefore, increases the risk of COPD development. However, it remains unclear if this increase risk is universal or if a genetic factor plays a major role.

The influence of gender on COPD has also received little attention. Men and women have been suggested to respond phenotypically different to tobacco smoke (*129*), with men more

likely to develop an emphysematous phenotype than females and females more likely to develop an airway predominant phenotype (*129, 130*). Although more males are diagnosed than females, the COPD-related mortality in women, caused by COPD, is higher (*129, 131, 132*). Females tend to be younger and suffer from more dyspnoea, more severe bronchial obstruction, and more exacerbations (*133*). Although the reason for this observation remains unknown, these studies concluded that women may be at a greater risk of smoking induced lung function impairments.

Body mass index (BMI) allows the estimate of body adiposity and has been found to contribute to a functional lung capacity (*134*). From a study of 1664 patients, it was revealed that very obese and cachectic individuals had a decreased functional lung capacity than those of normal weight. Unfortunately, this study was not segregated for smokers and non-smokers. It was known at the time of the study that more cachectic patients were smokers than those of normal and obese patients, and so the results may be biased to tobacco smoke exposure. Regardless, no plausible evidence has yet emerged for this result but it is hypothesised that in subjects with low BMI, air becomes trapped and hyperinflation can occur (*134*). In comparison, the weight of the very obese individuals may be the cause of impairment on ventilatory and bodily functions.

It has been well established that tobacco smoke is the major risk factor of COPD. However, little is known about the effect of length and amount of smoking. In 2013, a study was performed on 139 patients in which sputum production and chronic cough were investigated in smokers, categorised by pack years (*135*). The study demonstrated that smokers of less than 10 pack years and greater than 10 pack years had a 19% and 35% risk of increase sputum production, respectively. It was also identified that 42% and 77% of smokers of less than 5 pack years and greater than 50 pack years, respectively, had a chronic cough. Liu *et al.* further determined a positive linear relationship between smoking duration and the severity of

COPD (*132*), consistent with findings established by a Norwegian study nearly 20 years previous (*136, 137*). However, in the same study Liu *et al.*, identified that the prevalence of COPD was lower in former smokers who quit more than 10 years ago (*132*).

In summary, COPD is a complex disease, effected by an array of key features. There is evidence to suggest a genetic factor may be responsible for an increase in susceptibility to COPD. To date, little is known about the expression of OCTN1 under varying conditions like age, weight and sex and if there is a correlation between these factors. And so, this research aims to quantify the expression of the transporter, in patients of varying lifestyles and to identify if OCTN1 does play a role in the pathogenesis of this disorder.

3.2. Materials and Methods

Patient samples were provided from bronchial epithelium of COPD sufferers at the time of their bronchoscopy. All patients fulfilled the criteria of the lung disease declaration established by St. James' Hospital. Written informed consent was obtained from all participants. This study was approved by the local ethical committee. Bronchial epithelial cells were removed from the cytology brush by forceful pipetting and centrifuged at 17,000x*g* for 5 min at 4°C. The supernatant was removed and 500 µl of Tri-Reagent was added to the cell pellet and incubated at room temperature for 5 min.

3.2.1 Quantification of SLC22A4 expression

Total RNA isolation

One-hundred microlitres of chloroform (Sigma-Aldrich) was then added. The tube was inverted several times and allowed to rest for 15 min before centrifuging at 12,000x*g* for 15 min at 4°C. The top layer was transferred to a new nuclease free tube and 0.8 µl of glycogen from oyster (Fischer Scientific Ltd, Dublin, Ireland) was added to trap the nucleic acid. Two hundred and fifty microliters of isopropanol (Sigma Aldrich) was added to the tube and the sample was centrifuged at 12,000x*g* for 15 min at 4°C. The supernatant was completely removed to reveal a small white pellet, which was later washed with 500 µl of 75% ethanol (Sigma-Aldrich), followed by gentle vortexing and a final centrifugation step at 7,500x*g* for 5 min at 4°C. The supernatant was completely removed and the pellet was allowed to dry at room temperature.

Fifty microlitres of nuclease free water (ThermoFischer Scientific) was added to dissolve the RNA pellet. The RNA solution can be used immediately or stored at -80°C.

RNA quantification

The isolated RNA from each sample was quantified using a NanoDrop ND-1000 spectrophotometer (Fischer Scientific Ireland Ltd, Dublin, Ireland) and ND-1000 software.

The optical surfaces of the instrument were cleaned with RNA free wipes and it was initialised using nuclease free water. The NanoDrop was then blanked using the elution solution. Each sample is measured by loading 1 µl onto the lower optical platform and lowering the arm gently. The surfaces were wiped clean between each measurement. The RNA concentration was automatically calculated by the software from the absorbance at 260 nm and given as ng/µl. Purity of the sample was primarily assessed by the 260/280 ratio which was again automatically calculated by the software and should be approximately 2. A further measure of purity was the 260/230 ratio which should be approximately 2.0-2.2. These ratios serves as a rule of thumb for purity assessment. All samples were diluted to 1 µl/10µl with nuclease free water.

PCR Amplification

Real-time PCR (qPCR) was performed on 96 fast well plates according to Applied Biosystems' protocol. A total volume of a 10 µl was required and prepared as described in Table 3.2, using ViiA ™ 7 Real-Time PCR System.

Table 3.2: SYBR green reagents and proportions used in preparation for PCR

Component	Quantity per well (µL)
RT-PCR Master Mix	5
Forward primer	0.1
Reverse primer	0.1
Quantifast RT-Mix	0.1
RNA	Variable
Water	Variable
Total	**10**

The thermal cycler conditions consisted of an initial denaturation at 50°C for 5min and 95°C for 10 min (Hold Stage); 40 cycles at 95°C for 10 s and annealing at 60°C for 30 s (PCR Stage); dissociation curve analysis of 15 s at 95°C, 1 min at 60°C and finally 15 s at 95°C (Melt curve stage). All samples were analysed in triplicate and threshold cycles were calculated by instrument's software and normalised to β-actin:

$$\Delta C_t = C_{t\ \text{target gene}} - C_{t\ \text{ACTB}}$$

Relative gene expression levels were calculated as follows:

$$R = 2^{-\Delta CT} \qquad \text{Equation 3.1}$$

Table 3.3: Primer Sequences of OCTN1 for PCR

Primer	**Gene**		**Sequence**	**Size (bp)**	**Gen Bank Accession No.**
OCTN1	SLC22A4	Forw	CTG AGA ACG CTG TCA TCA CC	182	NM_003059
		Rev	GCC AGG AAC ACG ACT GAC AT		

3.2.2 Data Analysis

Results are expressed as means ± SEM. BMI is categorised into healthy weight i.e. 18.5-25 kg/m^2. All other weight is determined to be unhealthy for this analysis. The data were analysed by GraphPad Prism (La Jolla, CA) using Mann Whitney or Kruskal-Wallis test followed by Dunn multiple comparison test, and Minitab statistical package (State College, PA) using Two-way ANOVA followed by Bonferroni multiple test comparison, where appropriate. *P< 0.05 was considered statistically significant.

3.3. Results

3.3.1. RNA Purity

All RNA obtained for these studies were of good quality as illustrated by Table 3.4:

Table 3.4: RNA purity determination and quantification by Nanodrop 1000 given as an average reading of 9.

Sample	Average A260/230	Average A260/280	Average ng/µL
SJHBAL300	2.07	1.87	187.7
SJHBAL302	2.05	1.85	55.8
SJHBAL305	2.07	1.87	73.6
SJHBAL306	2.05	1.85	147.5
SJHBAL309	2.04	1.84	692.3
SJHBAL310	2.07	1.86	376.6
SJHBAL313	2.06	1.86	1002.6
SJHBAL314	2.08	1.88	773.4
SJHBAL315	2.06	1.86	54.1
SJHBAL316	2.07	1.87	96.5
SJHBAL317	2.09	1.89	354.4
SJHBAL318	2.07	1.87	348.9
SJHBAL320	2.08	1.88	207.4
SJHBAL323	2.09	1.89	262.8
SJHBAL331	2.07	1.87	205.7
SJHBAL335	2.07	1.87	259.7
SJHBAL336	2.06	1.86	576
SJHBAL338	2.05	1.85	444.1
SJHBAL339	2.05	1.85	382.8
SJHBAL340	2.08	1.88	444.2
SJHBAL342	2.07	1.87	359.5
SJHBAL343	2.05	1.85	286.5
SJHBAL344	2.06	1.87	132.6
SJHBAL345	2.03	1.83	341.6
SJHBAL346	2.07	1.87	268.1
SJHBAL347	2.07	1.87	265.6
SJHBAL348	2.05	1.85	278.4
SJHBAL349	2.03	1.83	314.8

RNA purity was determined by the $\frac{260}{230}$ and $\frac{260}{280}$ ratios. The $\frac{260}{280}$ can indicate if there is a contaminationwith residual phenol, guanidine or other extraction reagents. This value should be approximately 1.8 to represent pure RNA.The $\frac{260}{230}$ is a secondary measure which should be between 2.0-2.2. Abnormal values to this ratio may indicate a problem with the extraction protocol or the sample.

3.3.2. Patient characteristics

Smokers and ex-smokers were recruited when attending the bronchoscopy clinic at St. James' Hospital in order to quantify the gene expression of *SLC22A4*, which codes for the protein OCTN1 in patients suffering from COPD. Table 3.5 shows the clinical characteristics of patients recruited.

Table 3.5: Clinical characteristics of COPD patients recruited

	Bronchial Brushings of patients			
	Clinically diagnosed with COPD (*n*=10)		**Not clinically diagnosed with COPD (*n*=11)**	
	Characteristics	**Significance (*P* value)**	**Characteristics**	**Significance (*P* value)**
Age, years	57.00 ± 9	0.91	57.00 ± 11.59	0.19
Gender, male	6 (60%)	0.61	7 (64%)	0.86
BMI	26.71 ± 5.71	0.73	27.21 ± 7.05	0.07
Smoking status				
Current smokers, *n*	4 (40%)	0.61	4 (46%)	0.22
Ex-smokers, *n*	6 (60%)	0.61	7 (64%)	0.22

Pack years	23.90 ± 16.66	0.84	24.25 ± 14.34	0.06
FEV_1/FVC %	60.35 ± 9.67	0.02	84.25 ± 8.09	NA

Table 3.5 demonstrates that all patients in this study were of a similar age, independent of COPD diagnosis. The majority of patients recruited were male. In combination, most of the patients were ex-smokers and at least 5 months off cigarettes. Smokers and ex-smokers shared a history of 23.90 ± 16.66 and 24.25 ± 14.34 pack years for patients diagnosed with COPD and those who were not, respectively. Patients diagnosed with COPD had a much lower FEV_1/FVC % than those that did not, imperative for their diagnosis.

3.3.3 Gene Expression of *SLC22A4* in healthy and COPD patients.

Gene Expression was calculated as relative expression levels i.e. $2^{\Delta\text{-CT}}$, where the cycle thresholds (CT), values were calculated from QuantiStudio™ Real Time PCR Software v1.1 as illustrated by the PCR trace shown in Figure 3.1.

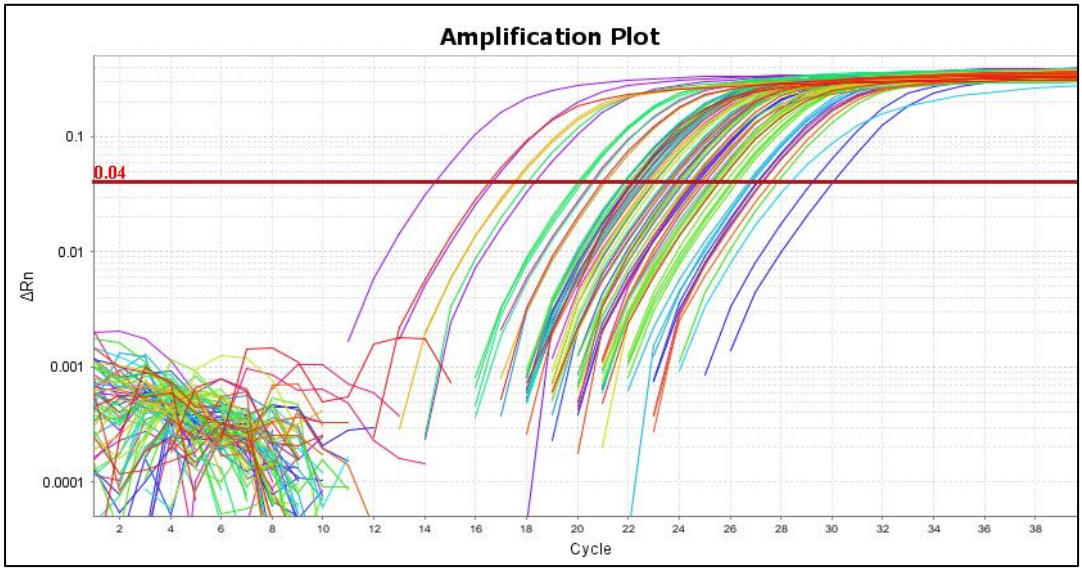

Figure 3.1: Amplification plot of patient samples revealing their cycle of threshold (CT) values using the QuantiStudio™ Real Time PCR Software v1.1.

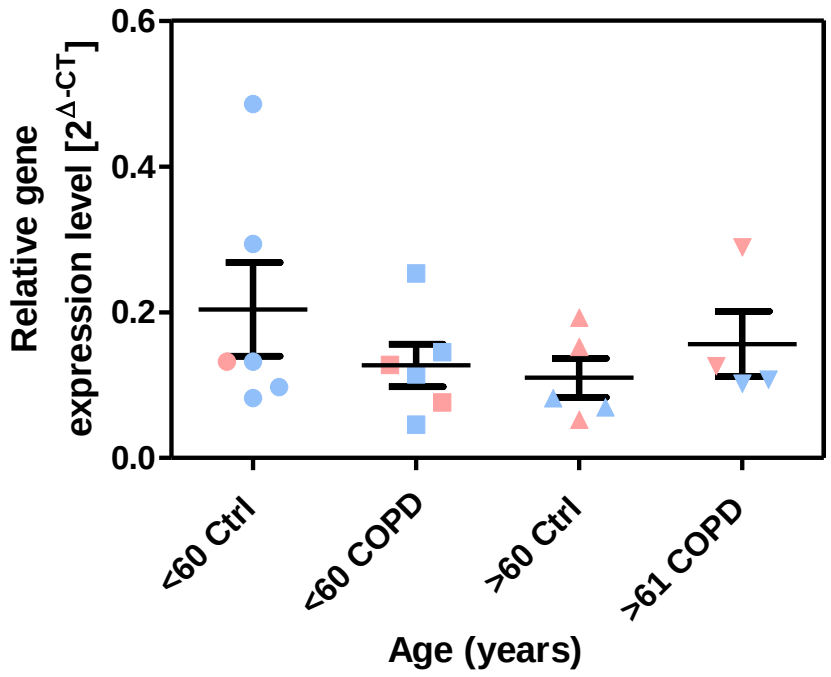

Figure 3.2: *SLC22A4* expression in bronchiolar epithelium of aged patients <60 years or >60 years) with/without COPD. Gene expression of the transporter appears to decrease with age in healthy individuals, however, an increase occurs with age in COPD patients. Data are presented as means ± SEM, (*n* = 20). Blue = male, female = pink.

As in Figure 3.2, *SLC22A4* gene expression appears to decrease with age. However, in sufferers of COPD, this increase in expression is reverted to an increase in expression with age. Men and female appear to be dispersed equally in the study.

No such difference in expression of *SLC22A4* occurs between males and females (Figure 3.3). An increase in expression occurs in female patients with COPD, whereas a decrease occurs in the expression of the gene in male patients with COPD compared to the control groups.

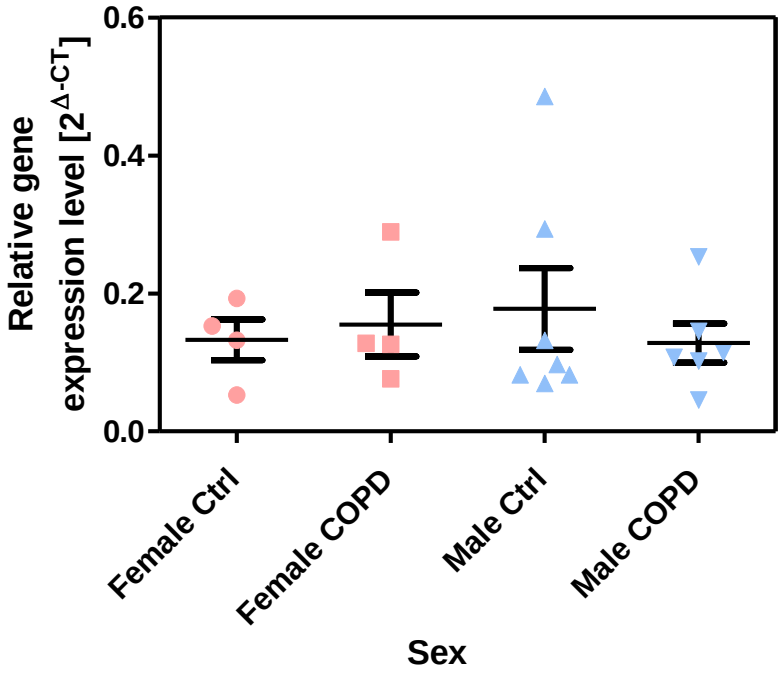

Figure 3.3: *SLC22A4* expression in bronchiolar epithelium of male and female patients with/without COPD. No trend is observed for expression of the gene in males or females. Data are presented as means ± SEM, (*n* = 20). Blue = male, female = pink.

The gene expression of the transporter was also characterised with regards to BMI (Figure 3.4). Patients with unhealthy BMI, i.e. <18.5 and >24.9, had an increased expression of *SLC22A4*, with the majority of patients being female. This increase in expression was further enhanced in patients with COPD.

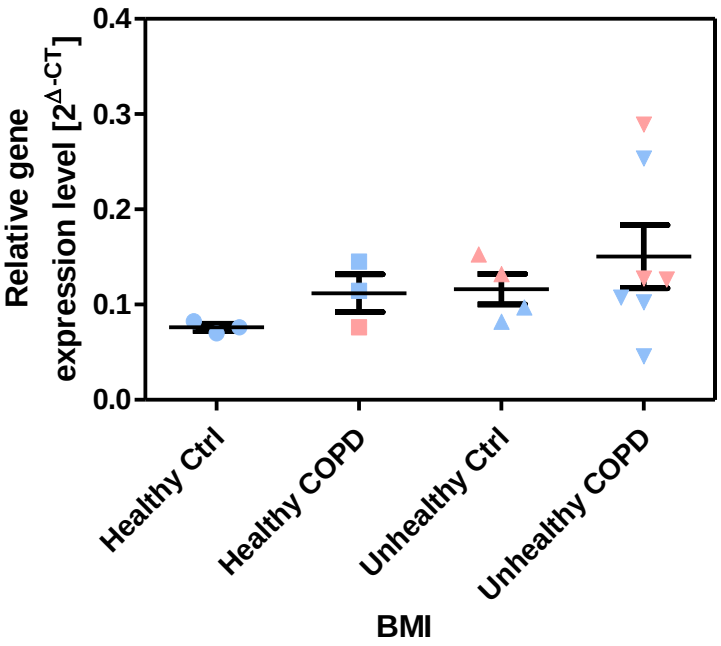

Figure 3.4: *SLC22A4* expression in bronchiolar epithelium categorised for BMI in patients with/without COPD, where healthy is a BMI of 18.5-24.9 an unhealthy BMI is <18.5 or >24.9. This data indicates that higher expression of *SLC22A4* occurs in patients who have a unhealthy BMI or suffer from COPD.Data are presented as means ± SEM, (*n* = 20). Blue = male, female = pink.

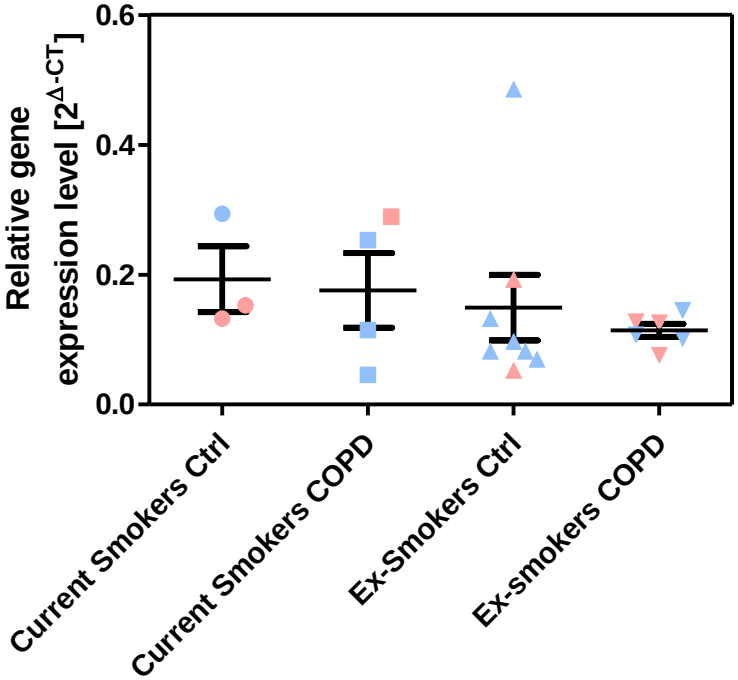

Figure 3.5: The smoking history of patients with/without COPD with reference to gene expression of *SLC22A4* expression in bronchiolar epithelium, where ctrl= healthy patients and COPD= COPD sufferers. These data suggest that ex-smokers tend have a lower expression of the *SLC22A4* gene compared to current smokers. Data are presented as means ± SEM, (*n* = 20). Blue = male, female = pink.

Both control and COPD groups illustrate an increase expression of *SLC22A4* in current smokers compared to ex-smokers. However, in patients with COPD this expression is slightly and non-significantly reduced compared to the control group (Figure 3.5).

Pack years were also investigated for the expression of *SLC22A4* in patients with COPD (Figure 3.6). An increase in expression of the gene is observed correlating with pack years. No difference in expression is observed in control and COPD groups when patients were of less than 20 pack years. However, in smokers of greater than 21 pack years a decrease in expression of the gene is observed. The majority of females had a pack year history of less than 20 but still suffered from the condition.

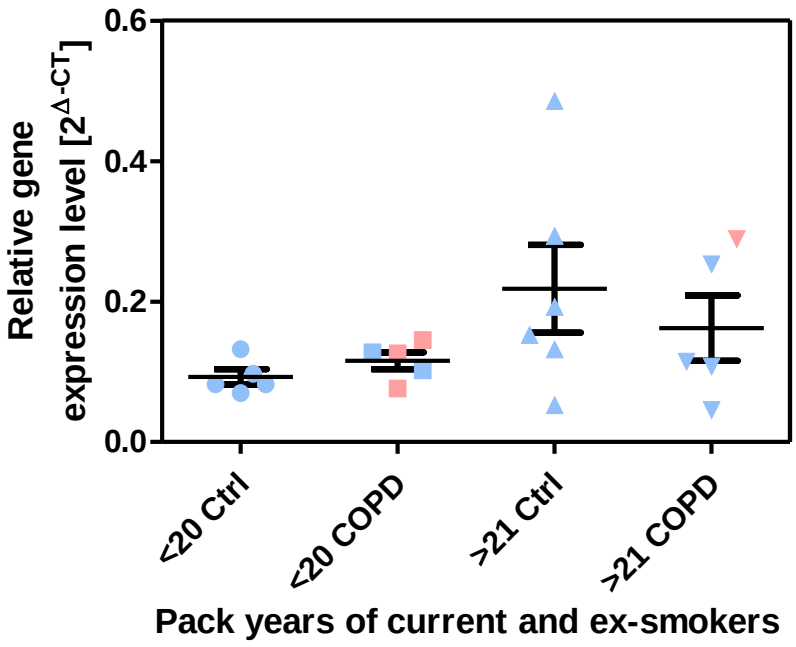

Figure 3.6: The pack year history of current and ex-smokers in patients with/without COPD was investigated for gene expression of *SLC22A4* expression in bronchiolar epithelium. Individuals who smoked more tended to have an increase in expression of *SLC22A4* with this increase attenuated in patients suffering from COPD. Data are presented as means ± SEM, (n = 20). Blue = male, female = pink.

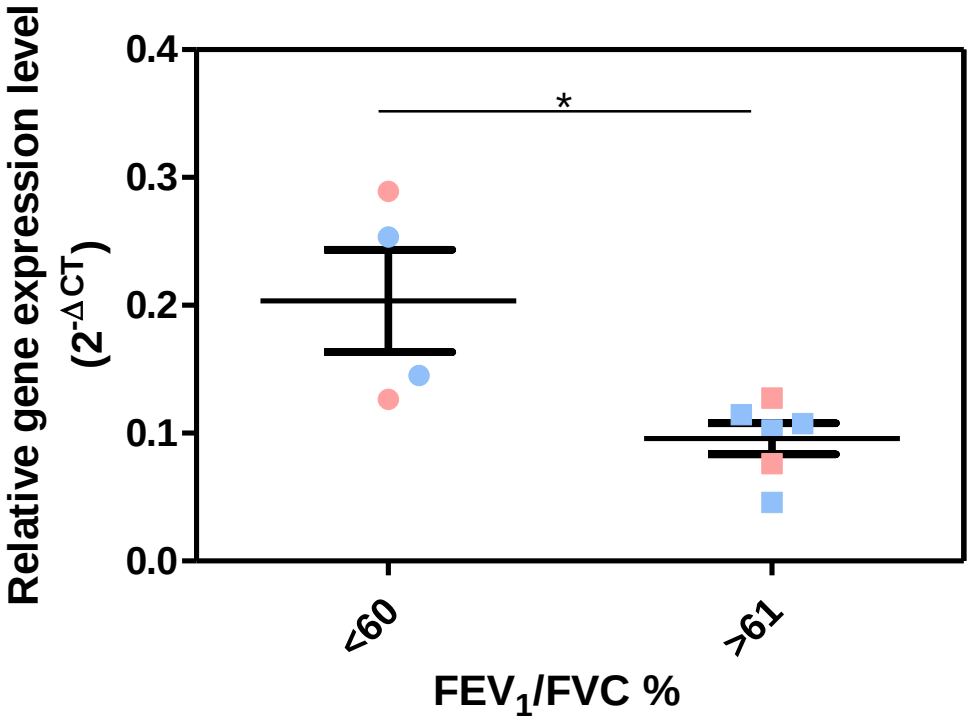

Figure 3.7: The expression of OCTN1 in patients with decreasing lung function as displayed by FEV_1/FVC was investigated. A significant increase in expression of *SLC22A4* occurs in patients whose lung function is less than 60 FEV_1/FVC%. Data are presented as means ± SEM, (*n* = 20). Blue = male, female = pink *P<0.05.

The expression of *SLC22A4* was characterised by FEV_1/FVC % in patients suffering from COPD (Figure 3.7). The expression of the transported was significantly lower in patients with FEV_1/FVC of greater than 61% and is displayed by Figure 3.6. Females were equally spread across the two groups.

The expression of *SLC22A4* was further explored with regard to smoking history and lung function to determine whether a correlation existed (Figure 3.7). Although no significance was detected due to the small sample size there is a strong suggestion present that current smokers with reduced lung function i.e. 60% has higher expression of the gene transcript in comparison to those of improved lung function (both ex and current) but also patients with a reduced lung function who are ex-smokers.

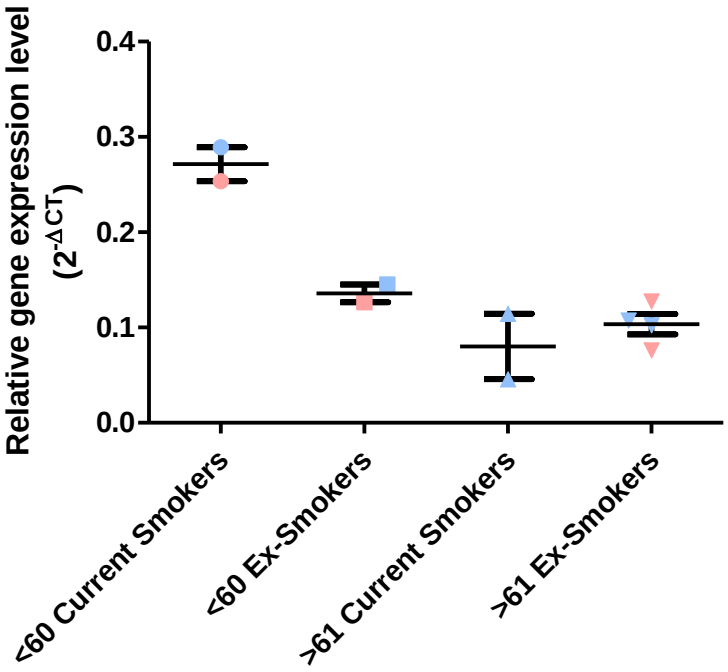

Figure 3.7: *SLC22A4* expression is attenuated in patients with reduced lung function who are current smokers compared to patients of reduced lung function who are exsmokers and those of a normal lung function i.e. >61 %FEV1/FVC% regardless of smoking history. Data are presented as means ± SEM, (*n* = 20). Blue = male, female = pink.FEV1/FVC% are displayed as <60 or >61.

3.4 Discussion

The data collected here indicates that OCTN1 expression is significantly related to lung function, a key determinant in the diagnosis of COPD (*138*). Although other factors such as age, sex, BMI, smoking history and pack years seem to follow a trend in the expression of OCTN1, no such significance is determined in this study.

Previous reports have stated that age causes a decrease in the functional lung capacity. They have also suggested that age increases the susceptibility to external insult (*128*). Our data suggests a decline in the expression of *SLC22A4* with increasing age in the control group. However, this trend is not observed in patients with COPD. In contrast, a slight increase in expression of the gene occurs. Previous studies have monitored the expression of *Slc22a4* in renal epithelium of rats by qRT-PCR, where gene expression was found to increase with age (*53*). This was supported by functional studies of OCTN1 in the kidneys, and it was found that the clearance of organic compounds occurred more slowly in infants and children than in adults. In comparison, human *SLC22A4* was strongly expressed in foetus compared to human adult liver and suggested that this is due to the potential increased foetal hepatotoxicity (*46*). However, in mice this increase in gene expression was also observed up to 2 weeks after birth, at which point it reached a steady state of expression (*55*). No such data has been reported for lung epithelium. Our studies suggest *SLC22A4* expression declines with age in control patients. However, in patients with COPD this expression is slightly increased suggesting that OCTN1 may be amplified to transport higher levels of its physiological substrate the antioxidant, ET, into the lungs of chronic inflammatory sufferers. Further studies are required to confirm this hypothesis.

Males are reported to be diagnosed more likely than females, which is similar with this study as the majority of patients recruited were male. Sakamoto *et al.* reported protein expression of OCTN1 to be 2-times higher in human lung tissue of females than in males by LC-MS/MS

(*139*). In female mouse lung, the expression of *Slc22a4* was also found to be higher when compared to males (*55*). Our data suggests a higher increase in expression to occur in females suffering from COPD. A decrease in expression in *SLC22A4* is observed in male patients with COPD compared to their controls. However, collectively, no such difference in gene expression is observed between the two genders. This is the first data to be reported on *SLC22A4* expression focusing on gender and COPD.

To date the gene expression of *SLC22A4* with regards to BMI has not yet been investigated. This is of interest as patients who are underweight or obese have been suggested to have lower lung function (18). The gene expression in both control and COPD groups was found to increase in patients who were not of normal BMI, i.e. 18.9-24.9. This increase in expression was further amplified in patients with COPD.

Smoking duration and COPD severity have been found to share a positive linear relationship (*132*). However, the development of COPD has been found to decline in ex-smokers who have quit less than 10 years ago (*132*). This is the first research that has investigated the expression of OCTN1 with regards to cigarette smoking. Previous findings carried out by our research group have revealed a slight increase in the gene and protein expression of OCTN1 upon incubation with CSE. Following, this study revealed that increase pack years (>21 pack years), increases the expression of *SLC22A4* in both control and COPD groups. No difference in expression of the gene is observed when patients have smoked <20 pack years. However, upon smoking more than 21 pack years, a further increase in the expression of the transporter is observed in patients with COPD compared to the control. And so, the expression of OCTN1 was investigated in current and ex-smokers. No difference in gene expression was observed in either control or COPD groups of current smokers. However, a decrease in expression of *SLC22A4* was observed in ex-smokers than that of current smokers. In combination with the above findings, it could be reasoned that this observed decrease in

expression of ex-smokers could be occurring due to a decrease in the requirement of an antioxidant to be transported.

Although key factors such as gender, age, BMI and smoking history remain insignificant with regards the expression of OCTN1, when collectively presented i.e. a male, 67 years of age, overweight and a current smoker with a pack year history of 50, highest expression of the transporter is revealed. This sample appears to be an outlier although it is not mathematically so.

As FEV_1/FVC is an important determinant of COPD diagnosis, it was imperative to investigate a relationship with the expression of *SLC22A4.* To date conflicting reports have been published regarding the expression of OCTN1 in patients with chronic inflammatory diseases. It has been reported that the SNP coding for the mistranslation of C1672T, resulted in a decreased expression of OCTN1 in the gastrointestinal epithelium of patients with CD (*121, 125*). Berg *et al.* reported high mRNA expression in central and peripheral lung samples with no difference between healthy and COPD tissues (*123*). However, Giardin *et al.* reported an increase in the protein of human intestinal biopsies of patients with CD (*140*). Similarly, Zhou *et al.* reported an increase in expression of OCTN1 in the basal cells of the lung of COPD patients (*123*). Data collected from this study performed on the bronchial epithelium of patients with COPD, suggests a significant increase in expression of the transporter as lung function declines. This is contradictory to findings of the University Medical Center, Groningen, who reported a decreased expression of *SLC22A4* in the bronchial epithelium.

Further, these data were investigated with regards to pack years and smoking history. A trend is evident when comparing smoking history and lung function with the expression of *SLC22A4*. This data indicates that expression of *SLC22A4* increases in patients with reduced lung function and who are current smokers, compared to individuals with reduced lung

function and who are ex-smokers, or those of normal lung function and are smokers or ex-smokers. This could suggest that these individuals are at greater risk of developing COPD, and OCTN1 expression is increased in an attempt to provide extra protection to the lungs of these subjects. Pack years did not demonstrate any trend when compared with lung function and its relationship with *SLC22A4* expression.

A study performed by Wotjal *et al.* reported that the expression of OCTN1 remained unchanged during inflammation (*141*), which could suggest that the expression of the transporter may be functionally related, and such increase in expression could be an attempt to transport greater quantities of the antioxidant ET into the chronically inflamed cells. However, functional activity of OCTN1 under these conditions is required.

3.4 Conclusion

This study for the first time investigated the expression of *SLC22A4* in the bronchial epithelium of COPD patients and compared this data to collected data of patients not suffering from the condition. It was determined that risk factors such as age, unhealthy weight, smoking resulted in an observed increase in expression in patients, both healthy and those suffering from COPD. An upregulation of the transcript also occurred in COPD patients with decreasing lung function, a criterion that determines the severity of the condition. Future work, could be to investigate the possible effects of corticosteroid use (the primary treatment of COPD), and whether their use could impact on the outcome of this study. In conclusion, for the first an association between COPD and *SLC22A4* was successfully determined.

Chapter 4

The Mechanism of Xenobiotic Detoxification by ET *in vitro*.

Abstract

The molecular mechanism of action of ET, as an antioxidant remains unclear. By studying potential reactions of ET, which have been previously reported for GSH, may reveal further insight into its role as an antioxidant. The structural form of ET was studied under conditions of oxidative stress i.e. CSE, to reveal the conversion of ET into ESO_3H. However, it was determined that unoxidised ET still remains intracellularly and so, its role in phase II metabolism was also investigated. Similar to GSH, ET can perform conjugation reactions for detoxification and so reaction with CDNB was confirmed by spectroscopy and also quantified intracellularly by LC-MS/MS. GST was identified to play a role in this formation, with MRPs responsible for the efflux of the metabolite. However, the molecular identity of the respective enzyme and transporter still needs to be elucidated. This novel research, for the first time, has confirmed that ET carries out its antioxidant properties in a similar way to GSH.

4.1 Introduction

A critical stage of pharmacokinetics is metabolism. Metabolism is the sum of all chemical reactions happening in the body. More specifically, metabolism is where compounds are transformed into new chemical entities to be more easily eliminated. Metabolism can occur via Phase I, where oxidation, reduction and hydrolysis reactions can take place, and/or Phase II, where chemical compounds may become conjugated, yielding ionised metabolites, which are later excreted.

Antioxidants in the body undergo all stages of metabolism and are compounds devout to the detoxification of ROS. In order to undergo Phase I metabolism, antioxidants must structurally have an easily oxidisable group, which will become the target for ROS in the cell.

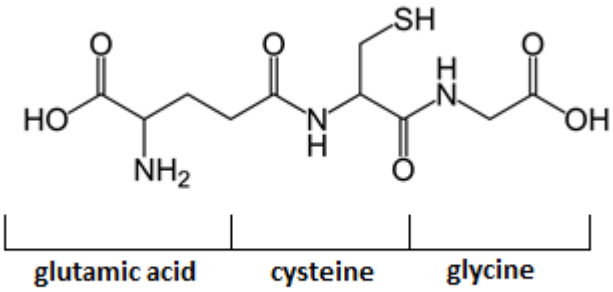

Figure 4.1: Chemical structure of glutathione (GSH) synthesised from glutamic acid, cysteine and glycine.

Glutathione (GSH) has been demonstrated to be the most effective antioxidant synthesised by the human body. In the presence of oxidative stress, the thiol group on the tripeptide becomes oxidised to form the disulfide dimer (GSSG), illustrated by Figure 4.1. In order to return to the reduced thiol GSH form, and to continue its behaviour as an antioxidant, the reaction requires, and is catalysed by a reducing enzyme. However, upon chronic inflammation, an imbalance between reducing enzymes and oxidative stressors occur, and without a competitor for ROS, oxidants favour and glutathione becomes depleted.

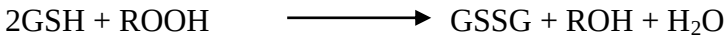

Scheme 4.1: Oxidation of glutathione with hydroperoxy.

Ergothioneine (ET), is reported to have superior antioxidant activity to that of GSH (*84*, *142*), as it is reported to not readily undergo oxidation like GSH (*142*). The tautomeric structure of ET allows for rapid equilibrium between the thiol and thione (Figure 1.2b) and so ET's nucleophilic action is reduced in comparison to that of GSH, which primarily remains as a thiol. Further, ET's redox potential is -0.06 V, compared to GSH's potential of 0.24 V (*142*). These characteristics account for the greater stability of ET (*142*) and prevents auto-oxidation as rapidly as other antioxidants. Therefore, the mechanism by which ET carries out its antioxidant properties remains unclear.

A recent publications by Servillo *et al.* (*4*) accounted for the structural changes occurring to ET once oxidised. At physiological pH, ET is majorly in the thione form (*1*) but it is reported that upon chronic inflammation, ET becomes oxidised to the disulfide just like GSH, which can oxidise to the disulfide monoxide (ESOSE), to further oxidise to the disulfide S-dioxide (ESO_2SE). ET can be reformed from each of these groups by disproportionation, with the formation of sulfenic (ESOH), sulfinic (ESO_2H) and sulfonic (ESO_3H) acid, respectively. ESOH can be further oxidised to form the unstable intermediate ESO_2H, which subsequently decomposes into hercynine (EH) and sulfurous acid (H_2SO_3). As a result, EH and ESO_3H have been found to be the major oxidised products of ET as in Figure 4.2(*4*).

Phase II metabolism is often referred to as 'the detoxifying step' as it involves the biotransformation of toxic compounds for their removal. GSH and its role in detoxification has been broadly studied. The thiol group of GSH behaves as a nucleophile attacking

electrophilic centres that are characteristic of many toxins, yielding a GS-adduct (Scheme 4.2).

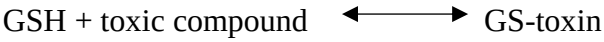

Scheme 4.2: Formation of a glutathione adduct

The forward reaction may occur enzymatically by glutathione S-transferase (GST) or non-enzymatically (*143*). GST are a family of isoenzymes of 16 members with 8 found in mammalian cells (α, μ, π, θ, ζ, ω, κ)(*144*, *145*). In human lung tissue, the predominant form of GST is alpha (*146*), with αGST reported to be responsible for the detoxification of carcinogenic metabolites, like those of cigarette smoke (*147*). GST is frequently investigated by studying the reaction of glutathione and GST's protypical substrate 1-chloro-2,4 dinitrobenzene (CDNB).

A)

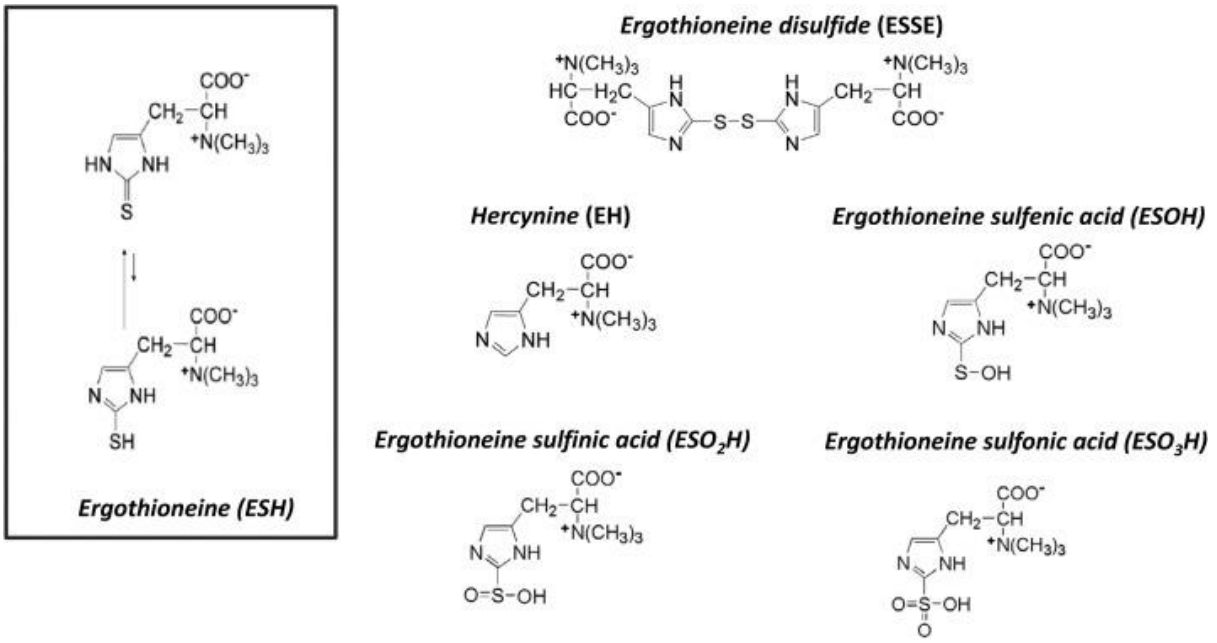

B)

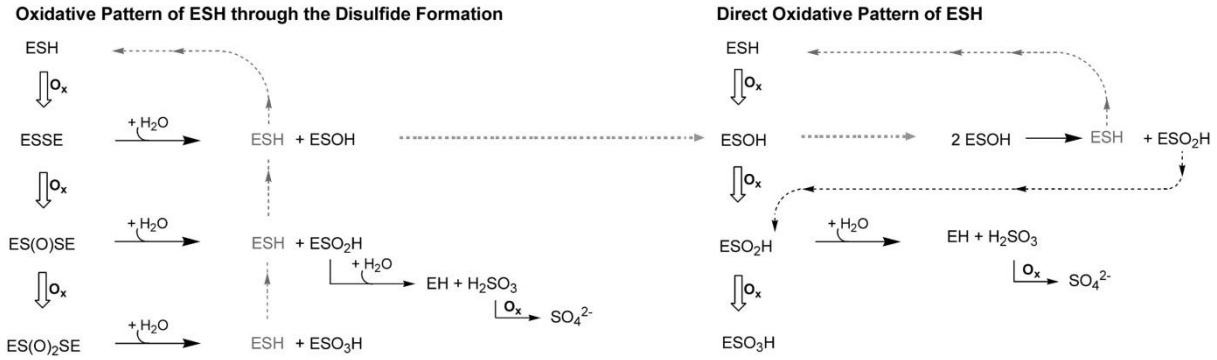

Figure 4.2: A) Oxidised products of Ergothioneine. **B)** The oxidation pattern of Ergothioneine either as a result of disulfide formation or direct oxidation of Ergothioneine (*1*).

This research will investigate the ability of ET to form oxidised products i.e. EH, ESO_3H in the absence and presence of CSE *in vitro.* Further, the ability of ET to participate in phase II metabolism will also be determined in order to elucidate its mechanism of action in cellular detoxification.

4.2 Materials and Methods

4.2.1 General procedures

All reagents used were of reagent grade and were used without further purification and purchased from Sigma-Aldrich and Merck.

4.2.2. Instrumentation

Thin layer chromatography (TLC)

TLC was performed using aluminium-backed silica gel 60 F_{254} (0.2 mm) precoated plates (Merck, Darmstadt, Germany). Plates were developed in a closed chamber at room temperature across a development distance of 15 cm. Specified mobile phases were used as development solvents. After development, the plates were dried in air, and visualized using shortwave (254 nm) ultraviolet fluorescence.

Nuclear Magnetic Resonance

^{1}H and ^{13}C nuclear magnetic resonance spectra were recorded at 27 ºC on a Bruker DPX 400 and an Agilent 400 MR DD2 spectrometer (400.13 MHz, 1H; 100.61 MHz, 13C). The data are reported as chemical shift (δ ppm) relative to the residual protonated solvent resonance, relative integral multiplicity (s=singlet, d=doublet, t=triplet, q=quartet, m=multiplet), coupling constant (*J* Hz), and assignment of signal, where applicable.

Infra-red Resonance

Infra-red spectra were obtained by mixing solid compound with dry KBr,grinding to a fine well mixed powder and forming a disc by applying high pressure before analysis being performed on a Perkin Elmer 205 FT infrared Paragon 1000 spectrometer.Band positions are given in cm^{-1}.

Mass Spectrometry

High resolution mass spectrometry (HRMS) was performed on a Thermo Scientific LTQ Orbitrap Discovery System in electrospray ionization mode.

Melting points

Melting points were recorded in open capillaries using a Stuart SMP11 melting point apparatus.

Solid Phase Extraction (SPE)

SPE was used for the extraction of DNP-ET due to the polarity of the compound and difficulty in separating it from the solvent i.e. methanol. Columns were purchased from Fisher Scientific and successful isolation was carried out according to the manufacturer's protocol.

4.2.3 Chemical Synthesis

Synthesis of [1-carboxy-2-(2-sulfo-1H-imidazol-4-yl)ethyl]trimethylazanium (ESO_3H)

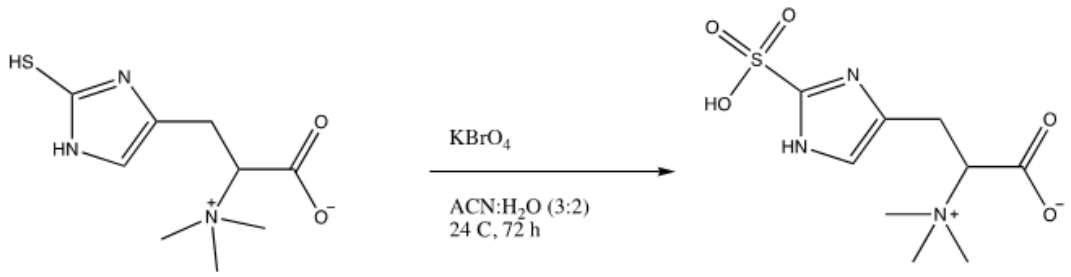

Scheme 4.3: Formation of ESO_3H

Ergothioneine (100 mg, 0.004 moles) was treated with potassium perbromate ($KBrO_4$, 200 mg, 0.012 moles) at 24˚C for 72 h in acetonitrile and water (3:2). Product formation was confirmed by thin layer chromatography using a mobile phase of acetonitrile and water (3:2). Purification was performed by precipitating $KBrO_4$ with $Ca(OH)_2$ followed by recrystallisation of the product with ethanol to produce a pale yellow solid (57 mg, 95%

yield) with melting point of 212-219˚C. **^{1}H NMR** (400 MHz, MeOD) δ ppm: 8.45 (1H,s), 7.24 (1H,s), 6.80 (1H,s), 6.58 (1H,s) 4.72 (1H, t, *J*=7.6 Hz), 3.46 (2H, d, *J*=6.5 Hz), 2.89 (9H, s). **^{13}C NMR** (100 MHz, MeOD) δ ppm: 171.28 (-C-), 160.47 (-CO-), 131.78 (-C-), 119.18 (-C-), 70.34(-CH-) 52.89 (-CH_3), 30.50 (-CH_2-). **IR** (nujol mull): 3238 cm^{-1} (-NH-), 1895 cm^{-1} (C-H), 1774 cm^{-1} (-C=O), 1298 cm^{-1} (-C-N-), 1176 cm^{-1} (S=O), 640 cm^{-1} (S-O). MS: Found: ($M+H^+$) =254, calculated $C_9H_{15}N_3O_5S^+$ =254.07

Synthesis of [1-carboxy-2-(1H-imidazol-5-yl)ethyl]-trimethylazanium (EH)

This compound is not novel

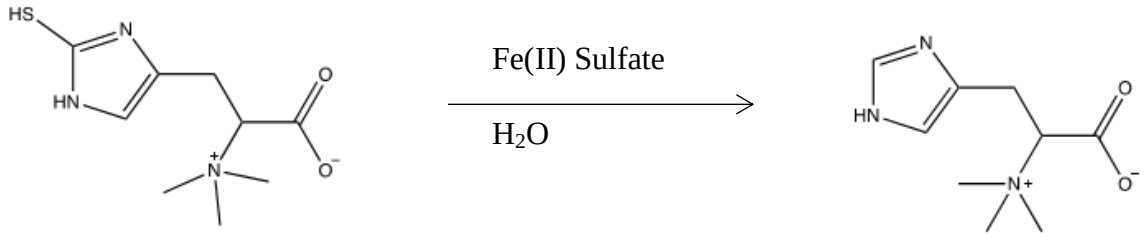

Scheme 4.4: Formation of EH

Ergothioneine (50 mg, 0.000218 moles) was treated with iron II sulphate (435 mg, 0.00218 moles) in 500 ml of water at 100˚C for 1 h. Product formation was confirmed by thin layer chromatography with mobile phase DCM:EtOH:MeOH (2:2:1). Purification was performed by precipitating with barium hydroxide. The precipitate was collected and dissolved in 150 ml of boiling water. The solution was filtered and the filtrate heated to boiling point before concentrated to 50 ml by vacuum evaporation. Finally the product was recrystallised from ethanol to produce a white solid (40 mg, 93% yield) with melting point of 247-249˚C (Literature: 237-238 ºC**) (*148*).^{1}H NMR** (400 MHz, DMSO) δ ppm: 12.72 (1H,s), 8.37 (1H,d, *J*=8.5 Hz), 7.83 (1H,d, *J*=7.3 Hz) 4.83 (1H, t, *J*=7.6 Hz), 3.30 (9H, m), 3.29 (2H, m),

2.49 (1H,s). **^{13}C NMR** (100 MHz, DMSO) δ ppm: 172.14 (-CO-), 135.90 (-CN-), 128.42 (-C-), 118.6 (-CH-), 88.1 (-CH-), 52.14 (-CH_3-), 19.3 (-CH_2-). **IR** (nujol mull): 3341 cm^{-1} (-NH-), 2958 cm^{-1} (O-H), 1726 cm^{-1} (C=O), 1474 cm^{-1} (aromatic C=C). HRMS: Found: ($M+H^+$) = 198, calculated $C_9H_{15}N_3O_2^+$ = 197.12

Synthesis of (carboxymethyl]trimethylazanium (DNP-ET)

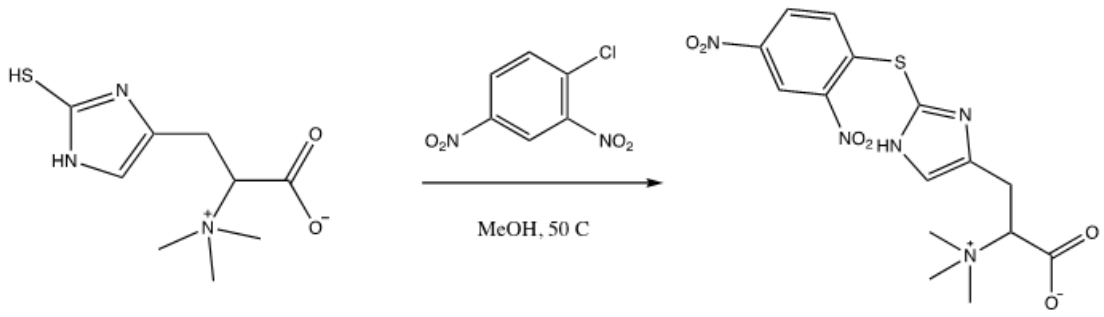

Scheme 4.5: Formation of DNP-ET

Ergothioneine (29 mg, 0.1265 moles) was treated with 1-chloro-2,4-dinitrobenzene (CDNB) (52 mg, 0.253 moles) at 50˚C for 24 h in methanol. Product formation was confirmed by thin layer chromatography. Purification was performed by solid phase extraction with mobile phase consisting of butanol, acetic acid and water (12:9:1), to produce an orange solid (25 mg, 50% yield) with melting point of 178-181˚C. **^{1}H NMR** (400 MHz, MeOD) δ ppm: 7.20 (s, 1H), 6.88 (dd, 1H, *J*=9.14 Hz), 6.69 (dd, 1H, *J*=9.14 Hz), 6.37 (d, 1H, *J*=8.5 Hz), 3.38 (m, 2H), 1.87 (m, 9H), 1.69 (m, 1H). **^{13}C NMR** (100 MHz, MeOD) δ ppm: 165.96 (-CO-), 143.96 (-C-), 142.36 (-C-), 134.12 (-C), 132 (-C-), 131.42 (-CH-), 127.29 (-C-), 125.73 (-CH-), 120.40 (-CH-), 119.31 (-CH-), 77.87 (-CH-), 50.29 (-CH_3-), 23.42 (-CH_2-). **IR** (nujol mull):

3102 cm^{-1} (-NH-), 1725 cm^{-1} (C=O), 1594 cm^{-1} (-C=C-), 1524 cm^{-1} (aromatic C=C). HRMS: Found: $(M+H^+)$ = 395.64, calculated $C_{15}H_{17}N_5O_6S^+$ = 395.09

4.2.4 Quantification of ESO_3H, EH, ET and DNP-ET.

Production formation was monitored by thin layer chromatography (TLC) facilitated by UV spectroscopy. To quantify product formation LC-MS/MS was utilised, using the previously established ET method. Selected reaction monitoring (SRM) was set at 198 and 155 m/z, for ESO_3H and EH, respectively, with collision energy set at 10 V to prevent complete fragmentation of the sulfonic acid group of ESO_3H to ensure differentiation between ESO_3H and EH was possible. SRM was set at 186 m/z for ET with collision energy of 16 V.

DNP-ET adduct production was monitored by UV spectroscopy at a wavelength of 405 nm. To increase sensitivity, DNP-ET formation was later detected and quantified by LC-MS/MS, using the previously established ET method. SRM was set at 352 m/z with collision energy 16 V.

Sample analyte content will be calculated from the analyte response ratio and the slope of the calibration curve, obtained by weighted linear regression.

4.2.5 Cell Culture

Human bronchiolar epithelium NCI-H441 (American Type Culture Collection, HTB-174, Teddington UK) were cultured at 37°C in 5% CO_2 atmosphere in Gibco RPMI-1640 medium (Biosciences, Dun Laoghaire, Ireland) supplemented with 5% foetal bovine serum (FBS), 1% sodium pyruvate, 1% penicillin streptomycin (all from Sigma Aldrich). NCI-H441 cells were routinely cultured in 75 cm^2 growth area tissue culture flasks (Greiner BioOne, Frickenhausen, Germany) and passaged when approximately 80% confluency. NCI-H441 cells were seeded at a density of 75,000 cells/cm^2 on well plates (Greiner). Twenty-four hours

prior to experimentation cells were serum starved 24 h prior to experimentation to prevent proliferation of cells. On the day of the experiment, cells were washed twice with warm, Kreb's Ringer Buffer (KRB) composed of 15 mM HEPES, 116.4 mM NaCl, 5.4 mM KCl, 0.78 mM NaH_2PO_4, 25 mM $NaHCO_3$, 1.8 mM $CaCl_2$, 0.81 mM $MgSO_4$ and 5.55 mM glucose, pH 7.4.

Transduction of NCI-H441 cells with OCTN1 shRNA lentiviral particles.

This was carried out by Dr. Sabrina Nickel

NCI-H441 cells at passage 60 were used to generate the knock-down cell line due to their ability to form good electrical resistance. Ahead of the lentiviral transduction, optimal concentrations of the cationic transduction enhancer polybrene (2.5 µg/mL, SantaCruz Biotechnology, Dallas, Texas) and minimal lethal dose (2 µg/mL) of the selection reagent puromycin dihydrochloride (SantaCruz Biotechnology) were determined using Alamar Blue (BioSciences Ltd, Dun Laoghaire, Dublin) cytotoxicity assay. NCI-H441 cells were seeded in a 12 well plate at a density of 100,000 cells/cm^2 in RPMI culture medium (5% FBS, 1% sodium pyruvate, 1% penicillin streptomycin) one day prior to transfection. Monolayers of 50-70 % confluency were used for viral transduction the following day. The culture medium was removed and replaced by transduction medium (RPMI, 5% FBS, 1% sodium pyruvate, 1% penicillin streptomycin, 2.5 µg/ml polybrene). Lentiviral particles were thawed at room temperature and the cells were transfected with $2x10^4$ Infectious Units (IFU) of the *OCTN1* shRNA lentiviral particles (SantaCruz Biotechnology) per well. One well was additionally transduced with scrambled shRNA lentiviral particles to create a control cell line. The cells were incubated for 24 h with the viral particles before the transduction medium was removed and replaced with culture medium. Following an additional 24 h incubation period, NCI-H441 cells were split at a 1:3 ration, seeded in culture medium onto 6 well plates and allowed to attach over-night. Subsequently, the culture medium was replaced by selection medium

(RPMI, 5% FBS, 1% sodium pyruvate, 1% penicillin streptomycin, 2 μg/ml puromycin hydrochloride). The selection medium was replaced every two to three days until resistant colonies could be observed. Colonies were picked and expanded in selection medium for another 3 weeks to ensure complete removal of non-transfected cells.

Cigarette smoke extract

Two Kentucky reference research cigarettes (2RF4) were ignited and the gaseous component bubbled through 20 ml of medium to yield 100% cigarette smoke extract (CSE) for 1.5 min. Two filters from unused Kentucky reference research cigarettes were bubbled through 20 ml medium to act as a control. All medium was sterilised by filtration before use.

4.2.6 Quantification of oxidised ET products *in vitro*

ET (250 μM) were incubated with and without various concentrations of CSE (1,5 and 10%). To identify the oxidative state of ET under oxidative stress *in vitro*, cells were incubated with ET on day of seeding. Twenty-four hours prior to experimentation, cells were serum starved and incubated with various concentrations of CSE. Experiments were stopped by washing the cell monolayer three times with ice-cold buffer. Cells were detached from the plate using 0.5 ml trypsin. The resulting solution was centrifuged at 12,000*x*g for 10 min before adding 1 ml of water to lyse the cells. The solution briefly sonicated and the resulting solution centrifuged at 17,000*x*g for 5 min. The supernatant was removed and filtered prior to analysis by LC-MS/MS. OCTN1$^{-/-}$ served as the positive control in this experiment.

4.3.7 Quantification of DNP-ET *in vitro*

DNP-ET formation was monitored in cells by LC-MS/MS. Cells were incubated with various concentrations of CDNB (1-200 μM) with and without ET (1-200 μM). After incubation for 2 h at 37°C, cells were washed twice with fresh pre-warmed KRB, and then finally washed with ice cold KRB. Cells were then lysed with 1 ml of water, which was then treated with

sonification to ensure the lysis of cells. The resulting solution was then centrifuged at 12,000*x*g for 10 min. The resulting supernatant was taken for analysis by LC-MS/MS and the formation of ET-adduct *in vitro* determined.

4.2.8 Cytotoxicity of DNP-ET adduct in the presence/absence of GST inhibitor and MRP inhibitor

NCI-H441 cells were seeded on a 96 well plate (Greiner) and the medium exchanged every alternative with or without 250 μM ET. However, on the day prior to experimentation, cells were fed with serum free medium. On the day of the experiment cells, were washed twice with warm, fresh KRB. Cells were incubated with different concentrations of CDNB (1-200 μM) and ethachrynic acid (1 μM, EA), and MK-571 (0.75 μM), the GST inhibitor and the MRP inhibitor, respectively. Cells were then incubated with 1X concentration Alamar Blue for 4 h in the dark. Thirty minutes prior to the end of incubation cells were incubated with 1% Triton-X-100, to act as a negative control. After the 4 h incubation cells were measured using FLUOstar Optima spectrophotometer and Optima software at an excitation of 570 nm and an emission of 585 nm. The percentage cell survival was calculated by $(F_T\text{-}F_n)100$ where F_T is the fluorescence of the treated wells and F_n the fluorescence of the negative controls.

4.2.9 Formation of DNP-ET in the presence/absence of GST inhibitors and MRP inhibitor

NCI-H441 cells were seeded on a 6 well plate (Greiner) and the medium exchanged every alternative day. On the day prior to experimentation, cells were fed with serum free medium. On the day of the experiment, cells were incubated with 250 μM ET for 30 min. Cells were then washed twice with KRB to be later incubated for 2 h with CDNB.

4.3 Results

4.3.1 Synthesis of ESO_3H, EH and DNP-ET

The succesful synthesis of ESO_3H, EH and DNP-ET was confirmed by ^{1}H and ^{13}C NMR, IR and MS Spectroscopy.

ESO_3H was prepared at 24˚C, by treating ET (1 equiv.) with $KBrO_4$ (3 equiv.) to convert it to its respective sulfonic acid. TLC monitored the generation of ESO_3H. Product formation was confirmed after 72 h. TLC with mobile phase acetonitrile and water (3:2) identified a spot appearing at R_f 0.71. The product was purified by recrystallisation with ethanol and obtained in 95% yield.

^{1}H NMR confirmed the structure formation of ESO_3H. Three peaks were identifiable for the protons attached to heteroatoms. Three singlets with integral 1 were detected at 8.45, 6.8, 6.58 ppm representative for the sulfonic acid proton, the amine proton and the hydroxyl proton, respectively. The proton associated with the aromatic region was detected at 7.24 ppm with integral 1. A triplet at 4.72 ppm was assigned to the methine group positioned next to the nitrogen of the trimethylamine group. This signal was disturbed by a solvent peak for deuterium oxide. Following, a doublet indicative of the aliphatic methylene group registered at 3.46 ppm with an integral of 2. Finally the signal for the three methyl groups was displayed as a singlet at 2.89 ppm with an integral of 9. Carbon^{13} NMR confirmed these peaks when integrated in a COSY. DEPT at 90 °C displayed an inverted signal at 30.50 ppm representative of the methylene group as shown in Figure 4.3.

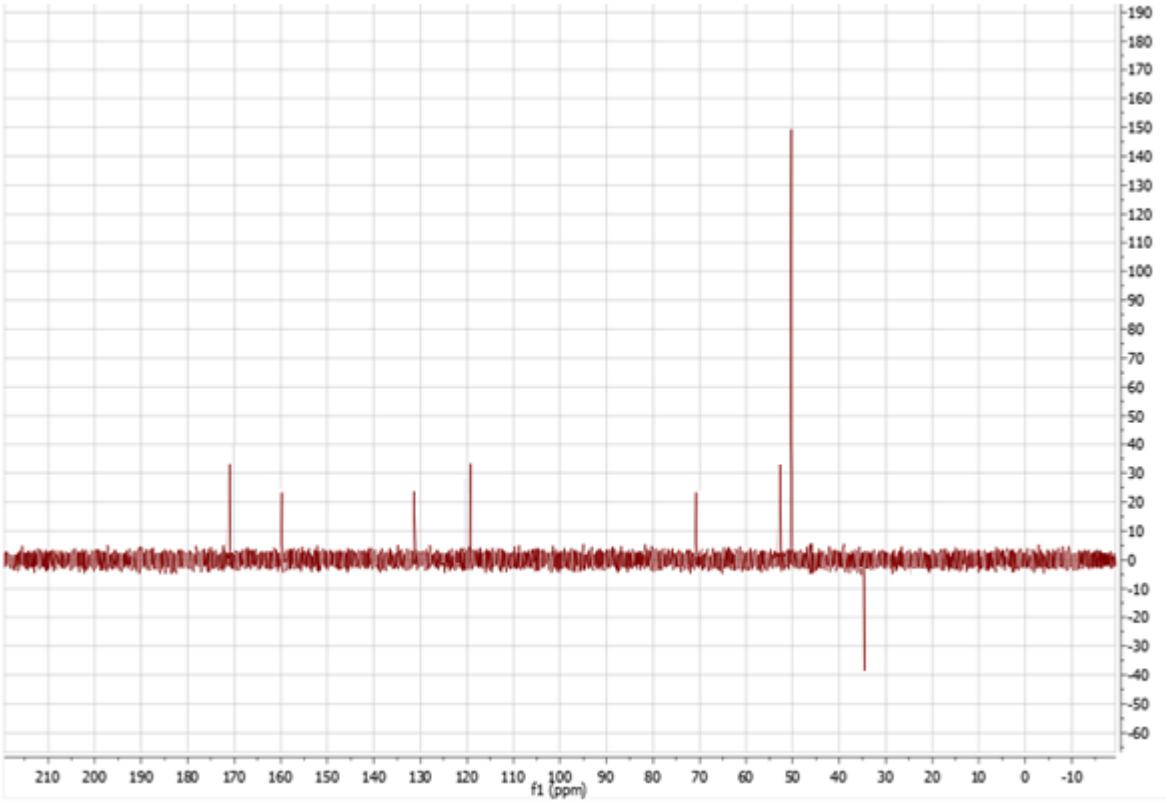

Figure 4.3: ^{13}C DEPT NMR at 90 °C illustrating the methylene carbon at 30.50 ppm

By IR spectroscopy, the presence of the sulfonic acid group was confirmed at 1176 cm^{-1} and 640 cm^{-1} for SO_3 and S-O, respectively. Mass spectrometry detected a signal at 254 m/z, with chromatograms displayed below (Figure 4.4). However, this signal was fragmented further to 198 m/z by tandem mass spectrometry. This was due to the cleavage of the energetically unstable carboxylic acid group and the release of the tertiary amine.

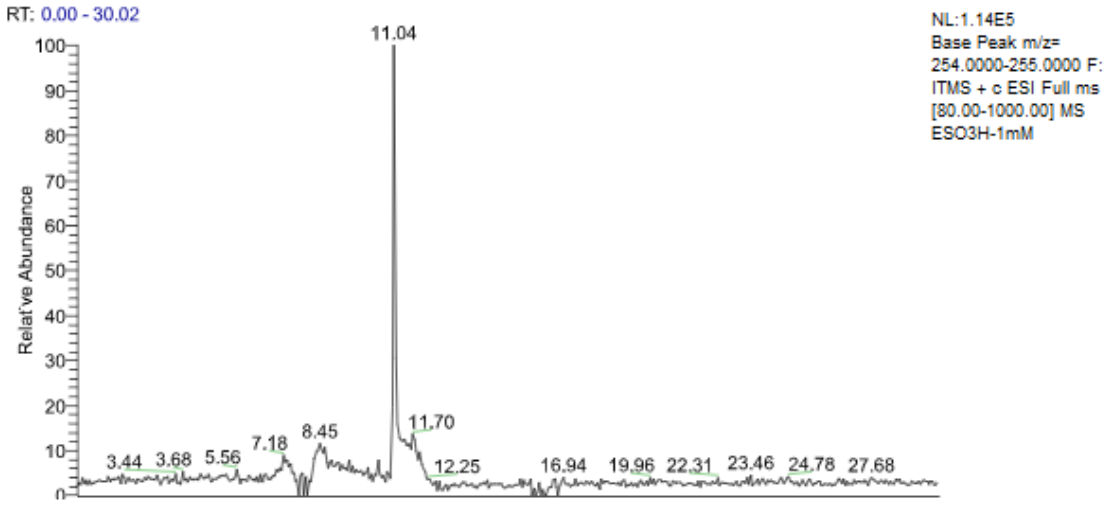

Figure 4.4: LCMS chromatogram of ESO_3H with a molecular weight of 254 m/z.

EH was prepared at 100˚C, by treating ET (1 equiv.) with $Fe(II)SO_4$ (10 equiv.) to convert it to hercynine. TLC monitored the generation of EH. Product formation was confirmed after 1 h. TLC with mobile phase dichloromethane, ethyl acetate and methanol (2:2:1) identified a spot appearing at R_f 0.38. The product was purified by recrystalisation with ethanol and obtained in 93% yield.

^1H NMR confirmed the structure formation of EH. Two peaks were identifiable for the protons attached to heteroatoms of oxygen and nitrogen at 12.72 ppm and 2.49 ppm, with integrals of one. The protons associated with the aromatic region were detected at 8.37 ppm and 7.83 ppm both with integral 1. The signal representative of the proton at the meta position of the imidazole ring was of higher chemical shift (8.47 ppm) due to the higher electronegativity of the adjacent nitrogen atoms. A triplet was observed at 4.83 ppm representative of the methine group with integral 1. A multiplet was observed at 3.30 ppm with an integral of 9. This is representative of the three methyl groups attached to the amine and the methylene group. Carbon^{13} NMR confirmed these peaks. By IR spectroscopy, the presence of the carboxylic acid group was confirmed at wavelengths of 2958 cm^{-1} and 1726

cm^{-1} for O-H and C=O, respectively. The N-H and aromatic C=C were identified at 3341 cm^{-1} and 1474 cm^{-1}, respectively. Mass spectrometry detected a signal at 198 m/z, shown in Figure 4.5. However, this signal was fragmented further to 154 m/z by tandem mass spectrometry. This was due to the cleavage of the energetically unstable carboxylic acid group and the release of the tertiary amine.

DNP-ET was prepared at 50˚C, by treating ET (1 equiv.) with CDNB (2 equiv.) to convert it to its respective adduct. TLC monitored the generation of DNP-ET. Product formation was confirmed after 2 h. However, to maximise yield, 24 h incubation was decided. TLC with mobile phase butanol, acetic acid and water (12:9:1) identified a yellow spot appearing at R_f 0.42. The product was purified by solid phase extraction with the same mobile phase and obtained in 50% yield.

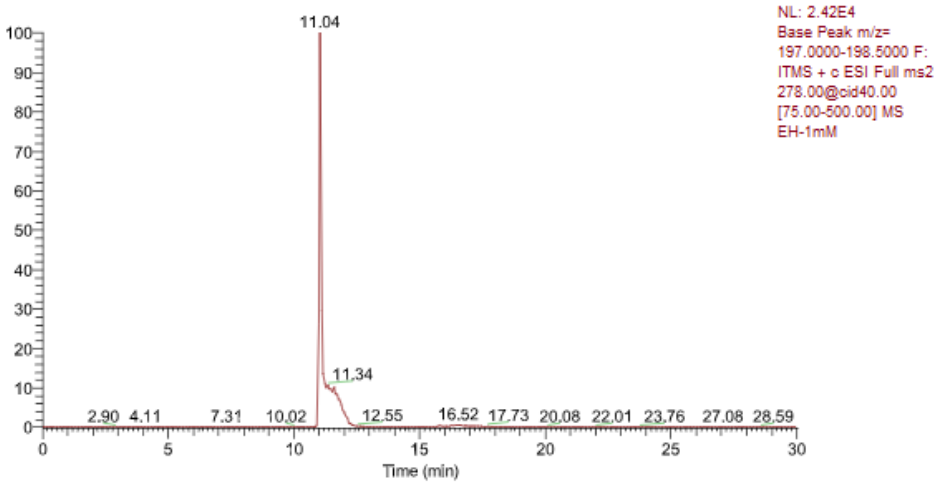

Figure 4.5: LCMS/MS chromatogram of EH with a molecular weight of 198 m/z.

^{1}H NMR evidenced confirmation of the structure (Figure 4.6). Four peaks were identifiable in the aromatic region confirming the presence of 4 aromatic protons. A doublet at 7.2 ppm was assigned to aromatic -CH- positioned next to two nitro groups. This peak was observed due to splitting nature of the proton in planar symmetry to the proton of the methine group.

Following, two further protons on the same aromatic ring were displayed as double doublets at 6.88 and 6.69 ppm. The final aromatic proton at 6.37 ppm corresponded to the -CH- group of the imidazole ring and appeared as a doublet. Three more signals appeared further upfield. These correspond to non-aromatic protons. The multiplet at 3.38 ppm represents the -CH_2- group, which is confirmed by the integral 2. The methyl groups attached to the nitrogen atom appear at 1.87 ppm. Unfortunately, this signal is hidden by a solvent peak, but a COSY confirmed this signal (Figure 4.8). Finally, the methine group is identified at 1.69 ppm by a multiplet with an integral 1. The carbonyl group was confirmed at 165.96 ppm on the carbon NMR spectrum, with the methylene group confirmed by DEPT at 90 °C at 23.42 ppm (Figure 4.7)

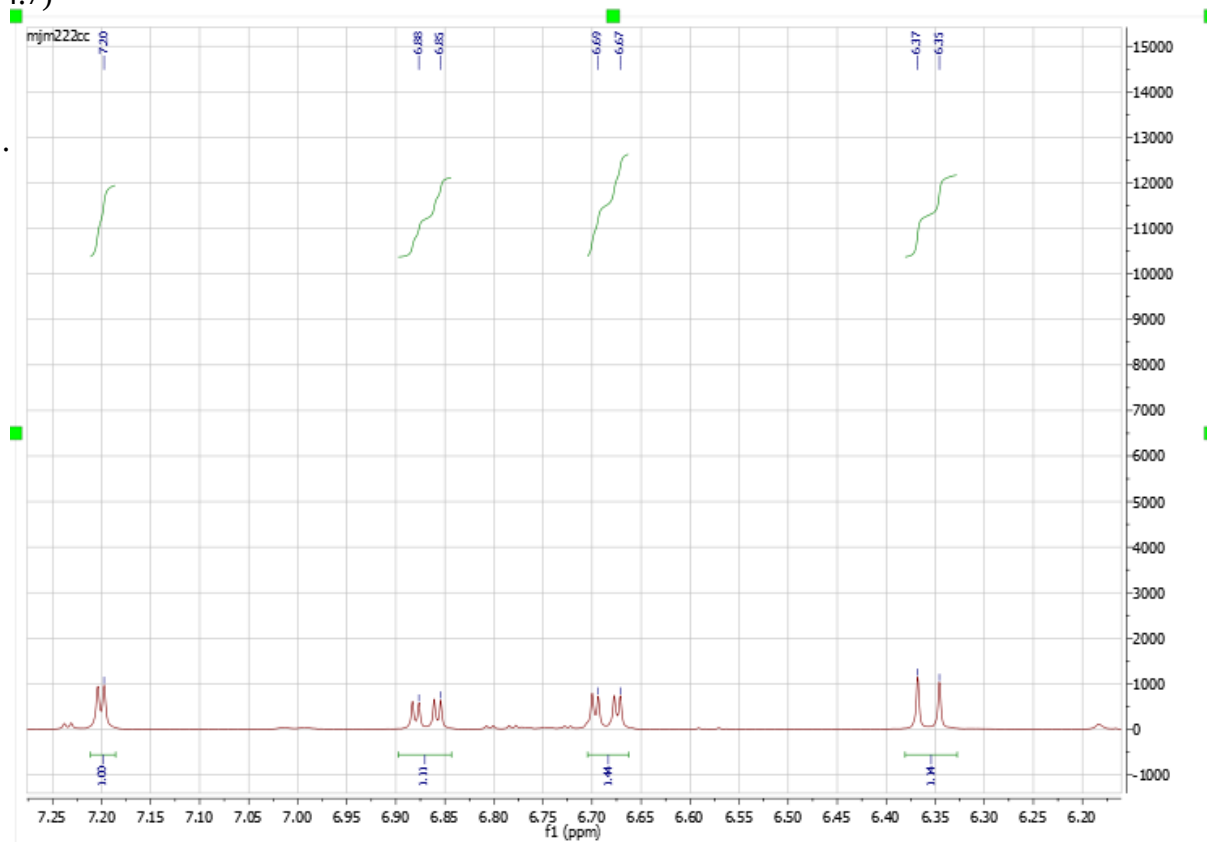

Figure 4.6: ^{1}H NMR (400 MHz, MeOD) illustrating four aromatic protons attached to DNP-ET

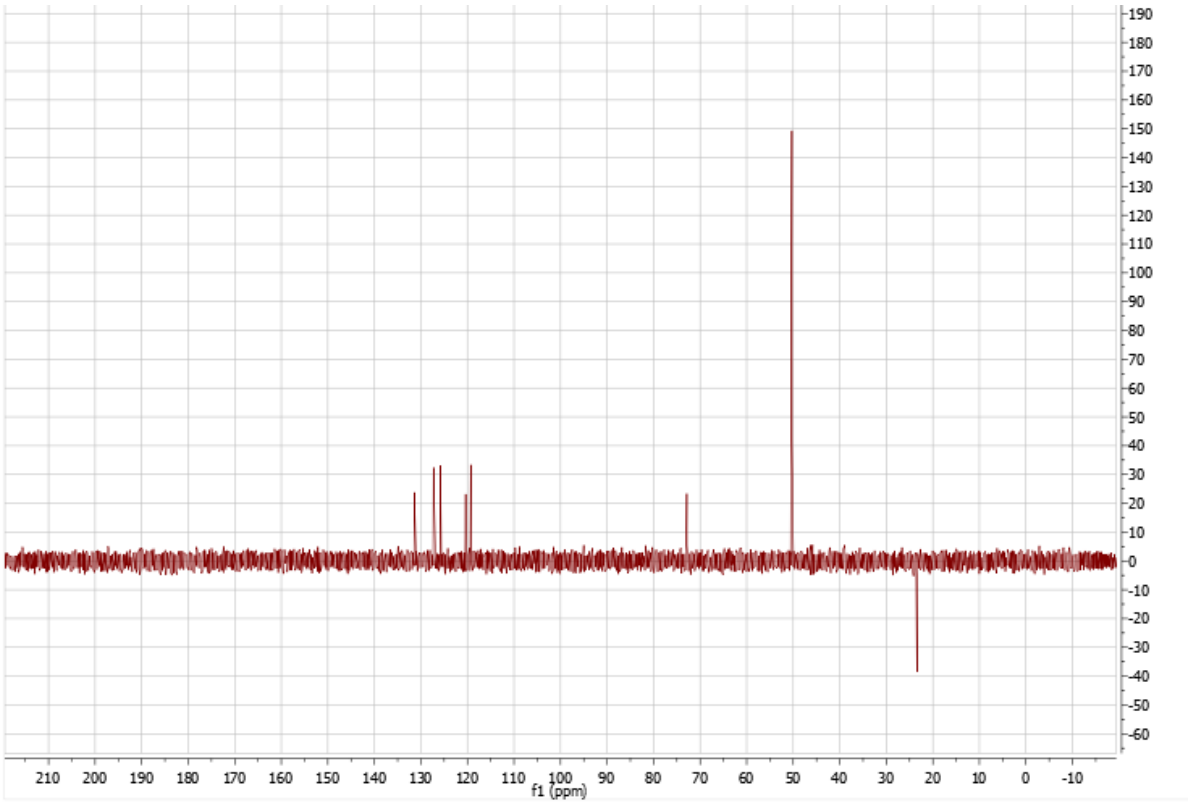

Figure 4.7: ^{13}C DEPT NMR at 90 °C illustrating the methylene carbon at 2.43 ppm

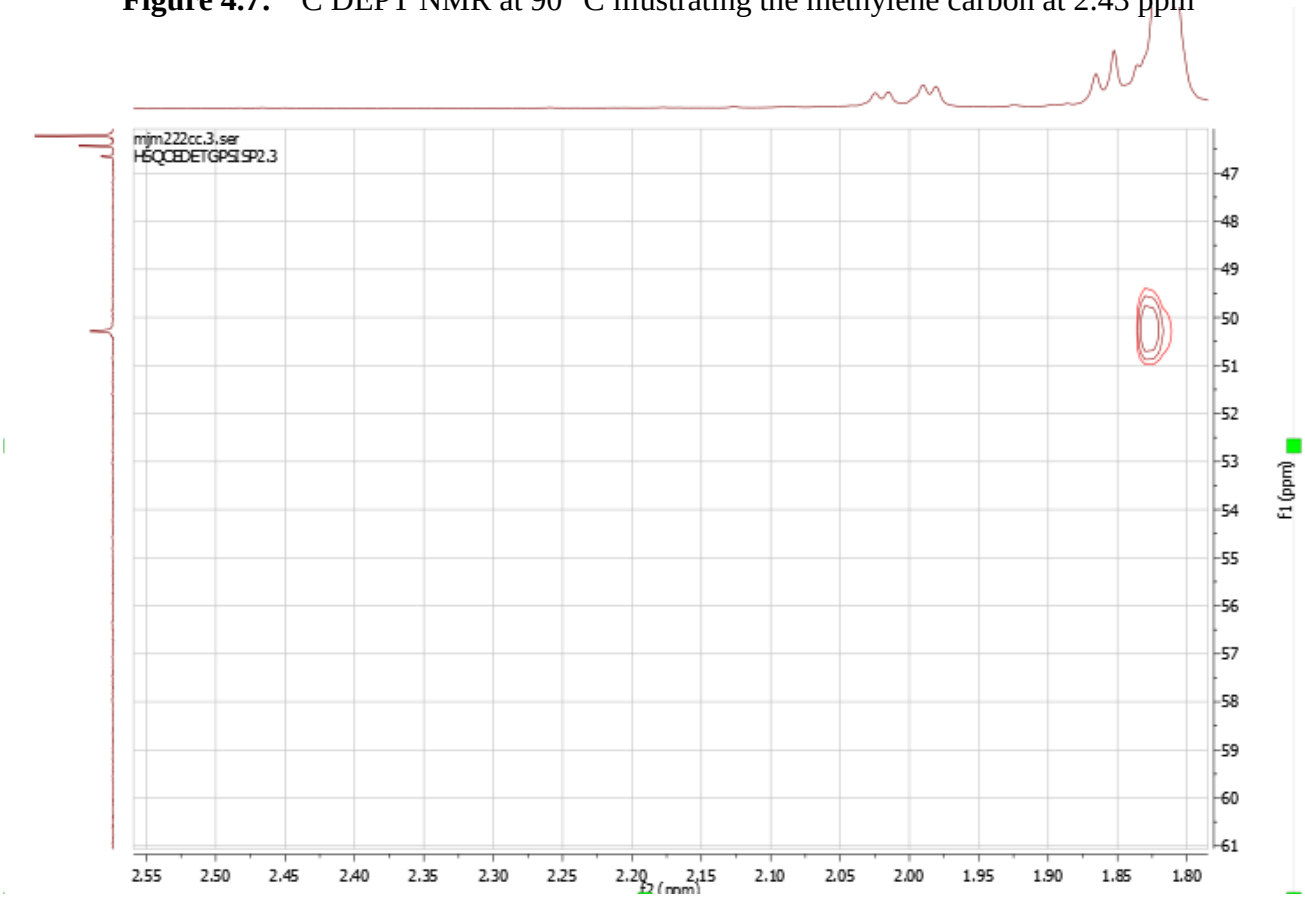

Figure 4.8: COSY NMR (400 MHz) confirming the presence of three methyl groups attached to the nitronium ion

Mass spectrometry detected a signal at 395 m/z as seen in Figure 4.9. However, this signal was fragmented further to 352 m/z by tandem mass spectrometry.

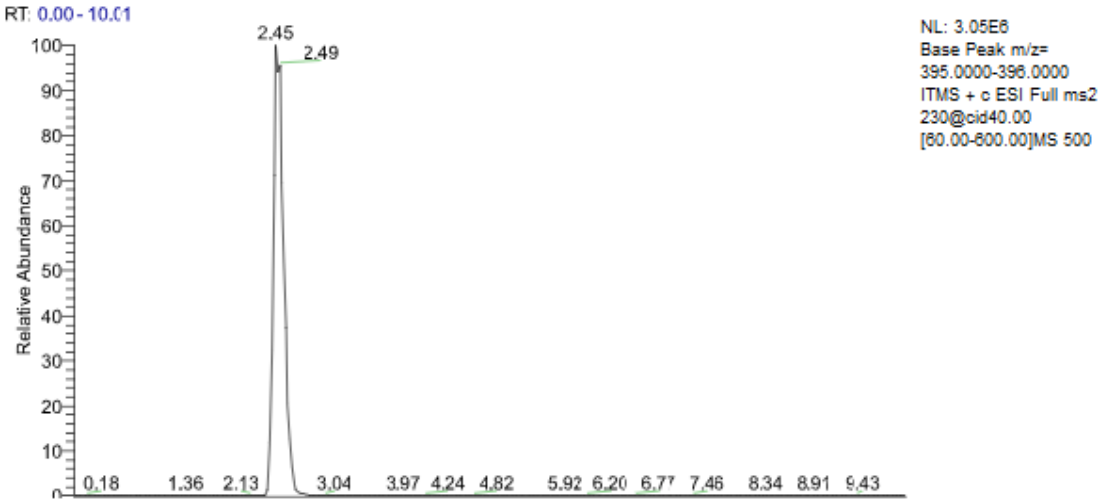

Figure 4.9: LCMS/MS chromatogram of DNP-ET with a molecular weight of 395 m/z.

4.3.2 Quantification of ESO_3H and EH by LC-MS/MS

ESO_3H, EH and DNP-ET were successfully quantified by LCMS/MS in water as low as 500 nanomolar (nM) displaying very good linearity (Figure 4.10). The limit of detection for ESO_3H, EH and DNP-ET was 7 nM, 6 nM and 9 nM respectively. All compounds had a limit of quantification in KRB 5 nM, with good linearity (r^2 = 0.9298 ± 0.07020) (Figure 4.10). The method for separation by chromatography was that previously established by the Ehrhardt group for ET.

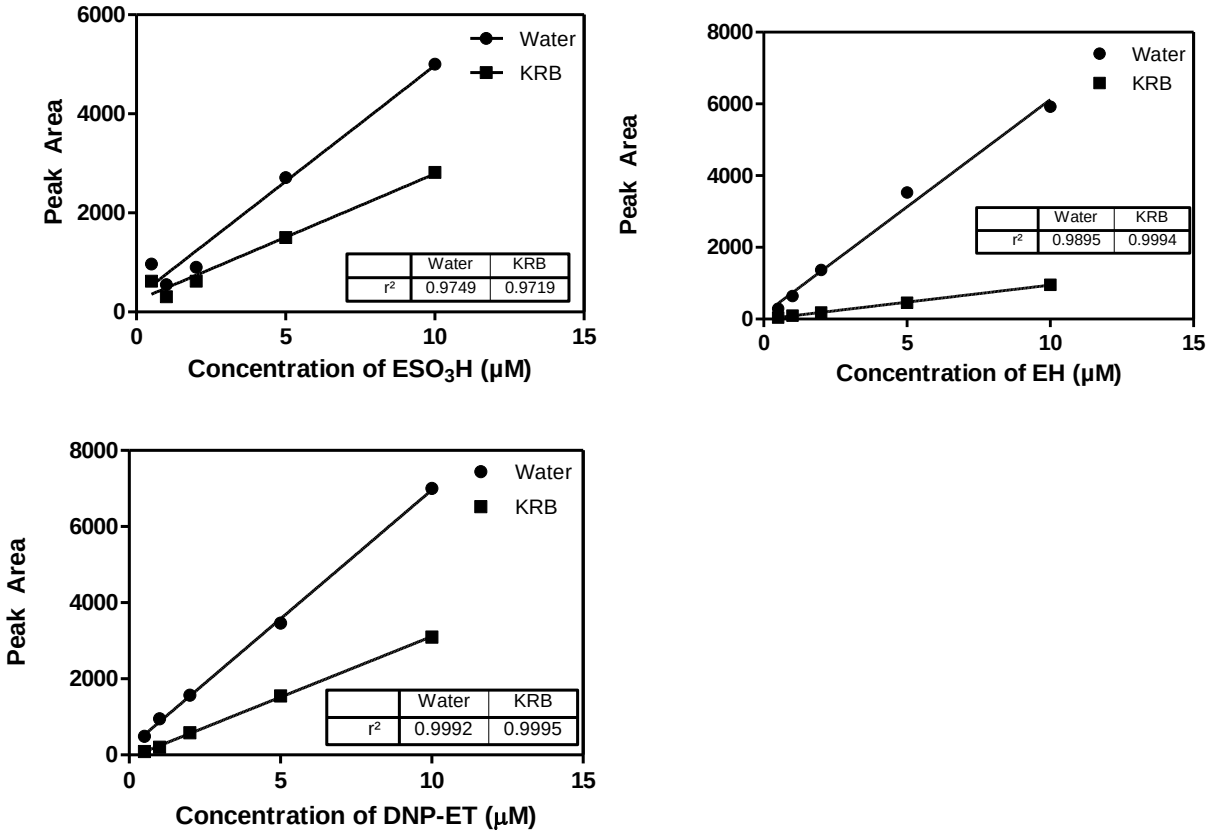

Figure 4.10: Quantification of ESO_3H (198), EH (154) and DNP-ET (352) by LC-MS/MS in water and KRB with SRM in parethesis. These data confirm excellent linearity for the quantification of each of the three compounds. Graphs represent (n=9).

4.3.3 Oxidation states of ET *in vitro.*

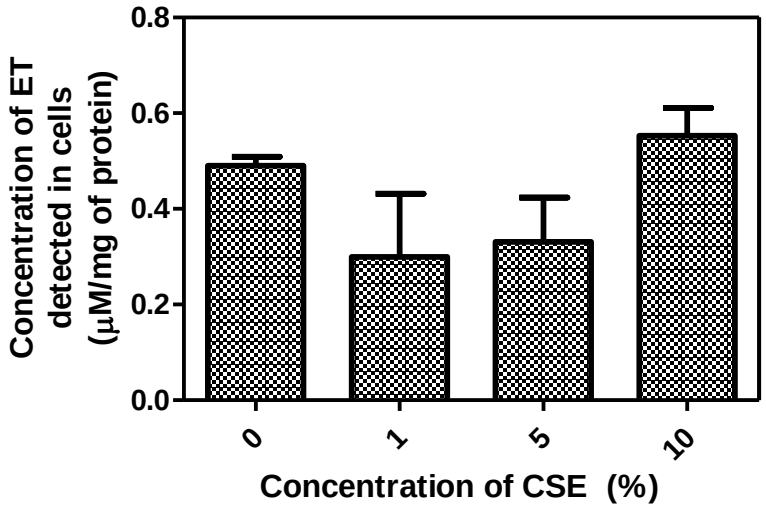

Figure 4.11: Concentration of 250 μM ET uptake into NCI-H441 cells when incubated with and without CSE (0-10%) for 24 h. CSE at low concentrations (1%) results in a decrease in the concentration of ET detected *in vitro.* However, increasing concentrations of ET (5-10%) result in a consecutive increase in the accumulation of ET. Graphs represent means ± SEM, (*n*=3).

As predicted, stable concentrations of ET accumulated intracellularly in the absence of CSE. However, upon incubating with CSE a drop in the level of ET detected in the cell occurred. Upon increasing the concentration of CSE, a further increase in the amount of ET was detected in the cell. This is demonstrated in Figure 4.11.

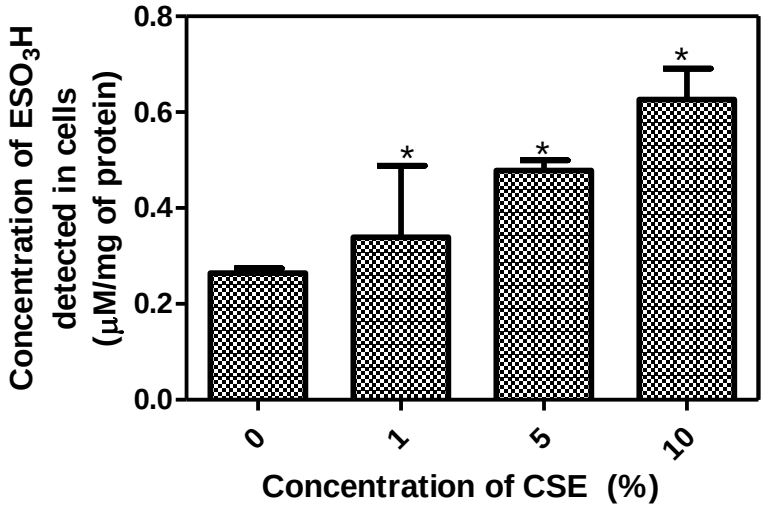

Figure 4.12: Increased concentrations of the oxidised form of ET i.e. ESO_3H was detected in the cell upon incubation with increasing concentrations of CSE (0-10%) for 24 h. Graphs represent means ± SEM (*n* = 3) and **P*<0.05.

From Figure 4.12, it can be identified that levels of ESO_3H were lower than levels quantified for ET. Further, levels of ESO_3H were significantly lower in the absence of CSE. Upon incubating with increasing CSE, a significant increase in the levels of ESO_3H was quantified. $OCTN1^{-/-}$ served as a positive control for these experiments with negligible quantities of ET and ESO_3H under all conditions of CSE.

Levels of EH failed to be detected and quantified in the cell.

4.3.4 Formation of DNP-ET *in vitro*

Formation of DNP-ET was confirmed *in vitro* by analysis of DNP-ET in knock-out OCTN1 NCI-H441. All cells were incubated with ET prior to being washed and incubated with CDNB. DNP-ET detection was significantly lower in $OCTN1^{-/-}$ compared to wildtype OCTN1 cells (Figure 4.13). When wildtype cells were incubated independently with ET and CDNB, intracellular concentration of DNP-ET increased with increasing concentration of ET.

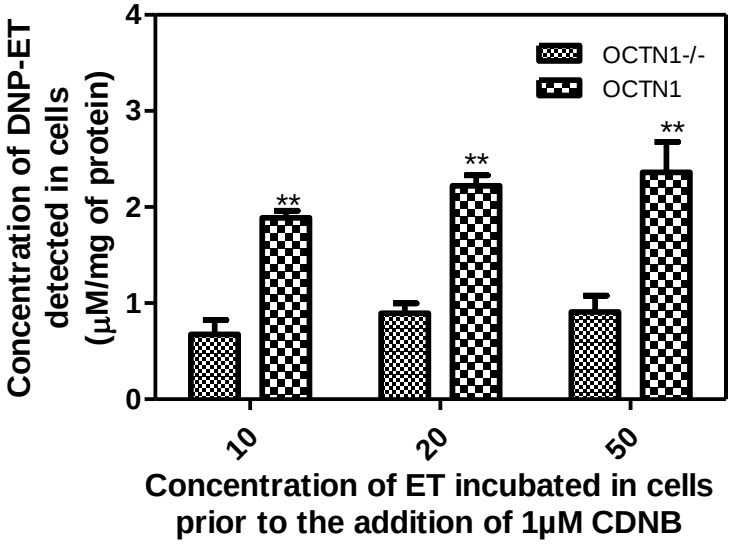

Figure 4.13: DNP-ET formation was confirmed to occur *in vitro.* Concentrations of DNP-ET were found to increase with increasing concentrations of ET (10-50 µM). Graph represents means ± SEM, (*n*= 3-6), ***P*<0.01.

To determine if GST plays a role in the formation of DNP-ET intracellularly, cells were incubated with inhibitors of GST i.e. CB and EA (Figure 4.14). At concentrations of 50 µM ET in the presence of 10 µM CDNB, only, was a significant reduction in DNP-ET formation observed intracellularly in the presence of CB. EA resulted in a decreased formation of DNP-ET over all concentrations of ET.

A)

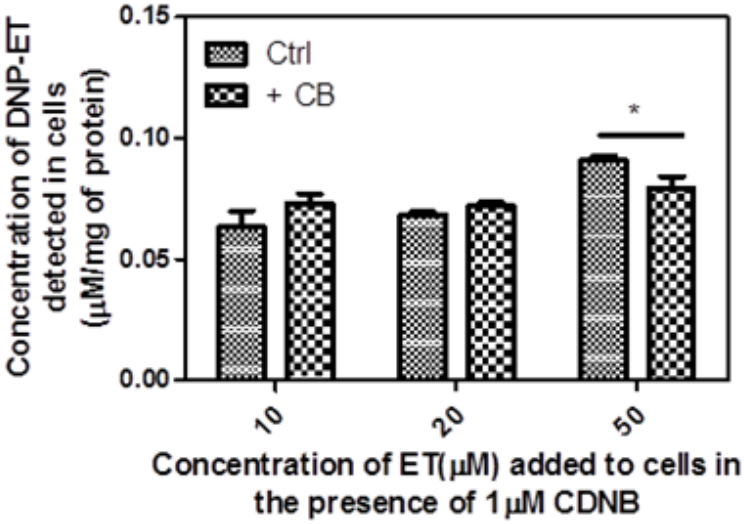

B)

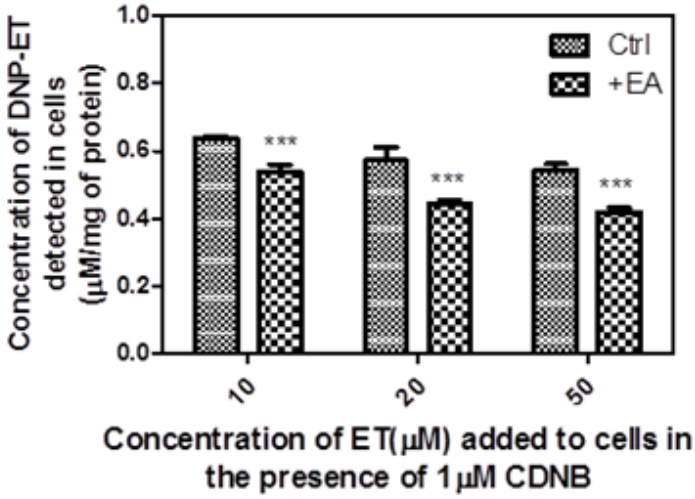

Figure 4.14: Quantification of ET-DNP in NCI-H441 cells in the presence/absence of GST inhibitors was found to decrease in the presence of GST inhibitor **A)** Cibracron Blue (CB) at high concentrations of ET (50 µM) and **B)** Ethacrynic Acid (EA) at all concentrations of ET. This suggests GST plays a role in the formation of DNP-ET. Graph represents means ± SEM, (n = 3-6), *P<0.05, ***P<0.001.

The cytotoxicity of CDNB was investigated in the presence and absence of the GST inhibitor EA, and the antioxidant ET (Figure 4.15). Cell viability decreased upon incubation with CDNB. This decline cell viability was non-significantly improved upon incubation with ET. When EA was added in combination to CDNB, a significant decrease in cell viability is observed. However, upon incubation with ET, the cell death observed for CDNB+EA was resolved, and a further significant increase in cell viability was observed compared to CDNB incubation alone.

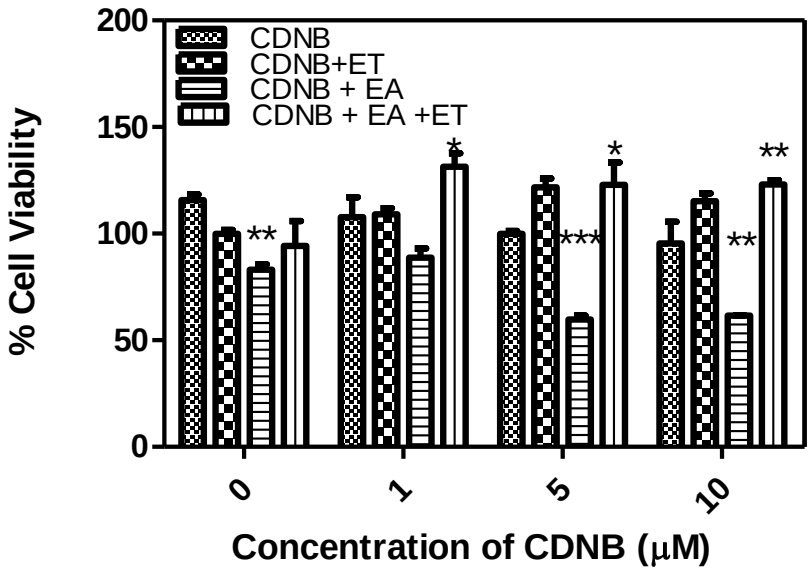

Figure 4.15: Cytotoxicity of CDNB in the presence and absence of 25 μM EA, the GST inhibitor and 250 μM ET was determined. It was determined that CDNB results in a decrease in cell viability and is improved upon incubation with ET. However, upon incubating with EA, a decrease in cell viability occurred. A significant increase in cell viability occurs when cells are incubated with CDNB, EA and ET suggesting that an alternative enzyme, other than EA may be responsible for catalysing ET for complete detoxification. Graph represents means ± SEM, (n = 6), *P<0.05, **P<0.01, ***P<0.005.

Formation of DNP-ET was measured intracellularly overtime. Concentration of DNP-ET formation peaked after 30 min incubation with ET and CDNB. Following, a drop in

concentration was observed. Hence, no such linearity in the formation of adducted was detected with time (Figure 4.16).

Therefore, DNP-ET was later detected in the supernatant of the cell overtime. With increasing time, increase concentrations of DNP-ET were detected in the supernatant of the cell (Figure 4.17).

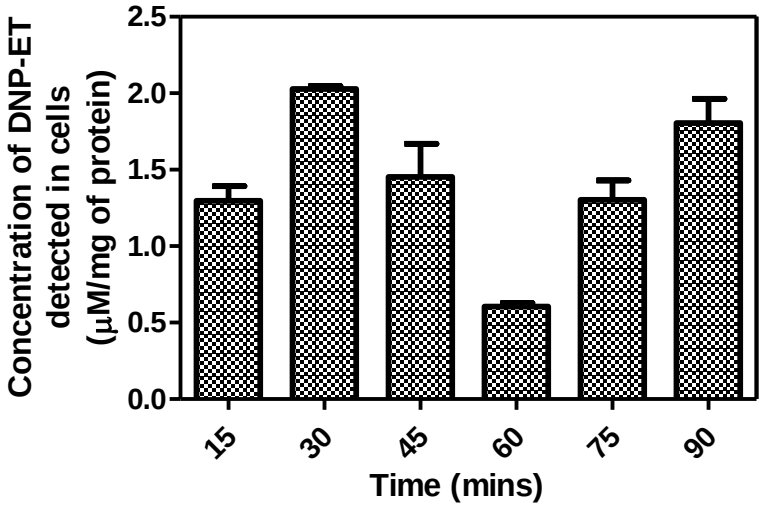

Figure 4.16: Quantification of DNP-ET was detected intracellularly by LC-MS/MS and it was found that variable concentrations of DNP-ET resulted. Graph represents means ± SEM,(*n* = 3).

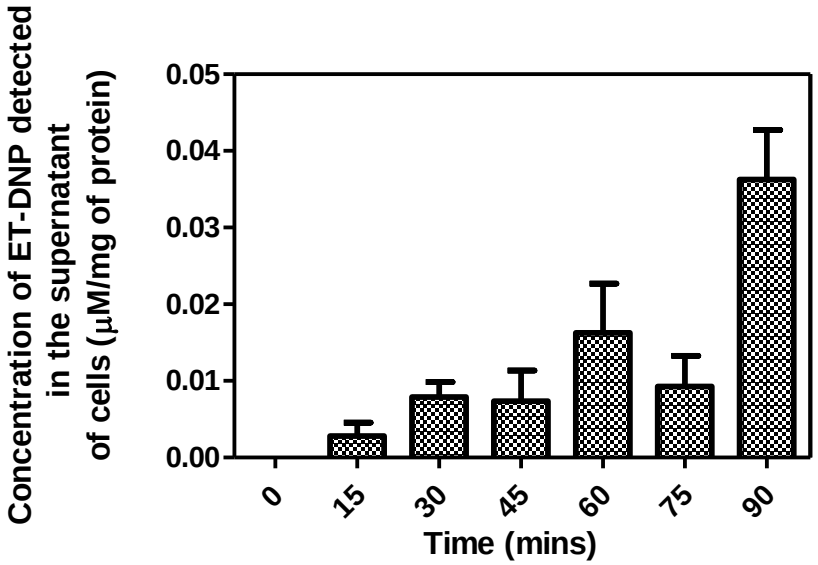

Figure 4.17: DNP-ET concentrations increased in the supernatant overtime. This demonstrates that DNP-ET is being effluxed from the cell. Graph represents means ± SEM, (*n* = 3).

To determine if MRP transporter proteins are responsible for the efflux of the DNP-ET, NCI-H441 cells were incubated with MK571, an inhibitor of MRPs. A significant decrease in DNP-ET was quantified in the supernatant of the cells when incubated with DNP-ET (Figure 4.18).

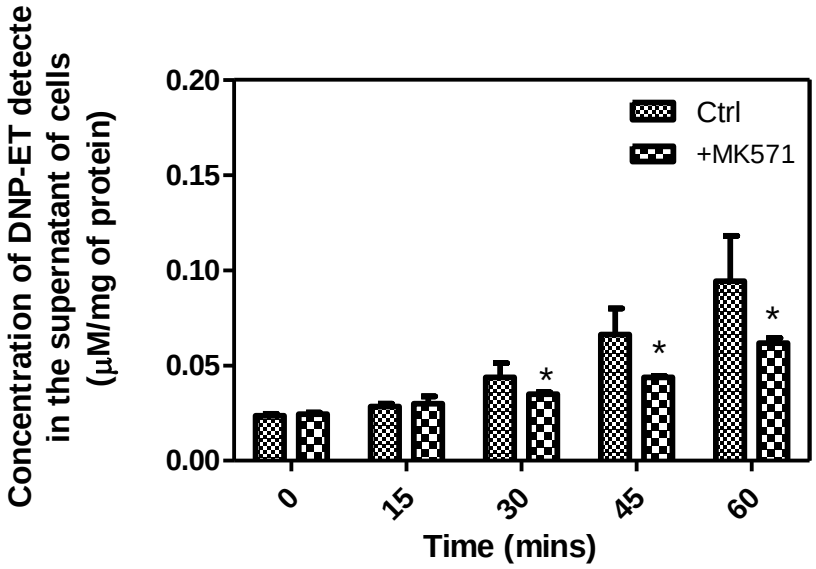

Figure 4.18: Quantification of DNP-ET detected in the supernatant overtime in the presence of the MRP inhibitor, MK-571. A significant reduction in the formation of DNP-ET occurred upon incubating with the MRP inhibitor. This would suggest that MRPs are responsible for the efflux of DNP-ET. Graph represents means ± SEM, (n = 3).

4.4 Discussion

ET is reported to behave as a potent antioxidant (*142*). However, its mechanistic pathway *in vitro* remains unexplored.

One such method to elucidate the protective role of ET *in vitro* was to monitor the oxidised states of ET. Previously, Servillo *et al.* determined that the primary oxidised products of ET were ESO_3H and EH that were produced by neutrophils during oxidative burst and quantified by MS (*149*). And so, LC-MS/MS methods specific for the successful detection of ET, EH and ESO_3H were developed and optimised. It was determined that upon incubation with increasing concentrations of CSE, the levels of ET also increased. An initial decrease in concentration of ET could be as a result of ET becoming oxidised into ESSE or other oxidised products. The subsequent increase could be hypothesised to be due to reformation of ET as a byproduct of its oxidised products as previously explained by Servillo *et al. (1).* Alternatively, previous findings of the Ehrhardt research group demonstrated the upregulation of OCTN1 in the presence of CSE. And as a result, higher levels of ET may accumulate intracellularly.

As predicted, lower levels of ESO_3H were quantified in the cell compared to levels of ET. This supports previous findings established by Servillo *et al.* (*149*). These levels were significantly lower in the absence of CSE compared to when incubated with CSE. CSE stimulated the production of ESO_3H in a concentration dependent manner.

Unfortunately, levels of EH failed to be detected intracellularly. This is likely to be due to their concentrations being lower than the LOD and could support the hypothesis that the main oxidised mechanistic pathway proposed by Servillo *et al.* is via ESO_2SE to form ESO_3H (*1*). No previous data was identified to confirm production formation ratios in order to support this theory. Further, work is required to quantitatively analyse EH production during oxidative stress.

ET shares similar cytoprotective properties to GSH. However, increased stability of ET prevents autoxidation as readily as other compounds like GSH and as a result limits the production of free radicals (*150*). Consequently, ET can only react with some sulfhydryl containing compounds (*142, 150*). Therefore, issues arise to whether ET can play a role in phase II metabolism in a similar way to GSH. Therefore, this research focuses on the mechanistic role of ET and whether it too can form bioconjugates in the cell. NCI-H441 cells were used for this analysis as it is reported to express OCTN1, the physiological transporter of OCTN1 (*73*). $OCTN1^{-/-}$ cells acted as a control to ensure formation of the adduct was occurring within the cell. It was determined that ET does react with CDNB intracellularly and that this reaction is concentration dependent on ET. This data, for the first time, has identified a possible mechanism of ET in phase II metabolism.

The reaction between CDNB and GSH has previously only been reported in the context of GST. Tang *et al.* first investigated the role of GST from Octopus digestive gland, and its role in the formation of GSH and CDNB, the prototypical substrate of GST (*151*). It was determined that GST is responsible for the promotion of proton dissociation of the GSH thiol (*152*)**.** By steady state analysis, they confirmed that this reaction occurs via SN_2 Bi Bi kinetic mechanism, meaning the substrates are in rapid and independent equilibrium with the enzyme (*151*). This was further confirmed by Labrou *et al.* who investigated the role of GST from maize, which was cloned in *Escherichia Coli* (*152*)**.** The consequence of this, is that inhibition of the enzyme by conjugates may occur non competitively (*151, 152*). The rate limiting step was confirmed to be product release from GST with the dissociation constants calculated as 1.6 mM and 2.2 mM for GSH and CDNB, respectively (*152*).

An array of GST inhibitors has previously been investigated. For this research, CB and EA are used. CB successfully inhibited DNP-ET formation only at high concentrations of ET, whereas EA was successful in the inhibition of DNP-ET formation at all concentrations of

ET. This contradicts previous findings of Wang *et al.* who identified CB to be a stronger inhibitor of GST than EA (*153*). This could suggest that an alternative enzyme is present for the formation of DNP-ET and that EA is more specific than CB, in its inhibition.

Conflicting reports currently surround the toxicity of CDNB incubation. Previously in Pacific Oyster *Crassostrea gigas* hemocytes CDNB was reported to have no effect on cell viability but contributed to levels of ROS only at high concentrations of CDNB i.e. 50 µM (*154*). However, in P388D1 macrophages, a TC_{50} value of 63 ± 6 µM was calculated for CDNB (*155*). Further, Caco2 cells were reported to result in 50% survival when incubated with 10 µM CDNB (*155*). Upon incubating NCI-H441 cells with CDNB, a reduction in cell viability of up to 30% occurred with 10 µM CDNB. Reports have found that upon incubating with both CDNB and GSH, no improvement in cell viability resulted. However, a reduction in the intracellular concentration of GSH occurred, possibly due to the formation of DNP-SG (*154*). Our results indicate a slight improvement in cell viability upon co-incubating NCI-H441 cells with CDNB and ET. Although, this improvement in cell viability was not statistically verified.

It has been reported that EA increases the sensitivity to cellular damage of HT-29 human colon adenocarcinoma cells (*156*). Further, CB incubation for 24 h has been found to reduce cell viability in adult worm and microfilariae with an IC_{50} of 0.05 mM and 0.025 mM respectively (*157*). Our results indicate that a reduction of 32% in cell viability occurs upon incubating with EA alone and this decrease in viability is further reduced when co-incubated with CDNB, by down to 55% cell viability. No reports to date have analysed the effect of co-incubation of CDNB, GST-inhibitor and GSH or specifically for this study ET. Our results indicate that a significant increase in cell viability results when incubated with CDNB, EA and ET. This could suggest that upon inhibition of GST, ET may react with an alternative

enzyme to facilitate its detoxifying conjugation reactions, which is in agreement with the hypothesis of our earlier findings.

Further, the formation of DNP-ET was monitored overtime with no trend appearing. This was identified to be due to DNP-ET being effluxed by appearing in the supernatant of the cell. Overtime, an increase in the concentration of DNP-ET in the supernatant resulted, representing a time dependent curve. Previous findings have detected GS-conjugates in the supernatant of Caco-2 cells and concluded that this too was occurring in a time dependent manner (*158*).

Previously, MRP1, 2, 3, 4 and MRP5 have been identified to be responsible for the efflux of anionic conjugates, particularly DNP-GS (*159, 160*). And so it was important to determine if MRPs were also responsible for the efflux of DNP-ET. MK-571 was previously identified to be an inhibitor of DNP-GS and GSSG across erythrocyte membranes (*160*). Therefore, cells were incubated with MK-571 and it was determined that a significant reduction in DNP-ET efflux occurs correlating to findings of Wu *et al.* Therefore, MRPs do play a role in the elimination of DNP-ET, and so further work is required to identify which transporter/s is/are responsible for the elimination of ET metabolites.

4.5 Conclusion

For the first time this research investigated the molecular action of ET. ET oxidisation to EH and ESO_3H was successfully synthesised and characterised by NMR and IR spectroscopy. It was identified that ET can become oxidised to ESO_3H intracellulary upon exposure to oxidative stress. However, no such successful detection of EH occurred, suggesting that ESO_3H to be the main oxidised product of ET oxidisation. It was further identified that ET can perform conjugation reactions similar to GSH, in an attempt to detoxify the cell through phase II metabolism. It was further determined, that GST plays a role in the formation of the adduct and that upon formation of the metabolite MRP transporters are responsible for its efflux, to complete detoxification. In conclusion, ET carries out its antioxidant properties in similar ways to that of GSH.

Chapter 5

RT-PCR analysis of transporters in NCI-H441 cell line and freshly isolated human alveolar epithelial cells in primary culture

Abstract

Membrane transporters and channels play a fundamental role in the absorption, distribution and elimination of xenobiotics and endogenous compounds. However, their expression in distal lung epithelial cells under various culture conditions remains unclear. In this study, 23 ABC, 56 SLC, 8 SLCO transporters and 3 AQP channels are investigated under AIC and LCC conditions in the NCI-H441 cell line by RT-PCR. This expression data is also compared with expression data generated from freshly isolated ATII and ATI-like human alveolar epithelial cells in primary culture. This research aims to provide evidence for the suitability of NCI-H441 cells as an *in vitro* model for the study of drug disposition at the human distal lung epithelium.

5.1 Introduction

Membrane transporters belong to the largest family of membrane proteins in humans, with over 400 members currently identified (*161*). They play a fundamental role in the absorption, distribution and excretion of xenobiotics and endogenous compounds. The activity of transporters can be examined *in vitro* using the original *Xenopus oocyte* model (*162, 163*)**,** cell lines such as HEK-293, which shares a metabolistic character similar to the original cell type (*164*) and/or Caco-2 cells, which can form tight junctions and are therefore suitable for vectorial transport studies (*165*) or isolated cell membranes or vesicles of insects, mammalian or primary cells in which the relevant transporters are over expressed. *In vivo* models can also be utilised such as rat and mice models. With the emerging genomic engineering technology like Zinc-Finger Nuclease, TALEN, CRISPR/Cas based, transgenic mice or knockout models can be generated to further study the gene of interest (*166*). *Ex vivo* models are also available and include Isolated Perfused Lung (IPL) and lung slices, which have been reported to solve deficiencies of *in vivo* and *in vitro* models and are useful in the kinetic predictions of macromolecule disposition (*167*). In combination, these models are powerful tools for the determination of kinetics of substrate transport and hence, the physiological role of transporters can be determined.

ATP-Binding Cassette (ABC) and SoLute Carrier (SLC) transporters are the largest families of transporters. ABC transporters are transmembrane proteins that are responsible for the movement of molecules in an energy dependent manner. Many of these transporters act as efflux pumps suggesting a pivotal role in the elimination of toxic compounds, important for both disease prevention and progression. MRP1 is reported to be specific for the removal of GSH. However, later studies determined MRP2, MRP3, MRP4, MRP5 and MRP7 to be also involved (*168*). This was confirmed through the inhibition of MRPs by MK-571 or through the knock-down of the transporters, resulting in an increase in cellular damage and

inflammation (*169*). ABC-transporters are abundantly expressed in the lung, of which MRP1 and BCRP (breast cancer resistant protein) are highest in bronchial epithelium. MRP1 is highly expressed on the basolateral membrane of lung epithelium (*170*) and so may assist with the efflux of noxious compounds and their metabolites from the cell into the interstitial fluid (*171*). BCRP is thought to be solely responsible for resistance against toxins and several chemotherapeutic agents. Studies carried out by van der Deen *et al.* found no expression of BCRP on alveolar macrophages and so concluded that BCRP may not play a role in the innate immune response (*171*).

SLC transporters consist of approximately 400 members belonging to 52 subfamilies. SLC22 are mostly responsible for the bidirectional transport of nutrients, metabolites, ions and drugs across cellular membranes, with SLCO primarily behaving as uptake carriers fundamental for the influx of xenobiotics for Phase I and Phase II metabolism, before elimination by ABC transporters. Without this family of transporters, cell detoxification would not occur (*172, 173*). This family of transporters are highly expressed in the kidney, liver and intestine due to its role in absorption, metabolism and elimination of compounds but also expressed at varying levels in diverse organs such as heart, brain, placenta, salivary glands, testes and lung (*172*).

Aquaporins (AQP) are ubiquitous transmembrane proteins involved in the passive transport of water, of which 13 have been identified. AQPs are homotetramers embedded in the lipid bilayer with each monomer behaving as a single channel pore. This research will focus on the expression of AQP1, AQP7 and AQP9. AQP1 investigated in human kidney epithelial cells was found to play a role in the removal of toxic wastes and high concentrations of ions that may alter the pH of the blood. Its expression was determined at both the apical and basolateral membranes of these epithelial cells (*174, 175*)**.** AQP7 and AQP9 are responsible for the transport of water, glycerol, urea and a small number of neutral solutes. However,

their exact function remains unknown. Yet, it is hypothesised that these channels may play a role in energy metabolism (*176*). Investigation into this relatively new family of transporters may provide further insight into their physiological role in detoxification and/or metabolism.

Well characterised *in vitro* models are fundamental to determine transporters' expression and their functional role. One example is the NCI-H441 adenocarcinoma cells, which resemble human distal lung epithelial cells. This cell line is advantageous as it can form polarised cells for transport studies. Cells grown under Air Interface Culture (AIC) conditions have been found to establish tight junctions and form simple monolayers representative of terminal bronchial epithelium giving rise to an *in vitro* model representative of an *in vivo* airway (*177*). And so, expression of the transporters must be investigated under AIC and Liquid Covered Culture (LCC) and to further compare these expression data with expression data obtained from human alveolar epithelial primary cells (hAEpCs) displaying an alveolar type II (ATII) and alveolar type I-like (ATI-like) phenotype. This will allow for future investigations of drug transporter function under optimal culture conditions in NCI-H441 cells.

5.2 Materials and Methods

5.2.1 Cell culture

NCI-H441 cells

Human NCI-H441 (American Type Culture Collection, HTB-174, Teddington UK) were seeded at a density of 200,000 cells/cm^2 and grown at 37°C in 5% CO_2 atmosphere in Gibco RPMI-1640 medium (Biosciences, Dun Laoghaire, Ireland) supplemented with 5% foetal bovine serum (FBS), 1% sodium pyruvate, 1% penicillin streptomycin (all from Sigma Aldrich) on Transwell Polyester Clear filters (12 mm diameter with 0.4 µm pore size, Corning). The following day, medium was exchanged for fresh medium additionally supplemented with 10 µM dexamethasone and 1X concentration of Premix Insulin Transferrin Selenium (ITS+). On day 3, medium was carefully removed with a pipette tip. For AIC, 1000 µl of medium was added to the basolateral compartment. For LCC, 1500 µl of medium was added to the basolateral compartment in addition to 500 µl added to the apical compartment. When cells reached a TEER >350 $\Omega \times cm^2$ (*88*) around approximately 6-8 days, cell were then isolated for total RNA.

Bioelectric measurements

The time of the cellular layers reaching confluence was determined by measuring transepithelial electrical resistance (TEER) as a function of days in culture. TEER was measured daily with an epithelial volt-ohm meter equipped with STX-2 electrodes (WPI, Berlin, Germany) and corrected for the background value contributed by the Transwell Clear filter and medium.

Human alveolar epithelial cells

Human alveolar type II epithelial cells were freshly isolated from non-tumour lung tissue obtained from patients undergoing lung lobectomy. The use of human material was approved by Saarland State Medical Board, Germany. Isolation of ATII cells was performed according

to a protocol adapted from Ehrhardt *et al.* (*178*). Purified ATII cells were seeded at a density of 400,000 cells/cm^2 on collagen (Sigma-Aldrich) and fibronectin (BD Biosciences) coated plastics using complete small airways growth medium (SAGM, Lonza) supplemented with penicillin, streptomycin and 1% FBS. ATII cells were either used after 24 h or after transdifferentiation into monolayers of ATI like phenotype, following 8 days of culture.

Total RNA isolation

Five-hundred microlitres of 100% Tri-reagent (Sigma-Aldrich) was added to the well plate for 5 min at 37 °C. Following, this solution was transferred to an Eppendorf tube and 100 µl of chloroform was added. The tube was inverted several times and allowed to rest for 15 min before centrifuging at 12,000×*g* for 15 min at 4°C. The top layer was transferred to a new nuclease free tube and 0.8 µl of glycogen from oyster (Fischer Scientific Ltd, Dublin, Ireland), was added to trap the nucleic acid. Two hundred and fifty microliters of isopropanol (Sigma Aldrich) was added to the tube and the sample was centrifuged at 12,000×*g* for 15 min at 4°C. The supernatant was completely removed to reveal a small white pellet, which was later washed with 500 µl of 75% ethanol (Sigma-Aldrich), followed by gentle vortexing and finally centrifugation at 7,500×*g* for 5 min at 4°C. The supernatant was completely removed and the pellet was allowed to dry at room temperature.

Fifty microlitres of nuclease free water (Fischer Scientific Ireland Ltd, Dublin, Ireland) was added to dissolve the RNA pellet. The RNA solution can be used immediately or stored at -80°C.

RNA quantification

The isolated RNA from each sample was quantified using a NanoDrop ND-1000 spectrophotometer (Fischer Scientific Ireland Ltd, Dublin, Ireland) and ND-1000 software. The optical surfaces of the instrument were cleaned with RNA free wipes and it was initialised using nuclease free water. The NanoDrop was then blanked using the elution

solution. Each sample is measured by loading 1 µl onto the lower optical platform and lowering the arm gently. The surfaces were wiped clean between each measurement. The RNA concentration was automatically calculated by the software from the absorbance at 260 nm and given as ng/µl. Purity of the sample was primarily assessed by the 260/280 ratio which was again automatically calculated by the software and should be approximately 2. A further measure of purity was the 260/230 ratio which should be approximately 2.0-2.2. These ratios serve as a rule of thumb for purity assessment. All samples were diluted to 1 µl/10 µl with nuclease free water.

5.2.2 Quantitative RT-PCR analysis of transporters expressed in NCI-H441 and hAEpCs.

Reverse transcription

RNA samples were converted to single stranded cDNA using High Capacity cDNA Reverse Transcription kit (Applied Biosystems) according to the manufacturer's protocol. The kit components were thawed on ice and for each sample; the quantities required were calculated based on the number of samples as per Table 5.1. Equal volumes of the 2x RT master mix and the diluted RNA samples (10 µl) were added to nuclease free reaction tubes, inverted several times and centrifuged at 8,000×g for 15 s.

Table 5.1: Components of High Capacity cDNA Reverse Transcription kit and volumes required per reaction.

Kit Component	Volume/Reaction (µl)
10x RT Buffer	2
25x deoxyribonucleotide triphosphate (dNTP) mix (100 mM)	0.8
10x RT random primers	2
Multiscribe™ reverse transcriptase	1
Nuclease free water	4.2
Total per reaction	**10**

The heat cycles required for reverse transcription were carried out using a Realplex^2 Mastercycler (Eppendorf UK Ltd) using the following cycles: step 1, 25°C for 10 min, step 2, 37°C for 120 min, step 3, 85°C for 5 min and step 4, 4°C until samples were collected. The cDNA samples were used immediately or stored at -20°C.

Real Time Quantitative Polymerase Chain Reaction (qPCR)

Real Time qPCR was carried out using pre-designed TaqMan Gene Expression Assays (Applied Biosystems) according to the manufacturer's protocol. The master mix including cDNA was prepared as per Table 5.2 below.

Table 5.2: Components of TaqMan gene expression assay and volumes per well.

Component	**Volume per well (µl)**
cDNA + DNase-free water	5
TaqMan universal master mix II no UNG	5
Total	**10**

Each 10 µl samples was added to each well of the pre-designed assay. Heat cycles required for PCR were run on ViiA™ 7 Real-Time PCR System and consisted of step 1, 95°C for 10 min, step 2, 95°C for 15 s, step 3, 60°C for 60 s. Steps 2 and 3 were repeated for 40 cycles and the measuring point for the reaction was set at the 60°C step.

Data Analysis

Real-Time qPCR data were analysed using realplex 1.5 software. Relative quantitation was carried out by the comparative C_T (threshold cycle) method and categorised based on their relative gene expression levels i.e. <25 high expression, 25-30 moderate expression, 30-35 low expression, >35 no expression. The gene 18S served as a positive control in all the RT-PCR reactions.

5.3 Results

5.3.1 RNA purity

All RNA obtained for these studies were of good quality as illustrated by Table 5.3:

Sample	Average A260/230	Average A260/280	Average ng/µL
P77 AIC	2.05	1.85	277.94
P77 LCC	1.98	1.78	312.6
P78 AIC	2.02	1.8	259.2
P78 LCC	2.06	1.84	884.7
P81 AIC	2.08	1.84	524.3
P81 LCC	2.05	1.84	217.4
hAEpCs AIC	2.12	1.92	146.1
hAEpCs LCC	1.99	1.81	819.2

Table 5.3: RNA purity determination and quantification by Nanodrop 1000 given as an average reading for different passages of NCI-H441 and for a single isolation of hAEpCs.

As per section 3.3.1, RNA purity was determined by the $\frac{260}{230}$ and $\frac{260}{280}$ ratios. The $\frac{260}{280}$ can indicate if there is a contaminationwith residual phenol, guanidine or other extraction reagents. This value should be approximately 1.8 to represent pure RNA.The $\frac{260}{230}$ is a secondary measure which should be between 2.0-2.2. Abnormal values to this ratio may indicate a problem with the extraction protocol or the sample.

5.3.1 RT-PCR analysis of ABC, SLC, SLCO transporters and AQP Channels

Gene Expression is represented as the respective cycle thresholds (CT), values as calculated from QuantiStudio™ Real Time PCR Software v1.1 as illustrated by the PCR trace shown in Figure 5.1.

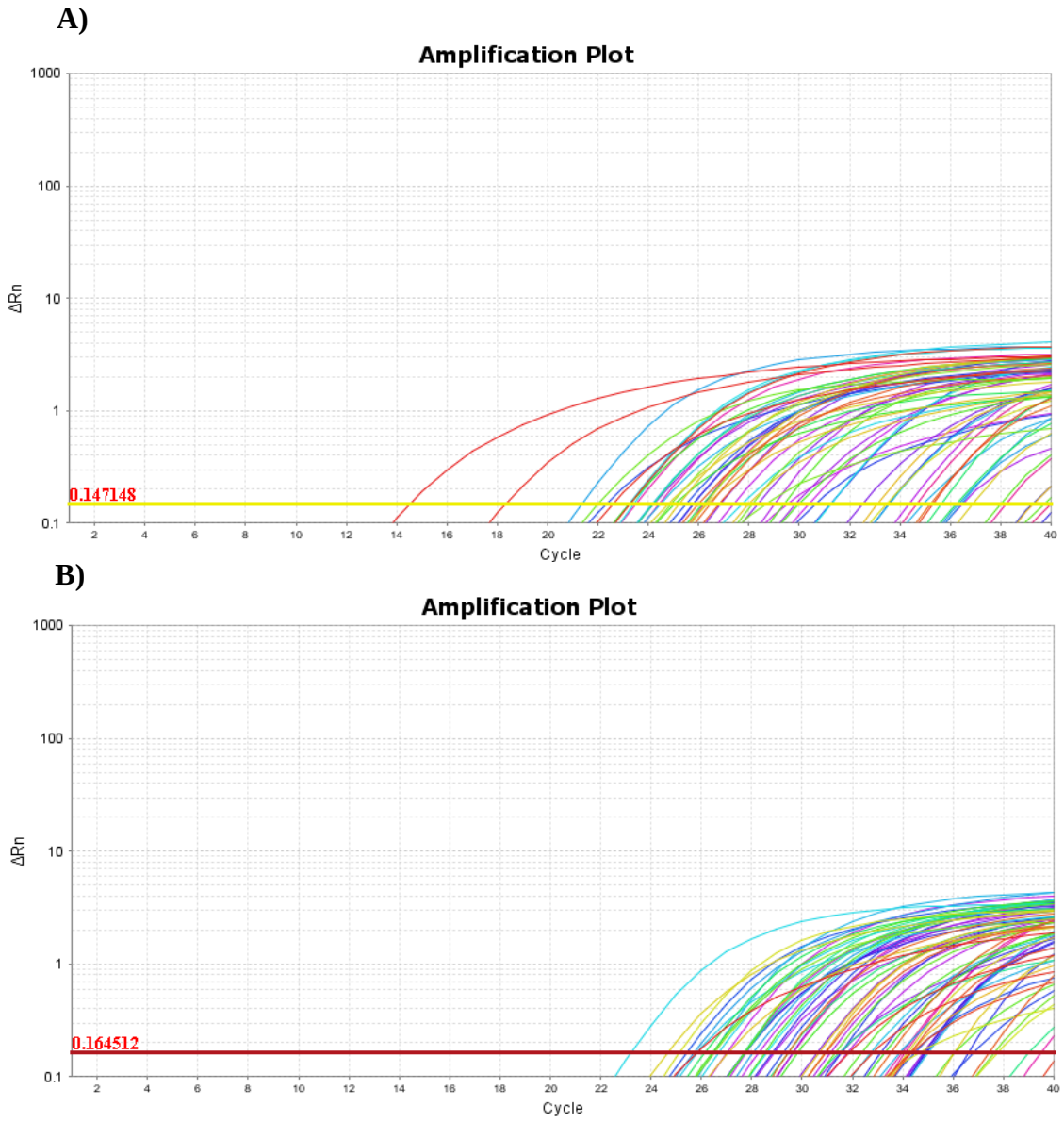

Figure 5.1: Amplification plot revealing their cycle of threshold (CT) of A) NCI-H441 cells under air interface and liquid covered culture and B) hAEpCs displaying an ATI-like and ATII phenotype. Data is calculated utilising QuantiStudio™ Real Time PCR Software v1.1.

The expression profiles for selected transporters and channels in human bronchiolar epithelium in the cell line NCI-H441 under AIC and LCC condition, and in hAEpCs with an ATII and ATI-like phenotype, were calculated by semi-quantitative RT-PCR and displayed as CT values. The gene 18S served as a positive control in all the RT-PCR reactions. Levels

of 18S were consistently detected in the highest quartile throughout all the different mRNA samples analysed as illustrated in Table 5.4

Table 5.4: RT-PCR expression profiles of selected Housekeeping Gene (18S) in the immortalised NCI-H441 cell line under AIC and LCC culture conditions and hAEpCs displaying an ATII and ATI-like phenotype. Results are displayed as CT values, where red=high expression.

Housekeeping Gene				
	NCI-H441		hAEpCs	
	AIC	LCC	ATII	ATI-like
18S	10.643	12.128	10.052	15.16484604

Table 5.5: RT-PCR expression profiles of selected ABC Transporters in the immortalised NCI-H441 cell line under AIC and LCC culture conditions and human alveolar epithelial cells displaying an ATII and ATI-like phenotype. Results are displayed as $2^{-\Delta CT}$, where red = high expression, orange = moderate expression, yellow = no expression and grey = no expression.

ABC Transporters				
	NCI-H441		hAEpCs	
	AIC	LCC	ATII	ATI-like
ABCB1	-	37.353	38.221	25.613
ABCB4	-	-		
ABCB5	-	-	-	34.486
ABCB6	27.43	26.473	34.508	34.434
ABCB11	34.81	33.411		
ABCC1	26.515	23.143	31.449	24.4
ABCC2	32.941	31.232	34.485	28.16
ABCC3	25.471	26.989	29.971	34.896
ABCC4	27.424	28.002	33.914	31.639
ABCC5	25.793	23.803	31.444	25.931
ABCC6	35.357	35.51	31.089	37.044
ABCC10	24.914	26.394		
ABCC11	34.778	33.29		
ABCC12	37.022	35.932	35.599	35.209
ABCF1	24.914	21.139	27.042	24.507
ABCG2	26.554	25.466	34.449	36.563
ABCG8	-	-	-	37.658
ATP6V0C	25.284	27.2		
ATP7A	26.34	24.867	31.534	26.597

ATP7B	28.174	23.549	35.694	32.747
MVP	23.401	21.532	27.091	25.433
TAP1	27.694	25.789	29.971	25.86
TAP2	25.803	25.046	31.201	26.8

Table 5.5 illustrates the expression profiles of ABC transporter mRNA in NCI-H441 cells cultured under AIC or LCC conditions and hAEpCs with an ATII and ATI-like phenotype.

The majority of ABC transporters were found to be detected at a moderate-high level in NCI-H441 cells. A change in gene expression of 5/23 of transporters occurred, when comparing AIC to LCC condition. Four transporter genes resulted in an increased expression from moderate to high levels under LCC such as, *ABCC1*, *ABCC5*, *ATP7A*, *ATP7B*, and only *ABCC10* resulting in an increase in expression under AIC condition (high to moderate). The remaining ABC transporters resulted in no difference in expression under culture conditions. In hAEpCs, 12/19 ABC transporters investigated changed expression during transdifferentiation from ATII to ATI-like. Eight of which increased their expression profiled in an ATI-like phenotype with 4 decreasing their expression in an ATI-like phenotype, compared with an ATII. The remaining transporters presented no difference between the two phenotypes. When comparing NCI-H441 cells under LCC with hAEpCs a striking difference in five transporters were detected i.e. *ABCC1*, *ABCC5*, *ATP7A*, *ATP7B.* All genes were highly expressed in NCI-H441 cells with only a low expression level detectable in ATII cells. *ATP7B* was stastically different under both ATII and ATI-like phenotypes compared to NCI-H441 LCC cells.

Table 5.6: RT-PCR expression profiles of selected SoLute Carriers (SLC) in the immortalised NCI-H441 cell line under AIC and LCC culture conditions and human alveolar epithelial cells displaying an ATII and ATI-like phenotype. Results are displayed as CT, where red = high expression, orange = moderate expression, yellow = no expression and grey = no expression.

SLC Transporters				
	NCI-H441		hAEpCs	
	AIC	LCC	ATII	ATI-like
SLC2A1	24.156	22.389	29.685	27.13
SLC2A2	-	-	-	24.918
SLC3A1	35.993	35.32	33.319	34.786
SLC3A2	22.191	21.422	27.398	-
SLC5A1	36.158	36.433	33.156	-
SLC5A4	-	-	-	-
SLC5A7	35.047	35.544	35.243	-
SLC6A1	-	-	35.095	-
SLC6A2	-	-	-	-
SLC6A3	23.84	34.103	-	-
SLC6A4	-	-	-	-
SLC6A6	29.39	-	-	-
SLC7A5	21.566	24.44	29.279	-
SLC7A6	25.731	26.273	26.744	27.305
SLC7A7	28.327	30.18	26.214	24.162
SLC7A8	32.016	30.234	33.148	21.765
SLC7A9	36.019	35.54	30.378	-
SLC7A11	25.824	30.36	34.568	31.361
SLC10A1	36.944	-	-	34.249
SLC10A2	-	38.632	-	34.671
SLC15A1	36.259	-	35.613	36.464
SLC15A2	29.952	27.765	28.23	25.836
SLC16A1	29.473	30.262	31.645	30.357
SLC16A2	-	-	35.209	37.013
SLC16A3	23.995	25.855	32.665	32.015
SLC19A1	24.797	22.412	29.534	23.983
SLC19A2	26.469	27.473	27.325	32.608
SLC19A3	-	37.87	30.161	27.369
SLC22A1	34.896	34.266	33.99	34.871
SLC22A2	-	-	-	34.96
SLC22A3	34.15	32.346	26.937	26.436
SLC22A4	35.263	-	35.438	35.598
SLC22A5	29.344	26.874	30.266	24.989
SLC22A6	36.464	-	-	36.697
SLC22A7	-	-	-	34.385
SLC22A8	-	-	-	33.086

SLC22A9	-	-	-	33.92
SLC23A1	34.686	34.495	35.377	-
SLC23A2	27.031	27.152	28.849	29.487
SLC25A13	24.144	23.118	29.935	-
SLC28A1	36.113	-	36.909	28.118
SLC28A2	37.661	-	-	29.169
SLC28A3	31.698	30.952	30.381	34.906
SLC29A1	24.101	23.013	28.143	37.613
SLC29A2	27.081	29.154	28.836	24.125
SLC29A3	27.537	25.19	31.757	24.897
SLC29A4	30.632	29.468	32.463	-
SLC31A1	25.147	25.137	27.352	32.117
SLC38A2	24.167	27.54	26.075	26.398
SLC38A5	34.682	35.129	33.356	23.954
SLC44A1	24.431	22.589	28.851	24.259
SLC44A2	24.275	21.019	28.164	24.199
SLC44A3	26.415	25.434	28.4	22.141
SLC47A1	-	-	30.627	24.058
SLC47A2	37.036	-	37.627	27.462

Approximately 20% of SLC transporters were of the highest transporter genes expressed in NCI-H441 cells including; *SLC2A1*, *SLC3A2*, *SLC7A5*, *SLC16A3*, *SLC19A1*, *SLC25A13*, *SLC29A1*, *SLC38A2*, *SLC44A1*, *SLC44A2*, *SLC44A3*. Of this group of transporters, 9/56 changed expression under different culture conditions, only 1 of which resulted in an increase in expression under LCC: *SLC29A4*. The remaining transporters resulted in an increase expression under AIC conditions i.e. *SLC6A3*, *SLC6A6*, *SLC77A7*, *SLC7A11*, *SLC16A1*, *SLC16A3*, *SLC29A4*, *SLC38A2*, *SLC38A5*. The remaining SLC transporters resulted in no difference in expression under culture conditions. Fifty-four SLC transporters were investigated in hAEpCs, of which 12 were detected in high expression when displaying an ATI-like phenotype, i.e. *SLC2A2*, *SLC3A2*, *SLC7A5*, *SLC7A8*, *SLC22A5*, *SL29A1*, *SLC29A3*, *SLC31A1*, *SLC38A5*, *SLC47A1*, *SLC47A2*. Thirty-one of the fifty six transporters have altered expression. The majority displayed an increased expression when displaying an ATI-

like phenotype. The remaining SLC transporters were determined to show no difference in expression regardless of phenotype. Thirteen of this group of transporters tested displayed significant differences in expression when comparing NCI-H441 cells under LCC conditions and hAEpCs, all of which were displaying an ATI-like phenotype. Eight of these were more highly expressed in ATI-like cells i.e. *SLC2A2, SLC7A7, SLC7A8, SLC28A1, SLC28A2, SLC38A5, SLC47A1, SLC47A2.* The remaining 5 were more highly expressed in NCI-H441 cells under LCC conditions i.e. *SLC3A2, SLC7A5, ALC25A13, SCL29A1, SCL29A4.*

SLCO transporters were also investigated, none of which were detected in the high quartile range. Of the 8 SLCO transporters investigated, two increased expression under LCC conditions, i.e. SLCO1B1 and SLCO1B3 with only *SLCO4C1* increasing in expression under AIC conditions. Eight SLCO transporters were investigated in hAEpCs with only one transporter of this family expressed at a higher level under an ATII phenotype, i.e. *SLCO1A2*. *SLCO2A1* were detected at higher levels under an ATI-like phenotype. The remaining SLCO transporters represented no change under the different phenotypes.

Table 5.7: RT-PCR expression profiles of selected SoLute Carrier Organic anion (SLCO) genes. Transporters in the immortalised NCI-H441 cell line under AIC and LCC culture conditions and human alveolar epithelial cells displaying an ATII and ATI-like phenotype. Results are displayed as CT, where red = high expression, orange = moderate expression, yellow = no expression and grey = no expression.

SLCO Transporters				
	NCI-H441		**hAEpCs**	
	AIC	**LCC**	**ATII**	**ATI-like**
SLCO1A2	-	-	32.3	-
SLCO1B1	-	34.353	-	-
SLCO1B3	38.06	34.902	35.198	-
SLCO2A1	33.772	33.739	33.227	28.477
SLCO2B1	39.442	-	35.155	-
SLCO3A1	33.194	32.27	27.946	28.367
SLCO4A1	28.236	27.873	35.215	-
SLCO4C1	30.264	-	-	-

Table 5.8: RT-PCR expression profiles of selected Aquaporin (AQP) Channels in the immortalised NCI-H441 cell line under AIC and LCC culture conditions and human alveolar epithelial cells displaying an ATII and ATI-like phenotype. Results are displayed as CT, where red = high expression, orange = moderate expression, yellow = no expression and grey = no expression.

AQP Channels				
	NCI-H441		**hAEpCs**	
	AIC	**LCC**	**ATII**	**ATI-like**
AQP1	33.33	21.508	24.97	24.285
AQP7	-	23.409	-	39.442
AQP9	-	25.803	33.955	36.992

Finally, 3 aquaporins were selected for this analysis including *AQP1*, *AQP7* and *AQP9*, all of which were highly expressed only under LCC conditions. A reduced expression was observed in all three transporters under AIC culture. Further, *AQP1* was expressed at high levels in hAEpCs with no expression of *AQP7* occurring in ATII hAEpCs and moderate expression occurring in ATI-like phenotype. *AQP9* was moderately expressed in hAEpCs.

5.4 Discussion

The functional role of many transporters remains unclear. Previously, Grainger *et al.* determined Calu-3 cells under AIC to display a more morphological similar phenotype to airway epithelium than LCC cells (*179*). This research aimed to provide NCI-H441 as a suitable *in vitro* model for the investigation of transporter activity in distal lung by studying the expression of various transporters under AIC and LCC conditions and comparing this to their expression in an ATII and ATI-like phenotype of human alveolar epithelial primary cells (hAEpCs). The expression of 23 ABC, 56 SLC, 8 SLCO transporter and 3 AQP channel genes were examined. Genes were selected based on their potential roles in the detoxification of xenobiotics or endogenous compounds. Where blanks occur in tables is as a result of an error in manufacturing of plates.

Expression analysis of ABC transporters by RT-PCR.

ABC transporters are expressed in all tissue types due to their ability to transport a wide variety of substrates across biological membranes in an energy dependent manner (*171*).

ABCB1 that codes for the multi-drug resistance protein MDR1, otherwise known as P-glycoprotein (P-gp) plays a role in cellular defence (*180*). It is apically expressed in organs involved in excretion (*181*). In the lung this transporter is expressed on ciliated epithelium or collecting ducts and on apical and lateral surfaces of serous cells of bronchial glands but not in goblet cells (*182*). Strong expression of the transporter was detected in trachea and bronchi whilst smaller bronchi expression of P-gp is absent or patchy (*182*). Endter *et al.* by RT-PCR determined low-moderate expression in primary human bronchial epithelial cells (hBEpC) and ATII and ATI-like cells, with no-high expression in the cell lines Calu-3, 16HBE14o-, BEAS-2B, A549 and Caco-2 (*183*). This was in parallel with findings of Salomon *et al.* who further determined no difference in gene expression when cultured under AIC or LCC**.** In comparison, Bleasby *et al.* detected low expression of P-gp in human lung tissue by gene

array with Campbell *et al.* determining expression of P-gp only in ATII cells by RT-PCR (*171, 184*). Sakamoto *et al.* reported no expression of MDR1 in the cell line NCI-H441 by LC-MS/MS (*185*). However, our studies suggest that no change in expression occurs under culture conditions of AIC and LCC in NCI-H441 cells. In hAEpC with an ATII phenotype, no expression of *ABCB1* was determined, with this expression increasing to moderate levels when displaying an ATI-like phenotype. This is in contradiction to findings of Endter *et al.* who found a higher expression of *ABCB1* in ATII rather than ATI-like cells (*183*).

RNA quantification of the gene encoding MDR3 (*ABCB4)* was absent in cell lines detected by van der Deen *et al.,* with further evidence concluding that it is absent in human and mouse lung and trachea (*171, 186, 187*)**.** However, Courcot *et al.* did detect low expression of *ABCB4* by RT-PCR in the cell line NCI-H727 and lung tissue of humans (*188*)**.** Our results detected no expression of *ABCB4* in NCI-H441 cells when cultured under AIC or LCC conditions. However, expression of the transporter was detected at moderate levels in hAEpCs displaying an ATI-like phenotype.

A role of *ABCB5* in glycolysis modulation in melanoma cells has been reported (*189*)**.** Previously, Courcot *et al.* failed to detect any expression of *ABCB5* in any immortalised cell line or lung tissue (*188*). This research failed to detect any transcript expression of the transporter in NCI-H441 cells regardless of culture conditions. However, in hAEpCs of an ATI-like phenotype, detection of the transporter was detected at low levels.

A protective role of the *ABCB6* orthologue in heavy metal tolerance in *C. elegans* has previously been reported (*190*)**.** Moderate-high expression of *ABCB6* was detected in all cell types and lung tissue detected by Courcot *et al.* (*188*). Our analysis confirmed these findings, with expression detected at moderate levels in NCI-H441 cells regardless of culture conditions and a lower expression in hAEpCs displaying an ATII or ATI-like phenotype.

Detection of *ABCB11* in lung tissue has not been reported on. *ABCB11* has been found to play a role in bile transport and weak detection has been reported in hepatocytes (*66*)**.** For the first time, our research indicated low expression of the transporter in NCI-H441 cells regardless of culture conditions. The transporter was not analysed in primary cells.

Previous reports investigating primary and immortalised cell types; human bronchial epithelial primary cells (hBEpCs), ATII and ATI-like cells, 16HBE14o-, BEAS-2B, Calu-3, Caco-2 and A549 cells, indicated that no-low expression of *ABCC4* and *ABCC11* with low-moderate expression of *ABCC2* and *ABCC6* and moderate-high expression of *ABCC1, ABCC3* and *ABCC10. ABCC5* displayed varying degrees of expression over all cell types (*171, 183*). Various expression profiles of *ABCC12* have not yet been reported on. *ABCC4,* ABCC6, *ABCC11, ABCC12,* displayed no change in expression when cultured under AIC or LCC. An upregulation of *ABCC1, ABCC2* and *ABCC5* occurred when cultured under LCC conditions with an upregulation of *ABCC3* and *ABCC10* when cultured under AIC conditions. Interestingly, a striking change in expression is observed for *ABCC1* and *ABCC5* when directly comparing NCI-H441 under LCC conditions and hAEpCs displaying low expression in ATII phenotype. Even though, *ABCC2* expression was not detected in human lung tissue by Bleasby *et al*. (*184*), moderate expression of the transcript was detected by Endter *et al.* and Van der Deen *et al.* Endter *et al.* previously determined a decrease in expression of *ABCC2* in ATI-like cells compared to ATII like cells (*183*). However, our research indicates that in hAEpCs an increase in expression of *ABCC2* occurred in ATI-like, with only a significant increase in expression observed in *ABCC1* when cultured under ATI-like conditions.

ABCF1 is unique to the ABC family of transporters as it lacks the characteristic transmembrane domain and has been found to be a risk gene for autoimmune diseases such as pancreatitis and arthritis (*191*). It is hypothesised to play a role in the innate immune response

by interacting with eukaryotic translation initiation factor 2 (eIF2). Further, in *ABCF1*$^{-/-}$ Hela cells, it was determined that a significant reduction in general protein synthesis occurred (*192*). *Abcf1* was detected in adult mouse lung by Northern blot and was expressed at high levels similar to that of liver, small intestine, retina and cerebral cortex. Our studies have indicated for the first time, high expression of *ABCF1* in NCI-H441 cells. This expression level was similar to hAEpCs under an ATI-like phenotype with moderate expression detected in ATII cells. Therefore, future work is required to further elucidate the role of *ABCF1* particularly in the lung.

ABCG2 responsible for the coding of the BCRP, which is involved in resistance against toxins (*171*). Detection of the protein has been determined to be lower than P-gp or MRP1 but has been localised to the epithelial cell layer and in seromucinous glands (*186, 193*). Van der Deen *et al.* detected moderate-strong expression of BCRP in solid lung tumours. High detection of *ABCG2*/BCRP was identified in all immortalised lung cell lines excluding BEAS-2B and NCI-H727 (*185, 188*). Sakamoto *et al.* determined that BCRP was undetectable in human alveolar tissue with quantification only in the bronchiolar epithelium (*185*). Our results confirmed findings of Sakamoto *et al.* whereby moderate expression of *ABCG2* was detected in NCI-H441 cells. However, no-low expression of *ABCG2* was detected in hAEpCs under an ATII and ATI-like phenotype, respectively. This was in contradicion to findings of Endter *et al.* (*183*) but in line to studies carried out by Nickel *et al.* no change in expression of BCRP occurred between different culture conditions of NCI-H441 cells, with a decrease in expression occurring during transdifferentiation of hAEpCs (*194*)**.**

No detection of *ABCG8* was determined in NCI-H441 cells. This confirms findings of Courcot *et al.* who failed to identify any expression in 11 immortalised lung cell lines and 4 types of human lung tissue (*188*).

The functional role of *ATP6V0C* remains unclear. It is thought to be involved in mediating the acidification of eukaryotic intracellular organelles (*195*). Courcot *et al.* investigated its expression in a range of lung cell models and found very high expression in all (*188*). Our findings confirm moderate expression of this gene in NCI-H441 cells. This transporter was not investigated in primary cells but could be a potential candidate for monitoring the acidity of the cell caused by inflammatory diseases.

ATP7A and *ATP7B* have also been identified by Courcot *et al.* to be moderately expressed in lung cell models and human lung tissue (*188*). These 2 transporters are required for copper homoeostasis which is fundamental for the reduction of oxidative stress. Our findings confirm the presence of these transporters in NCI-H441 cell line and suggest that both gene expression levels are dependent on cell conditions, i.e. under AIC conditions a lower expression is detected. An increase in expression occurred when transporters were investigated under ATI-like phenotypes compared to ATII with no expression of *ATP7B* when displaying an ATII phenotype. And so, when directly comparing these two genes under LCC conditions in NCI-H441 cells and in hAEpCs displaying an ATII phenotype, a dramatic change in expression is observed.

The Major Vault Protein (MVP) was investigated in normal human lung tissue**.** It was determined to play a role in the protection against toxic substances. Scheffer *et al.* detected strong expression in the cytoplasm of bronchiole and bronchiolar epithelium (*186*). Further, Courcot *et al.* also determined high expression in all lung models tested (*188*). Our findings are similar with high and moderate expression of *MVP* detected in NCI-H441 and hAEpCs, respectively, regardless of culture conditions or phenotype.

Transporters associated with antigen processing; *TAP1* and *TAP2* were also investigated. These transporters are essential for the delivery of antigen peptides into the lumen of the endoplasmic reticulum, which will form assemblies with Major Histocompatibility

Complexes (MHC) for initiation of T lymphocytes (*196*)**.** Previously, it has been identified that low expression of *TAP1* and *TAP2* are found in A549 and NCI-H1355 with higher expression of *TAP1* in 16HBE14o- (*188*). Our results indicated that moderate expression of *TAP1* and *TAP2* in NCI-H441 cells occurred. Following, hAEpCs were also investigated for *TAP1* and *TAP2* expression and found to also be moderately expressed with only *TAP2* expressed at low levels when displaying an ATI-like phenotype.

Expression analysis of SLC transporters by RT-PCR

The expression of 56 SLC transporter genes in NCI-H441 cells and hAEpCs were investigated. Although the role of this family of transporters is primarily in the uptake of small molecules (*184*)**,** these transporters are highly expressed in organs responsible for the elimination of xenobiotics and endogenous compounds such as kidney and liver (*197, 198*)

SLC2 genes code for GLUcose Transporters (GLUT) for which there are 14 expressed in humans (*199*). All have been found to transport hexoses/polyoles yet their primary substrates remain unknown (*199, 200*). GLUT1 (*SLC2A1)* functions in the primary transport of glucose but transport of mannose, galactose, glucosamine and reduced ascorbate also can occur (*200*). Highest expression of this gene, have been found in human erythrocyte membranes (*199*). It is believed glucose is in equilibrium with blood serum and red cell cytoplasm to ensure optimum concentrations accumulate intracellularly (*199*), as glucose is essential for cellular oxidation, metabolism, growth, surfactant synthesis, differentiation and host defence (*201*). Courcot *et al.* detected high expression of *SLC2A1* in all cell lines tested, which is similar to our findings in NCI-H441 cells. In hAEpCs, moderate expression is detected regardless of cell type. GLUT2 (*SLC2A2*) was first studied in human and rat liver. Although GLUT2's main function is to transport glucose, it has been determined to have a low affinity for the transporter (K_m=17 mM) with a higher affinity for glucosamine (K_m 0.8 mM) (*202*). In the

intestine epithelium, GLUT2 has been reported to be localised to the basolateral membrane (*203, 204*). No such studies have been reported for GLUT2/*SLC2A2* in lung epithelium. In NCI-H441 cells, it was determined that no expression of the transporter was present. However, high expression of the transporter was detected when cells displayed an ATI-like phenotype in hAEpCs, which is strikingly different to the expression observed for NCI-H441 cells.

SLC5 genes are responsible for the coding of Sodium coupled GLucose Transporters (SGLT), which are vastly studied for intestinal absorption and renal reabsorption of glucose (*205*). *SLC5A1* has a high affinity and low capacity for glucose when studied for its reabsorption in the small intestine (*205*). *SLC5A4* is specific for reabsorption of mannose and *SLC5A7* a specific importer of choline required for acetyl choline synthesis. Quantification of *SLC5A7* was performed by Courcot *et al.* where low expression was detected in A549, Calu-1, NCI-H292, NCI-H727 and HBEC cell lines and low expression detected in the all human lung tissue types investigated by RT-PCR (*188*). In our studies performed on NCI-H441 cells, no expression was detected of these genes. *SLC5A1* was detected at low levels only in hAEpCs displaying an ATII phenotype.

Genes *SLC3* and *SLC7* are responsible for the transport of amino acids (*206*)**.** *SLC3* are responsible for the translation of Heteromeric Amino acid Transporters (HAT), which function in the transport of a broad spectrum of substrates that are crucial in renal and intestinal re-absorption and cell redox balance (*206*). Previously, *SLC3A1* was detected in moderate and low levels in A549 and Calu-1 cells, respectively (*188*). Our results indicated that NCI-H441 did not express *SLC3A1*, with low expression detected in hAEpCs. In comparison, *SLC3A2* was expressed at high levels in all cell types explored by Courcot *et al.* (*188*). Similarly, high expression was detected in NCI-H441 regardless of culture conditions. Further, moderate expression was detected in hAEpCs displaying an ATII phenotype with no

expression detected in an ATI-like phenotype, indicating a striking difference to the expression observed in NCI-H441 cells.

SLC7 transporters can be categorised into two groups i.e. Cation Amino acid Transporter (CAT) and L-Type Amino Acid Transporter (LAT). CAT transporters do not require energy for the entry and efflux of cationic amino acids, specifically L-arginine, which is required for the synthesis of NO (*206*). Our research focuses on LATs (*SLC7A5-9, SLC7A11).* This group of transporters are also called glycoprotein associated amino acid transporters. *SLC7A5* is involved in the sodium independent transport of neutral amino acids and are found in the microvessels of the central nervous system (CNS). *SLC7A6*, *SLC7A7* and *SLC7A8* are responsible for the sodium independent transport of cationic amino acids or large amino acids and are detected in the basolateral membranes of the lung. *SLC7A9* similarly transport cationic amino acids and large neutral amino acids, however no detection has yet to be confirmed in the lung. Finally, *SLC7A11* is responsible for the transport of small neutral amino acids and have also been detected in the lung. Courcot *et al.* detected low-high expression of *SLC7A5, SLC7A6* and *SLC7A11*. *SLCA7* was only detected in low-moderate levels in A549, Calu1, NCI-H292, NCI-H727, HBEC and all human lung tissue tested (*188*). *SLC7A8* failed to be detected in cell lines NCI-L132 and NCI-H358. *SLC7A9* was not investigated (*188*). All *SLC7* genes tested were detected in NCI-H441 cells with the exception of *SLC7A9. SLC7A7* and *SLC7A11* genes varied their expression depending on culture conditions with highest expression detected under AIC conditions. In hAEpCs, *SLC7A7, SLC7A8* generated a higher expression when displaying an ATI-like phenotype, especially *SLC7A8.* In comparison *SLC7A5* and *SLC7A9*, stimulated a decrease in expression under an ATI-like phenotype, particularly, *SLC7A5*. *SLC7A5, SLC7A7, SLC7A8* were markedly different in expression when comparing NCI-H441 cells under LCC conditions to hAEpCs only under an ATI-like phenotype.

SLC6 genes belong to about 20 structurally related symporters, that use a transmembrane electrochemical gradient to import substances mainly amino acids to which some are neurotransmitters (*207*). *SLC6A1* belongs to the transporter family Gamma Amino Butyric Acid (GABA) Transporters (GAT1), which are responsible for the regulation of GABA levels in the CNS (*208*). *SLC6A2* is responsible to the coding of the sodium and chlorine dependent Norepinephrine Transporter (NET). NET has also been found to uptake dopamine, however Dopamine Transporter (DAT), encoded by the gene *SLC6A3* is specific for this purpose**.** *SLC6A4* is responsible for the coding of the Serontonin Reuptake Transporter (SERT). Both NET and SERT have been detected by immunohistochemistry on the abluminal, and abluminal and luminal membranes of brain capillaries in mouse cerebral cortex (*209*). Detection of NET has been reported, although limited, in the lung (*210*). Decreased levels of SERT have been detected in inflamed mucosa lining of the intestine in comparison to healing mucosa and so is associated with Irritable Bowel Syndrome (IBS) and Inflammatory Bowel Disease (IBD) (*211*)**.** *SLC6A6* is responsible for the coding of the sodium and chloride dependent Taurine Transporter (TAUT). Prior to findings by Courcot *et al.* detection of these transporters in the lung had not been recorded, except for NET (*SLC6A2)* (*188*). Courcot *et al.* investigated the expression of *SLC6A3* and *SLC6A4* (*188*). *SLC6A3* was determined at low levels in 1HAEo- cells but also in squamous cell carcinoma and adenocarcinoma tissues (*188*)**.** *SLC6A4* remained undetected in the cell lines tested but was expressed at low levels in all lung tissue tested (*188*). Our studies identified expression of *SLC6A3* and *SLC6A6* in NCI-H441, with the latter only detected when cultured under AIC. *SLC6A3* decreased expression significantly when cultured under LCC. *SLC6A1, SLC6A2, SLC6A4* failed to be detected. All transporters of this family were undetectable in hAEpCs.

The SLC10 family is comprised of influx transporters of bile acids, steroidal hormones and various drugs and substances (*212*). *SLC10A1* and *SLC10A2* code for the proteins sodium-taurocholate co-transport peptide (NTCP) and apical sodium dependent bile acid transport (ASBT), respectively, hence this group of transporters are also known as the sodium bile salt co-transport family. Limited literature is present surrounding evidence of both these transporters in lung tissue. Courcot *et al.* was unable to detect any presence of mRNA of either transporter in the lung models and human lung tissues investigated (*188*). Our research is comparable with these findings with no detection of this family possible in NCI-H441 cells. However, in hAEpCs expression of both *SLC10A1* and *SLC10A2* were detected at low levels when in an ATI-like phenotype. This could suggest a preference of the transporter for alveolar cells rather than bronchiolar cells.

Members belonging to *SLC15* family play a role in the renal reabsorption of di or tripeptides and related drugs (*184*). Expression in the lung was quantified by LC-MS/MS of PEPT1 and PETP2 encoded by *SLC15A1* and *SLC15A2,* respectively in bronchiolar cultured human lung cells, with no detection in the cell lines tested by Sakamoto *et al.* (*185*). Gene expression for the transcripts too was absent from cell lines tested by Courcot *et al.* with few exceptions (*188*). *SLC15A1* was expressed at low levels in NCI-H727 and 16HBE14o^{-} with low expression also detected in all lung tissue except pulmonary parenchyma tested by Courcot *et al.* (*188*). *SLC15A2* was expressed at low levels in 16HBE14o^{-}, NCI-H292 with moderate expression also detected in all lung tissue (*188*). Endter *et al.* detected low to high expression of both genes in cell lines; Calu-3, 16HBE14o-, BEAS-2B, A549 and Caco-2 cells (*183*). *SLC15A1* failed to be detected in NCI-H441 cells either under AIC or LCC conditions and hAEpCs. *SLC15A2* was detected at moderate expression levels under AIC and LCC, in NCI-H441 cells and in hAEpCs. Findings of Groneberg *et al.* and Lu and Klassen *et al.* were able to confirm high expression of PEPT2 in lung tissue (*213, 214*)**.**

SLC16 codes for the family of monocarboxylate transporters (MCT), that have been localised to the chromosome 1p12 (*215*). Little evidence has been reported regarding this family in the lung. *SLC16A1* is associated with transport defects of erythrocyte lactate resulting in an acidic intracellular environment (*216*)**.** They reported this transporter to be proton dependent and located on the apical membranes of epithelial cells of the gastrointestinal tract (*216*). Courcot *et al.* only investigated *SLC16A1* and found high expression in cell models and lung tissues investigated (*188*). Our studies identified moderate and low expression of *SLC16A1* in NCI-H441 cells, when cultured under AIC and LCC conditions, respectively. Moderate expression of this gene was detectable in hAEpCs. No expression was detected for *SLC16A2* in NCI-H441 cells or hAEpCs. Finally, high expression of *SLC16A3* was detected in NCI-H441 cells when cultured under AIC conditions with moderate expression under LCC conditions and low expression in hAEpCs, with no change occurring with cell phenotype.

SLC19A1 belongs to the reduced folate carrier (RFT) (*217*)**,** where its function was first determined in rat brush border of jejunum epithelial cells (*218*)**.** Here, it was determined to be an organic anion antiporter that utilised high transmembrane organic phosphate gradients for active transport of folate (*217, 218*). Kawami *et al.* confirmed its mRNA expression by Northern blot in A549 cells (*218*). However it was later confirmed that human lung tissue has higher expression of the transcript than A549 (*218*). This was confirmed by Courcot *et al.* and detected moderate-high expression in all lung models chosen (*188*). Our results indicate high expression of *SLC19A1* in NCI-H441 cells and moderate to high in hAEpCs when displaying an ATII and ATI-like phenotype, respectively.

SLC19A2 and *SLC19A3* unlike *SLC19A1,* do not transport folate but instead transport thiamine, hence their respective proteins are called Thiamine Transporters 1 and 2 (ThTr1, ThTr2) (*219*). It was determined that ThTr1 is responsible for delivery to systemic organs whilst ThTr2 mediates intestinal thiamine absorption (*219*)**.** Courcot *et al.* further detected

moderate expression of *SLC19A2* in all cell types (*188*), which was confirmed by our findings in the cell line NCI-H441 and hAEpCs. When cells displayed and ATII phenotype higher expression of *SLC19A2* was detected. Courcot *et al.* further detected moderate expression of *SLC19A3* in only some cell types with no expression detected in Calu1, NCI-L132, NCI-H727 and HBEC (*188*). Our findings were in line with no expression detectable in the cell line NCI-H441. However, low-moderate expression was detectable in hAEpCs under an ATII and ATI-like phenotype, respectively.

SLC22A family have been broadly studied in lung epithelial membranes. They play a role in the mediated uptake and secretion of organic cations (*220*). The family encoded *SLC22A1-SLC22A3* code for the proteins OCT1-OCT3 and are responsible for the translocation of net charge across a membrane (*220*). It was determined by Endter *et al.* that low-moderate expression of *SLC22A1* was detectable in all cell lines tested (*183*). However, Courcot *et al.* failed to detect its transcript in NCI-L132, BEAS-2B, NCI-H358, NCI-H460, NCI-H727 but was present in all lung tissues tested (*188*). Protein expression by LC-MS/MS however, detected OCT1 in BEAS2B cells and in trachea and bronchial tissue but not in alveolar tissue (*185*). Regardless, Sakamoto *et al.* detected the transporter in the cell line NCI-H441, which is similar to results achieved in this study where *SLC22A1* was detected in low levels independent of culture conditions (*185*). The same level of expression was also detected in hAEpCs regardless of phenotype. In following, Endter *et al.* failed to detect any mRNA expression of *SLC22A2* in cell lines tested with only low expression detectable in Caco-2 cells (*183*). This is comparable with Courcot *et al*. (*188*) However, Sakamoto *et al.* did detect low protein expression in the cell lines BEAS2B, NCI-H292, NCI-H441and trachea, bronchial and alveolar tissue (*185*). Our results were similar with Endter *et al.* and Courcot *et al.* with no gene expression detectable in NCI-H441 cells (*183, 188*). However, in hAEpCs, low expression was detected when cells displayed an ATI-like phenotype only. Finally,

SLC22A3 was absent in 16HBE14o-, BEAS-2B, NCI-L132, NCI-H358, NCI-H460, NCI-H727 (*183, 188*). However, Courcot *et al.* confirmed the presence of the transporter in all lung tissue, although, protein expression failed to be detected when quantified by LC-MS/MS (*185, 188*). From the data gathered in this study, low expression levels of *SLC22A3* were detected in NCI-H441 cells, with moderate expression detected in hAEpCs.

The pH dependent transporters OCTN1 and OCTN2 encoded by the gene *SLC22A4* and *SLC22A5,* respectively have been proven to mediate the transport of cationic zwitterionic compounds, in particular the influx of ET and carnitine (*220*). Both protein and gene expression of OCTN1/ *SLC22A4* have been detected in all cell types and lung tissue with highest detection in the bronchiolar cell lines; NCI-H292 and NCI-H441, and bronchiolar tissue (*183, 185, 188*). In our investigations, *SLC22A4* expression was unable to be detected in NCI-H441 cells. This was similar to detection levels in hAEpCs under an ATII and ATI-like phenotype. *SLC22A5* was confirmed to be present in all lung models tested with varying degrees of expression (*183, 188*). However, Sakamoto *et al.* failed to detect any protein in A549 cells (*185*). Protein levels were also undetectable in lung tissue, which was previously detected by Courcot *et al.* at a transcript level (*185, 188*)**.** Moderate expression of *SLC22A5* was detected in NCI-H441 cells with expression levels significantly altering during transdifferentiation of hAEpCs from ATII (low) to ATI-like (high), with expression levels in parenthesis.

SLC22A6-SLC22A8, SLC22A9 in this study were also investigated. These genes are responsible for the coding of the transporters OAT1-OAT3, OAT7. They differ from previous OCT/Ns as their substrate specificity is not restricted to cationic compounds and their metabolites, as the name suggests. *Oat1* has been widely studied in rodents and found to be exclusively expressed in the kidney with localisation to the basolateral membrane of the proximal tubule (*221*) with expression of the gene in the lung only successfully detected in

Caco2 cells (*183, 188*). It is believed that this subfamily plays an important role in pathways of metabolism with *Oat1*$^{-/-}$ mice resulting in defects in the handling of important metabolites (*222, 223*)**.** Following, *SLC22A7,* which codes for OAT2 or previously the novel liver transporter. This transporter has been recently capable of transporting cyclic nucleosides which is thought to play a plausible role in intracellular signalling (*224*)**.** *Oat2* was studied in mouse embryo lung, however, more recently *Oat2* has been detected in adult lung. *SLC22A7* has only been detected in Caco-2 cells to date (*183, 188*)**.** However, protein expression was detected in low levels in bronchiolar human lung tissue. OAT3 encoded by *SLC22A8,* has been mainly investigated in the kidneys with highest detection of *Oat3* in mouse renal proximal tubule (*221*). The functional role of this transporter still requires further attention. Again, this transporter was only detected at moderate levels in Caco-2 cells with Sakamoto *et al.* quantifying low expression of OAT3 in bronchiolar human tissue (*183, 185, 188*). *SLC22A9* is responsible for the coding of OAT7 and although a lack of literature surrounds this protein it is thought to be a liver specific organic anion transporter (*225*). This transporter was investigated by Courcot *et al.* and expression remained undetectable. Our studies also failed to detect the presence of any OAT genes expression in NCI-H441 cells, with low expression of *SLC22A7, SLC22A8* and *SLC22A9* only detectable in hAEpCs when displaying an ATI-like phenotype.

SLC44 and *SLC47* are also transporters of organic compounds. *SLC44* is largely restricted for the movement of choline and structural analogues in a sodium independent manner hence, *SLC44* belongs to the family of Choline Like Transporters (CLT) (*226*). *SLC44A1* has been localised to the membrane of plasma and mitochondria, where it functions in cell growth and repair, and phospholipid production in the generation of lung surfactant (*227*). Blockage of *SLC44A2* has been reported to result in autoimmune disorders for example in transfusion related acute lung injury; antibodies targeting *SLC44A2* caused the deletion of granulocyte

aggregation (*227*). To date no reports have yet to identify a role of *SLC44A3.* This is the first study to determine the expression levels of *SLC44* transporters in lung cell models. All genes were highly expressed in NCI-H441 cells, with only moderate expression detected for *SLC44A3*. In hAEpCs, high expression was observed for all transcripts when displaying an ATI-like phenotype with moderate expression detected for ATII cells.

SLC47 genes belong to the Multidrug And Toxin Extruder (MATE) family. This family of transporters are often coupled with OCTs for the transepithelial secretion of organic compounds, and have been found to support apical organic compound efflux (*226*). MATE1 (*SLC47A1)* has been determined to coordinate with OCT2 for the vectorial renal elimination of organic cations. Polymorphisms in MATE1 have led to reduced elimination (*228*) with detection also reported to significantly lower levels in the lung (*229*). Courcot *et al.* determined low to high expression in all lung models tested with the exception of HBEC and bronchial mucosa tissue (*188*). No detection of *SLC47A1* occurred in NCI-H441 cells, with a huge contrast in hAEpCs, expressing the gene at moderate and high levels in ATII and ATI-like phenotypes. No function of MATE2 (*SLC47A2)* has yet to be determined. However, mRNA was detected by Northern blot to be most dominant in the colon, followed by the liver and lung (*229*)**.** Courcot *et al.* was only successful in the detection of this transcript in BEAS-2B, NCI-H358, HBEC and small cell carcinomas (*188*)**.** Our findings are similar, with no detection in NCI-H441 cells. However, moderate expression was observed only in ATI-like hAEpCs.

SLC23A1 and *SLC23A2* are responsible for the coding of the Sodium dependent Vitamin C Transporters; SVCT1 and SVCT2 (*230*). It has been determined that SVCT1 co-transports sodium and ascorbate in a 2:1 ratio (*231*), with *Slc23a1*$^{-/-}$ mice resulting in death within a few minutes of birth. Presence in the epithelium has been confirmed by Burzle *et al.* with apical localisation in human bronchiolar epithelium confirmed for SVCT2 by

immunohistochemistry (*232*). NCI-H441 cells for the first time displayed low and moderate expression for *SLC23A1* and *SLC23A2*, respectively. Only *SLC23A2* were expressed at moderate levels in hAEpCs regardless of phenotype.

SLC25A13, located on the chromosome 7, codes for the mitochondrial Aspartate Glutamate Carrier (AGC) with a central role in malate aspartate shuttle (*233*). Further investigation is required to fully elucidate the role of this transporter. Courcot *et al.* detected the gene transcript in all lung cell lines investigated in moderate to high expression levels, which was to findings achieved in this study (*188*). NCI-H441 cells highly expressed *SLC25A13* with moderate expression detected only in ATII hAEpCs. No such detection was possible in ATI-like hAEpCs.

Genes coding for *SLC28* and *SLC29* are responsible for the translation of Concentrative Nucleoside Transporters (CNT) and Equilibrative Nucleoside Transporters (ENT) (*234*). CNTs function in the sodium dependent transport of nucleosides, with CNT1 (*SLC28A1*) and CNT2 (*SLC28A2*) having a high specificity for pyrimidine and purine nucleosides, respectively and CNT3 (*SLC28A3*) responsible for the transport of both (*235*). ENTs are responsible for the transport of nucleosides bidirectionally in a sodium independent manner (*234*). It is hypothesised that CNTs and ENTs coordinate together for the transepithelial nucleoside transport (*234*). CNT1 has been found to be primarily localised to the apical membrane of epithelial cells with CNT2, CNT3, ENT1, ENT2, ENT3 sharing a much broader localisation (*234, 236*)**.** *Cnt3* was found to be the highest expressed in rat lungs compared to *Cnt1* and *Cnt2*. Courcot *et al.* failed to detect *SLC28A1* in lung models tested (*188*). *SLC28A2* was detected in bronchial mucosa at low levels with low expression of *SLC28A3* detected in NCI-H292, HBEC and all human lung tissue tested (*188*). These findings were similar with this study. No gene expression was detected for *SLC28A1* and *SLC28A2* with moderate expression detected for *SLC28A3* in NCI-H441 cells. In hAEpCs

however, a varying degree of expression of *SLC28* genes are observed. ATI-like phenotype displayed moderate levels of *SLC28A1* and *SLC28A2* with no detection possible in cells displaying an ATII phenotype. *SLC28A3* was expressed at low levels in hAEpCs, similar to NCI-H441 cells. Similarly, *Ent1* mRNA was highest expressed in the lungs of mouse and rat (*234*). This was comparable to findings of Courcot *et al.*, who detected highest expression of *SLC29A1* in human lung tissue, in comparison to *SLC29A2* and *SLC29A3* (*188*). *SLC29A3* failed to be detected in the cell line NCI-L132. Our investigation suggested high levels of *SLC29A1* to be detected in NCI-H441 with moderate expression detectable in hAEpCs only in an ATII phenotype. No expression was possible to be detected in ATI-like cells. Moderate expression was detected for *SLC29A2*, *SLC29A3* and *SLC29A4* in NCI-H441 cells with only *SLC29A4* expressed at low levels when cultured under AIC. A varying expression of all transporters was detected in hAEpCs. *SLC29A2* ranged from moderate to high expression depending on phenotype. *SLC29A3* was expressed at low levels under an ATII phenotype but a striking increase in expression occurs when displaying an ATI-like phenotype. Finally, *SLC29A4* was expressed at low levels in ATII cells with no expression detected when sharing an ATI-like phenotype.

SLC31A1 codes for the Copper TRansporter (CTR1) as it allows for monovalent copper accumulation in to the cell (*237*)**,** which is fundamental for redox coupling reactions**.** This transporter is a trimer with each subunit having 3 transmembrane regions. It is detected in all organs with highest expression detected in the liver and kidney (*238*). In lung cell models; A549 and NCI-H441, CTR1 was determined to be expressed at cytoplasmic compartments by immunohistochemistry (*239*)**.** Courot *et al.* detected moderate to high expression in all lung cell lines and tissues tested. This correlates to our findings with moderate expression in NCI-H441 cells detected, regardless of culture conditions. However, in hAEpCs, moderate

expression of *SLC31A1* was only detected in ATII cells, with ATI-like cells expressing low levels of the transcript.

SLC38 genes code for the Sodium coupled Neutral Amino acid Transporters (SNAT), which function in the movement of small aliphatic amino acids for example, glutamine from astrocytes to neurons in the CNS (*238*). *SLC38A2*, which codes for the transporter SNAT2 is ubiquitously detected (*240*). Courcot *et al.* detected high levels of this gene in all lung models tested (*188*), which is in correlation to our findings that found expression of the transporter at high and moderate levels for AIC and LCC culture, respectively, in NCI-H441 cells. In hAEpC, moderate expression was detected in hAEpCs. *SLC38A5* is reported to be expressed in astrocytes, glial cells and to the apical membranes of the intestine epithelial (*173, 238, 241*). Courcot *et al.* detected the transcript in all lung models tested with expression levels ranging from low-high (*188*). However, the transcript appeared absent from the cell lines 16HBE14o- and A549 (*188*). Our research indicates that low expression of *SLC38A5* is only detectable in NCI-H441 when cultured under LCC conditions, with low to high expression detected in hAEpCs when displaying an ATII and ATI-like phenotype, respectively.

Expression analysis of SLCO Transporters by RT-PCR.

SLCO genes are responsible for the coding of the Organic Anion Transporting Polypeptides (OATP). Previously, detection of these transporters in the lung remained negative and so were concluded to play no or minor role in drug absorption (*242*). However, these transporters have been detected in a variety of biological barriers and have a marked impact on xenobiotic absorption (*243*)

SLCO1A2 is a sodium independent uptake transporter of a broad range of substrates and is ubiquitously expressed in tissues such as liver, kidney, testes and lung with the highest

detection in the brain (*244*). Gene expression has previously been detected in hBEpC, Calu-3, BEAS-2B, A549, Caco-2, NCI-H292 and NCI-H727 and in all lung tissue except adenocarcinoma by RT-PCR (*183, 188*), with protein expression quantified by LC-MS/MS only in bronchiolar human lung tissue. Our findings are in parallel with Sakamoto *et al.* with no gene expression detected in the cell line NCI-H441. However, expression was detected in hAEpCs only under an ATII phenotype at low levels. *SLCO1B1* and *SLCO1B3* was previously detected by RT-PCR in A549, Calu-1, Calu-3 cells and BEAS-2B, NCI-L132, HBEC only for *SLCO1B3* (*183, 188*). Our findings indicate that low expression of *SLCO1B1* and *SLCO1B3* was only detectable in NCI-H441 cells when cultured under LCC. Further in hAEpCs no detection of these transcripts occurred.

SLCO2A1 codes for the transporter OATP2A1 also known as the ProstaGlandin Transporter (PGT*). Pgt* has been detected in ATII and ATI cells by immunohistochemistry in mouse lung (*173*). Prostaglandin has been found to have an antifibrotic effect in response to inflammation. In *Slco2a1*$^{-/-}$ mice, reduced prostaglandin levels were detected and hence promotion of fibrosis occurred when compared to their wildtype control (*173*). Courcot *et al.* detected *SLCO2A1* in all cell types apart from A549, BEAS-2B, Calu-1 and NCI-H460 (*188*) with Endter *et al.* only detecting its transcript in Caco-2 cells (*183*). *SLCO2A1* was detected in NCI-H441 cells at low levels. Expression was detectable in hAEpCs with moderate expression occurring in ATI-like cells.

SLCO2B1 has previously been detected in A549, NCI-H727, Calu-3 and Caco-2 cells and all human lung tissue tested (*183, 188*)**.** Protein expression was detected in trachea, bronchi and alveolar tissue by Sakamoto *et al.* (*139, 185*)**.** However, this study has identified no expression of the transcript in NCI-H441 cells or in hAEpCs. *SLCO3A1* (OAT3A1) is widely expressed in tissues such as testis, brain, heart, spleen, peripheral blood leukocytes, thyroid and lung. This transporter has also been found to have larger substrate specificity than other

OATPs (*245*). Expression of *SLCO3A1* has been detected in all lung models except Caco-2 with varying expression levels (*183, 188*)**.** Low expression of *SLCO3A1* was detectable in NCI-H441 cells with moderate expression detected in hAEpCs.

Members of the *SLCO4* family are responsible for the transport of iodothyronines (*246*)**.** *SLCO4A1* was investigated by Endter *et al.* and Courcot *et al.* in lung models and found to be expressed in moderate-high levels in lung models tested. In NCI-H441 cells, moderate expression was detected for both genes under AIC and LCC, except *SLCO4C1,* which was detected only at low levels under AIC conditions. These genes were also undetectable in hAEpCs.

Expression analysis of Aquaporins by RT-PCR.

AQPs are small integral proteins, detected across epithelium and endothelium of peripheral lung and airways (*247*)**.** They play a crucial role in water homoeostasis creating selective pores for rapid movement of water during airway hydration, alveolar fluid transport and submucosal gland secretion (*247, 248*)**.** It was determined by Verkman *et al.* that *AQP1* is localised primarily to the microvascular endothelial. However, high expression was detected in bronchial mucosa, pulmonary parenchyma, adenocarcinoma and moderate expression in squamous cell line (*188, 247*)**.** *AQP1* was only detectable in BEAS-2B and NCI-L132 cell lines (*188*). However, our research indicated presence of *AQP1* to be expressed at low and high levels when cultured under AIC and LCC, respectively, in NCI-H441 cells with high detection occurring in hAEpCs.

The main functional role of *AQP7* is to facilitate the efflux of glycerol from adipose tissue (*249*), hence, *AQP7* was detected in the plasma membrane of adipocytes and it was determined in *AQP7* knockout mice that an increase in weight gain occurred compared to

their wildtype control. *AQP7* was undetectable by any cell line tested by Courcot *et al.* with only low expression detected in bronchial mucosa and pulmonary parenchyma of human lung tissue (*188*). It was determined by our analysis that detection of *AQP7* only occurred in NCI-H441 when cultured under LCC. In hAEpCs, *AQP7* was only detected when cells displayed an ATI-like phenotype with moderate expression.

Highest expression of *AQP9* is detected in the liver where its main function is in the hepatic uptake of glycerol for the synthesis of glucose. However, high expression of *AQP9* was detected in bronchial mucosa (low), pulmonary parenchyma (moderate), squamous cell carcinoma (low) and adenocarcinoma (high) by Courcot *et al.* with expression levels in parenthesis, suggesting a possible niche for the uptake of glycerol, and subsequent glucose synthesis for respiration (*188*). Our analysis indicated that high expression of *AQP9* occurs when under LCC conditions in NCI-H441 cells and moderate expression in hAEpCs regardless of phenotype.

5.5 Conclusions

The data collected here provides information on ABC, SLC, SLCO Transporters and AQP Channels under AIC and LCC condition in NCI-H441 cells. Further, it provides expression data for these transporters in hAEpCs of an ATII and ATI-like phenotype. Only 5/23 ABC transporters investigated changed their expression under culture conditions in NCI-H441 cells. The majority were expressed at higher levels under LCC conditions with only *ABCC10* being displayed at lower levels under these conditions. Twelve of the nineteen transporters investigated in hAEpCS changed expression during transdifferentiation with 66% expressing at higher levels under an ATI-like phenotype and 33% detected at higher levels under an ATII phenotype. When directly comparing NCI-H441 transporter expression under LCC conditions with hAEpCs, a significant difference in expression is observed in the transporter genes; *ABCC1, ABCC5, ATP7A, ATP7B*, in which high levels are detectable in NCI-H441 cells but no-low levels when hAEpCs display an ATII phenotype.

Nine of the fifty-six SLC Transporters investigated changed expression under culture conditions, with only *SLC16A1* and *SLC16A3* expressing lower levels when cultured under LCC conditions. Again, after transdifferentiating of hAEpCs, differences in expression depending on their phenotype were observed. The majority of these transporters were expressed at higher levels when under an ATI-like phenotype. Further the genes; *SLC2A2, SLC3A2, SLC7A5, SLC7A7, SLC7A8, SLC25A13, SLC28A1, SLC28A2, SLC29A1, SLC29A4, SLC38A5, SLC47A1, SLC47A2* were strikingly different when comparing NCI-H441 cells to hAEpCs only when displaying an ATI-like phenotype.

Changes in expression were also observed for SLCO Transporters when cultured under various conditions in NCI-H441 cells, with the majority of transporters being expressed only under LCC at low levels. *SLCO1A2* was only expressed in ATII hAEpCs, with *SLCO2A1*

increasing its expression from low to moderate from an ATII to ATI-like phenotype and moderate expression detected for *SLCO3A1* in hAEpCs regardless of phenotype.

Finally, 3 AQP Channels were investigated and it was determined that significantly higher expression was detected when cultured under LCC conditions. This could suggest that AQPs play a role in fluid clearance and so maybe extremely important for lung function. *AQP7* was the only channel to change expression in hAEpCs from no to moderate levels depending on whether displaying an ATII or ATI-like phenotype respectively.

No change in expression was observed in the majority of ABC and SLC transporters investigated during transdifferentiation. However, care must be taking when investigating SLCO Transporters and AQP Channels under these conditions. Expression differences are observed in the majority of genes (82%) when NCI-H441 cells are compared to hAEpCs. And so care must be taken when utilising NCI-H441 as an *in vitro* model for human alveolar epithelial cells for the study of SLCO Transporters and AQP Channels.

In summary, care must be taken regarding cell culture techniques and comparison between the *in vitro* model NCI-H441 and hAEpCs when investigating drug transporters. However, as only one patient sample was possible for the investigation into hAEpCs, a need for a larger sample size is required to confirm the conclusions drawn from this study.

Chapter 6

General Conclusions

An association between OCTN1 and the chronic inflammatory lung disease, COPD has been established in this work. Although, much remains to be done regarding the elucidation of the exact molecular mechanism, novel insights are provided suggesting a role for OCTN1 and its physiological substrate ET in the distal lung epithelium.

I. OCTN1 belongs to the SLC family of transporters, which are involved in the bidirectional movement of organic cation molecules. Evidence surrounding the functional role of this transporter in inflammatory diseases is emerging. This work has identified 3 novel SNPs associated with the transporter in the cell line NCI-H441. Further, uptake and transport experiments of ET by OCTN1 were performed, to help determine the mechanistic role of OCTN1 in inflammatory diseases. It is suggested that OCTN1 is apically localised in the bronchiolar epithelium, as ET transport in an apical to basolateral direction is higher than *vice versa*. Finally, uptake of ET by OCTN1 has been proven to counteract ROS through, *inter alia* the stabilisation of the intracellular pH, supporting the hypothesis that OCTN1 plays a protective role against inflammatory disease.

II. It is hypothesised that higher expression levels of OCTN1 may increase the susceptibility of developing inflammatory diseases such as COPD. Therefore, *SLC22A4*, the gene responsible for the coding of OCTN1 was characterised in the bronchial epithelium of COPD patients. It was determined that increased expression of the gene occurs with age, with unhealthy weight, with pack years. A significant increase in expression of *SLC22A4* was observed with decreasing lung function, a key determinant in the diagnosis of COPD. Hence, OCTN1 has successfully been associated with COPD in Irish and Dutch population.

III. How exactly ET detoxification mechanisms work has not yet been identified. ET was therefore investigated under conditions of oxidative stress, i.e. CSE exposure. It was determined that ET converts into its oxidised forms EH and ESO_3H with only ESO_3H successfully detected intracellularly by LCMS/MS. However, ET stores are not depleted intracellularly and so it was imperative to determine, whether ET can undergo phase II metabolism similar to GSH. ET was successfully reacted with CDNB *in vitro.* It was further determined that GSTs plays a role in this formation, and that upon formation of DNP-ET, MRP transporters are responsible for its efflux. Therefore, this novel research has confirmed that ET plays a role in phase II metabolism by forming adducts with compounds intracellularly. It also has identified, for the first time that these metabolites take part in phase III metabolism via their efflux by MRP transporters. And so, it may be concluded, that ET's mechanism for detoxification is similar to that of GSH.

IV. A characterised *in vitro* model is required to fully determine the role of various drug transporters in the distal lung epithelium. Prior to this analysis, an investigation has yet to be made on the effect of culture conditions to the expression of different transporters. The expression of 23 ABC, 56 SLC and 8 SLCO transporters and 3 AQP channels were investigated in the cell line NCI-H441. The expression data gathered was compared to hAEpCs. This data gathered failed to provide a well characterised *in vitro* model for the study of transporters in human distal lung epithelium.

Collectively, this research has highlighted the physiological function of OCTN1 and its role in lung disease. The functional activity of OCTN1 in lung epithelial cells *in vitro* has been revealed to be temperature and pH dependent. There are suggestions for apical localisation of

the transporter on bronchial epithelium. However, without the presence of reliable antibodies for OCTN1, the exact spatial localisation of the transporter remains nebulous.

Three SNPs in the *SLC22A4* gene, responsible for the encoding of OCTN1, have been identified in the cell line NCI-H441. These SNPs are novel to any previously determined. Future work would require further investigation into their influence (if any) into the function of OCTN1.

Previous SNPs detected in *SLC22A4* have been frequently reported to be associated with inflammatory diseases. However, their causative role has been unclear to date. Reports suggest reduced activity of the protein when expressing the 503F haplotype (109). This reduced activity is suggested to be solely due to a change in the expression of the transporter and will not alter the susceptibility of developing an inflammatory disease (106). Therefore, the expression of *SLC22A4* was investigated in COPD patients for the first time and it was determined that any risk factors, i.e. age, unhealthy weight, smoking, resulted in an increase in the expression of the transcript. It is hypothesised, that OCTN1 may be upregulated to ensure optimum concentrations of ET are present within the cell to counterbalance oxidative stress caused by these risk factors. To confirm this hypothesis, quantitative studies of ET levels in the lungs of patients should be performed under these conditions.

The expression of transporters from different ethnic populations requires much investigation. The SNP responsible for the missense of L503F has been found to be linked to the development of CD in German, Swedish, and Chinese Han but not in Scottish people with conflicting data collected for Hungarian populations (98-101,105, 107.) Similarly, L503F has been associated with IBD in Scandinavian and Western populations but not in Chinese (103 104). Our studies determined an increase in expression of *SLC22A4* in the bronchial epithelium of Irish COPD patients. In contrast, a decreased expression of the gene was

detected in the bronchial epithelium of Dutch COPD patients. This supports the idea that ethnicity may impact the development of various mutations in *SLC22A4.*

GST was identified to play a role in the formation of DNP-ET. However, when incubated with CB, a more powerful inhibitor of GST compared to EA (68), formation of DNP-ET was only significantly reduced at high concentrations of ET. Further, surprising results were obtained when cell viability was investigated in the presence of CDNB, ET and EA. A significant improvement occurred when GST was inhibited in the presence of CDNB and ET. Collectively, these data suggest that GST may not be the sole enzyme for the catalysis of this reaction and that further investigations into alternative enzymes are now required.

It was also identified that MRPs are, at least partly, responsible for the efflux of the adduct, similar to DNP-SG. Further studies are required to identify which transporter/s is/are responsible for this efflux.

Finally, the cell line NCI-H441 was investigated for the expression of transporters and channels under culture conditions of AIC and LCC, and whether the expression detected was comparable to hAEpCs. It was identified that for the majority of ABC and SLC transporters expression was independent of whether NCI-H441 cells were cultured submersed or at an air-liquid interface. However, discrepancies were observed regarding the expression in AQP channels and SLCO transporters. These data observed for NCI-H441 cells was incomparable to hAEpCs. Therefore, a more suitable *in vitro* model for the analysis of human lung epithelial cells is required.

In summary, an association between OCTN1 and COPD in the Irish population has been established. OCTN1 is responsible for pH and temperature dependent transport of ET, which once taken up in the cell, undergoes phase II metabolism for detoxification of the xenobiotic. The resulting conjugate is then effluxed from the cell for complete detoxification by a MRP

transporter. This research has successfully provided further insight into the role of OCTN1 in the pathogenesis and development of COPD.

Appendices

I Acknowledgements

Dr. Carsten Ehrhardt, where to begin? Thank you for giving me the privilege of carrying out this research under your supervision. Thank you for your guidance, advice and patience. More importantly, thank you for your kind and light-hearted nature. No problem never seemed unsolvable with you around. Thank you for sharing your stories and experiences and making conferences fun and exciting places to learn, both personally and professionally. You have allowed me to develop from a 'young Irish girl' into hopefully a talented, competent young woman.

Dr. Sabrina Nickel and Mohammed Ali, without whom I would never have completed this piece of research. You were always there to lend a helping hand and provide tricks and tips to aid any experimental procedure. Thank you.

Brian Talbot, thank you for your patience and your willingness to help me, even when you had 100 more important jobs to do. Thank you.

To the Ehrhardt lab; Awfa, Damola, Juliane, Louise, Lisa, Katja, Karina, Maria, Matthias, Max, Melanie, Nagi, Stephany, Valentin but especially Johannes, Manoel and Ozlem. Thank you for bringing fun into our lab. You made this experience unforgettable with your witty jokes over a failing experiment or pint in Kennedys. I miss you and you will always have a tender spot in my heart.

To my fantastic colleagues; Andrew, Alan, Azizah, Chris, David, Emer, Grainne, James, Jason, Jeremiah, Kit, Kate, Maria, Melissa, Michelle, Nadihm, Sadhbh, Susan, Vanessa, Vilmar. Thank you for not only being colleagues, but true friends. I thank you for all the cakes and celebrations, even though my hips do not. I thank you for the unforgettable nights out. Long may they continue.

I would like to thank the technical staff and principal investigators in the School of Pharmacy especially, Dr. Maria Santos, Prof. John Gilmer, Dr. Astrid Sasse, Prof. Mary Meegan, Rhona

Prendergast, Ray Keaveny. Thank you for all for your help and guidance, with this research but also with laboratory practicals.

I would like to thank my friends, most especially Claire, Gloria, Jane, Niall, Tessa. Thank you for sticking by me and supporting me even when I didn't deserve it. I look forward to celebrating this achievement with you.

Finally, to my family, my grandparents; Mummy-2 and Daddy-2, Nana and Papa, Uncle Paddy, my sisters Noelle and Katie, but mainly, Daddy and Simone and most importantly, Mummy. Thank you for your encouragement. Thank you for your love. Thank you for your unconditional support, even though I may not seem to appreciate it. This achievement would not have been possible without you. Thank you for the endless cups of tea and frequent 50€ notes. I cannot wait to make you proud and return the benefits of this accomplishment to you.

II List of Abbreviations

4Py-S-S-Py4	4,4 dipyridyl disulfide
A1PI	Alpha 1 Antitrypsin Protease Inhibitor
AB	Apical-Basolateral
ABC	ATP-Binding Cassette
Ach	Acetylcholine
ACN	Acetonitrile
ADP	Adenosine Diphosphate
AGC	Aspartate Glutamate Carrier
AIC	Air Interface Culture
AIDS	Aquired Immune Deficiency Syndrome
ANOVA	Analysis of Variance
AQP	Aquaporin
ASBT	Apical Sodium Bile Transport
ATI	Alveolar Type I
ATII	Alveolar Type II
ATP	Adenosine Triphosphate
BA	Basolateral-Apical
BALF	Bronchol-Alveolar Lavage Fluid
BCRP	Breast Cancer Resistance Protein
BMI	Body Mass Index
bp	Base Pair
$Ca(OH)_2$	Calcium Hydroxide
Calu-3	Airway Epithelial Cells
CAT	Cation Amino Acid Transporter
CB	Cibracron Blue
CD	Crohn's Disease
cDNA	complementary DNA
CDNB	1-Chloro, 2,4-dinitrobenzene
CLSM	Confocal Laser Scanning Microscopy
CLT	Choline Like Transporters
CNS	Central Nervous System
CNT	Concentrative Nucleoside Transporters
CO2	Carbon Dioxide
COPD	Chronic Obstructive Pulmonary Disease
COSY	Correlation Spectroscopy
CSE	Cigarette Smoke Extract
CSE	Cigarettes moke extract
CT	Cycle Threshold
CTR1	Copper Transporter
d_20	Deuterated water
DAT	Dopamine Transporter

DCF	Dichlorofluorescein
DEPT	Distortionless Enhancement by Polarisation Transfer
DNA	Deoxyribose Nucleic Acid
DNP-ET	2,4 Dinitrophenyl-ergothioneine
DOPA	Dihydroxyphenylalanine
DTNB	Dithiobisnitrobenzoic acid
EA	Ethacrynic Acid
EH	Hercynine
eIF2	Eukaryotic Translation Inititaion Factor 2
ENT	Equlibrative Nucleoside Transporters
ESI	Electrospray Ionisiation
ESO_2H	Ergothioneine Sulfinic Acid
ESO_2SE	Ergothioneine Disulfide S-oxide
ESO_3H	Ergothioneine Sulfonic Acid
ESOH	Ergothioneine Sulfenic Acid
ESOSE	Ergothioneine Disulfide Monoxide
ESSE	Ergothioneine Disulfide
ET	Ergothioneine
FBS	Fetal Bovine Serum
Fe	Iron
FEV1	Forced Expiratory Volume
Fn	Fluorescence of negative control
FVC	Forced Volume Capacity
GABA	Gamma Amino Butyric Acid
GAT	GABA Transporter
GLUT	Glucose Transporters
GOLD	Global initiative for Obstructive Lung Disease
GPx	Glutathione Peroxidase
GSH	Glutathione
GSSG	Glutathione Disulfide
GST	Glutathione S-Transferase
H_20	water
H_2DCFDA	2,7-dichlorofluorescein diacetate
H_2O_2	Hydrogen Peroxide
H_2SO_3	Sulfurous Acid
hAEpC	Human Alveolar Epithelilal Cells
HAT	Heteromeric Amino Acid Transporters
hBEpC	Human Bronchiolar Epithelial Cells
HEK-293	Human Embryonic kidney cells
Hela cells	Henrietta Lacks; isolated from a cervical carcinoma
HIV	Human Immune-deficiency Virus
HPLC	High Performance Liquid Chromatography
HPRE	Human Pigmented Retinal Epithelial cells

HSSC18	Hollow Structure Section Carbon-18 column
IBD	Inflammatory Bowel Disease
IBS	Irritable Bowel Syndrome
IF	Immunofluorescence
IFNγ	Interferon Gamma
IFU	Infections Units
IL-1β	Interleukin 1 Beta
IR	Infrared
ITS	Insulin Transferrin Serum
$KBrO_4$	Potassium Bromate
Km	Michaelis Menten constant
KRB	Krebs-Ringer Buffer
LAT	L-Type Amino Acid Transporter
LC-MS/MS	Liquid Chromatography Tandem Mass Spectrometry
LCC	Liquid Covered Culture
LCIS	Live Cell Imaging Solution Buffer
LTQ	Linear Trap Quadrupole
MATE	Multidrug And Toxin Extruder
MCT	MonoCarboxylate Transporters
MeOD	Deuterated methanol
MeOH	Methanol
MHC	Major Histocompatibility Complex
MLE15	Mouse Transformed ATII cells
mRNA	Messenger Ribonucleic Acid
MRP	Multi-drug Resistance related Protein
MS/MS	Tandem Mass Spectrometry
MVP	Major Vault Protein
ND	Nanodrop
NET	Norepinephrine Transporter
NF-κB	Nuclear Factor Kappa B
NMR	Nuclear Magnetic Resonance
NO	Nitric Oxide
NO_2	Nitrogen Dioxide
NTCP	Sodium Tautocholate Co-transport Peptide
O_2	Oxygen
O_2*	Superoxide
OAT	Organic Anion Transporter
OATP	Organic Anion Transporting Polypeptide
OCT	Organic Cation Transporter
OCTN1	Organic Cation Transporter Novel 1
Papp	Apparent Permeability Coefficient
PFT	Pulmonary Functional Tests
PGE2	Prostaglandin E_2

Pgp	P-glycoprotein
PGT	Prostaglandin Transporter
PMN	Polymorphonucelar
ppm	parts per million
Q	Quinone
QH	Semi-quinone
QH2	Hydroquinone
qRT-PCR	Quantitiative ReverseTranscriptase-Polymerase Chain Reaction
RA	Room Air
ROS	Reactive Oxygen Species
RPMI	Roswell Park Memorial Institute Medium
RT-PCR	Reverse TranscriptasePolymerase Chain Reaction
SAM	Senescence Accelerated Mice
SD	Standard Deviation
SEM	Standard Error of the Mean
SERT	Serotonin Reuptake Transporter
shRNA	Short Hairpin Ribonucleic Acid
SHS	Second Hand Smoke
SLC	Solute Carriers
SLCO	Solute Carrier Organic Anion
SNAT	Sodium coupled Neutral Amino Acid Transporter
SNP	Single Nucleotide Polymorphism
SOD	Superoxide Dismutase
Src	Proto-oncogene tyrosine protein kinase
SRM	Selected Reaction Monitoring
SVCT	Sodium dependent Vitamin C Transporters
TAP	Transporters associated with Antigen Processing
TAUT	Taurine Transporter
TEA	Tetraethyl ammonium
TEER	Trans-Epithelial Electrical Resistance
ThTr	Thiamine Transporters
TLC	Thin Layer Chromatography
TNF-α	Tumour Nercrosis Factor Alpha
UV	Ultraviolet
Vmax	Maximum uptake rate
WB	Western Blot
WT	Wildtype

III References

1. L. Servillo *et al.*, An uncommon redox behavior sheds light on the cellular antioxidant properties of ergothioneine. *Free radical biology & medicine* **79**, 228-236 (2015).
2. M. a. P. o. C. Global Strategy for the Diagnosis, Global Initiative for Chronic Obstructive Lung Disease (GOLD) 2017.
3. C. T. U. S. N. H. L. a. B. I. A. f. t. o. o.-.-R. 2013-07-23.
4. L. Servillo, N. D'Onofrio, M. L. Balestrieri, Ergothioneine Antioxidant Function: From Chemistry to Cardiovascular Therapeutic Potential. *J Cardiovasc Pharmacol* **69**, 183-191 (2017).
5. K. Peckelsen *et al.*, Ergothioneine and related histidine derivatives in the gas phase: tautomer structures determined by IRMPD spectroscopy and theory. *Physical Chemistry Chemical Physics* **19**, 23362-23372 (2017).
6. J. C. Harfield, C. Batchelor-McAuley, R. G. Compton, Electrochemical determination of glutathione: a review. *The Analyst* **137**, 2285-2296 (2012).
7. L. Pochini *et al.*, The human OCTN1 (SLC22A4) reconstituted in liposomes catalyzes acetylcholine transport which is defective in the mutant L503F associated to the Crohn's disease. *Biochimica et Biophysica Acta (BBA) - Biomembranes* **1818**, 559-565 (2012).
8. T. Vos *et al.*, Years lived with disability (YLDs) for 1160 sequelae of 289 diseases and injuries 1990–2010: a systematic analysis for the Global Burden of Disease Study 2010. *The Lancet* **380**, 2163-2196 (2012).
9. WHO, The Global Burden of Disease A response to the need for comprehensive, consistent and comparable global information on diseases and injuries. *[serial on the Internet]*, (2003).
10. L. Schirnhofer *et al.*, COPD prevalence in Salzburg, Austria: results from the Burden of Obstructive Lung Disease (BOLD) Study. *Chest* **131**, 29-36 (2007).
11. European Health for All Datbase [database on the Internet]. (2007).
12. P. J. Landrigan *et al.*, The Lancet Commission on pollution and health. *The Lancet* **391**, 462-512 (2018).
13. J. B. Soriano *et al.*, Global, regional, and national deaths, prevalence, disability-adjusted life years, and years lived with disability for chronic obstructive pulmonary disease and asthma, 1990–2015: a systematic analysis for the Global Burden of Disease Study 2015. *The Lancet Respiratory Medicine* **5**, 691-706 (2017).
14. M. Decramer, W. Janssens, M. Miravitlles, Chronic obstructive pulmonary disease. *Lancet* **379**, 1341-1351 (2012).
15. W. A. Pryor, K. Stone, Oxidants in cigarette smoke. Radicals, hydrogen peroxide, peroxynitrate, and peroxynitrite. *Annals of the New York Academy of Sciences* **686**, 12-27; discussion 27-18 (1993).
16. D. F. Church, W. A. Pryor, Free-radical chemistry of cigarette smoke and its toxicological implications. *Environmental Health Perspectives* **64**, 111-126 (1985).
17. Y. Iwasawa, S. Ogasawara, T. Onishi, K. Tamaru, Dehydrogenation and dehydration of ethyl alcohol over a polynaphthoquinone containing various amounts of FeCl3. Selectivity of formation of acetaldehyde, ethylene and diethyl ether. *Journal of the Chemical Society, Faraday Transactions 1: Physical Chemistry in Condensed Phases* **70**, 193-201 (1974).

18. S. O. Yasuhiro Iwasawa, Catalytic hydrogen transfer reaction on the polynaphthoquinone -syntesis of aniline and decomposition of hydrogen sulfide. *Chemistry Letters* **3**, 845-848 (1974).
19. Y. Iwasawa, S. Ogasawara, Control of the selectivity and increase of the catalytic activity of polynaphthoquinone by various Lewis acids. *Journal of Catalysis* **37**, 148-157 (1975).
20. M. Chang, D. Lynn, *Haustoria and the chemistry of host recognition in parasitic angiosperms*. (1986), vol. 12, pp. 561-579.
21. R. R. Bartz, C. A. Piantadosi, Clinical review: oxygen as a signaling molecule. *Critical care (London, England)* **14**, 234 (2010).
22. L. Norma V, An overview of the vapor phase semivolatile and nonvolatile components of cigarette smoke. *Truth Tobacco Industry Documents*, (1969).
23. A. Ayala, M. Muñoz, S. Argüelles, *Lipid Peroxidation: Production, Metabolism, and Signaling Mechanisms of Malondialdehyde and 4-Hydroxy-2-Nonenal*. (2014), vol. 2014, pp. 360438.
24. W. A. Pryor *et al.*, Free radical biology and medicine: it's a gas, man! *Am J Physiol Regul Integr Comp Physiol* **291**, R491-511 (2006).
25. W. A. Pryor, D. G. Prier, D. F. Church, Electron-spin resonance study of mainstream and sidestream cigarette smoke: nature of the free radicals in gas-phase smoke and in cigarette tar. *Environ Health Perspect* **47**, 345-355 (1983).
26. B. M. Hybertson, B. Gao, S. K. Bose, J. M. McCord, Oxidative stress in health and disease: The therapeutic potential of Nrf2 activation. *Molecular Aspects of Medicine* **32**, 234-246 (2011).
27. I. T. Society, National Respitatory (COPD) Framework. (2008).
28. D. H. Au *et al.*, The effects of smoking cessation on the risk of chronic obstructive pulmonary disease exacerbations. *Journal of general internal medicine* **24**, 457-463 (2009).
29. L. Fromer, Diagnosing and treating COPD: understanding the challenges and finding solutions. *International journal of general medicine* **4**, 729-739 (2011).
30. E. Mortaz, G. Folkerts, F. Redegeld, Mast cells and COPD. *Pulmonary pharmacology & therapeutics* **24**, 367-372 (2011).
31. S. Eriksson, Studies in alpha 1-antitrypsin deficiency. *Acta medica Scandinavica. Supplementum* **432**, 1-85 (1965).
32. C. Larsson, Natural history and life expectancy in severe alpha1-antitrypsin deficiency, Pi Z. *Acta medica Scandinavica* **204**, 345-351 (1978).
33. O. Senn *et al.*, Circulating alpha1-antitrypsin in the general population: Determinants and association with lung function. *Respiratory Research* **9**, 35 (2008).
34. E. K. Silverman, Risk of Lung Disease in PI MZ Heterozygotes. Current Status and Future Research Directions. *Annals of the American Thoracic Society* **13**, S341-345 (2016).
35. M. F. Fromm, R. B. Kim, (Eds.), *Drug Transporters*. (Springer, 2011).
36. V. Vasiliou, K. Vasiliou, D. W. Nebert, Human ATP-binding cassette (ABC) transporter family. *Human Genomics* **3**, 281-290 (2009).
37. M. A. Hediger, B. Clemencon, R. E. Burrier, E. A. Bruford, The ABCs of membrane transporters in health and disease (SLC series): introduction. *Mol Aspects Med* **34**, 95-107 (2013).

38. H. Koepsell, The SLC22 family with transporters of organic cations, anions and zwitterions. *Molecular Aspects of Medicine* **34**, 413-435 (2013).
39. S. K. Nigam, What do drug transporters really do? *Nat Rev Drug Discov* **14**, 29-44 (2015).
40. J. J. Salomon, C. Ehrhardt, Organic cation transporters in the blood-air barrier: expression and implications for pulmonary drug delivery. *Ther Deliv* **3**, 735-747 (2012).
41. W. Kummer, K. S. Lips, U. Pfeil, The epithelial cholinergic system of the airways. *Histochem Cell Biol* **130**, 219-234 (2008).
42. W. Kummer *et al.*, Role of acetylcholine and polyspecific cation transporters in serotonin-induced bronchoconstriction in the mouse. *Respir Res* **7**, 65 (2006).
43. K. S. Lips *et al.*, Down-regulation of the non-neuronal acetylcholine synthesis and release machinery in acute allergic airway inflammation of rat and mouse. *Life sciences* **80**, 2263-2269 (2007).
44. K. S. Lips *et al.*, Polyspecific cation transporters mediate luminal release of acetylcholine from bronchial epithelium. *Am J Respir Cell Mol Biol* **33**, 79-88 (2005).
45. L. Pochini, M. Scalise, M. Galluccio, C. Indiveri, Regulation by physiological cations of acetylcholine transport mediated by human OCTN1 (SLC22A4). Implications in the non-neuronal cholinergic system. *Life sciences* **91**, 1013-1016 (2012).
46. I. Tamai *et al.*, Cloning and characterization of a novel human pH-dependent organic cation transporter, OCTN1. *FEBS letters* **419**, 107-111 (1997).
47. D. Grundemann *et al.*, Discovery of the ergothioneine transporter. *Proc Natl Acad Sci U S A* **102**, 5256-5261 (2005).
48. X. Wu *et al.*, Structural and functional characteristics and tissue distribution pattern of rat OCTN1, an organic cation transporter, cloned from placenta. *Biochim Biophys Acta* **1466**, 315-327 (2000).
49. D. Grundemann, The ergothioneine transporter controls and indicates ergothioneine activity--a review. *Prev Med* **54 Suppl**, S71-74 (2012).
50. J. J. Salomon *et al.*, Transport of the fluorescent organic cation 4-(4-(dimethylamino)styryl)-N-methylpyridinium iodide (ASP+) in human respiratory epithelial cells. *European journal of pharmaceutics and biopharmaceutics : official journal of Arbeitsgemeinschaft fur Pharmazeutische Verfahrenstechnik e.V* **81**, 351-359 (2012).
51. T. Nakamura *et al.*, Transport of ipratropium, an anti-chronic obstructive pulmonary disease drug, is mediated by organic cation/carnitine transporters in human bronchial epithelial cells: implications for carrier-mediated pulmonary absorption. *Mol Pharm* **7**, 187-195 (2010).
52. S. Grigat *et al.*, Probing the substrate specificity of the ergothioneine transporter with methimazole, hercynine, and organic cations. *Biochemical pharmacology* **74**, 309-316 (2007).
53. A. L. Slitt, N. J. Cherrington, D. P. Hartley, T. M. Leazer, C. D. Klaassen, Tissue distribution and renal developmental changes in rat organic cation transporter mRNA levels. *Drug metabolism and disposition: the biological fate of chemicals* **30**, 212-219 (2002).
54. I. Tamai *et al.*, Molecular and functional characterization of organic cation/carnitine transporter family in mice. *The Journal of biological chemistry* **275**, 40064-40072 (2000).

55. Y. Alnouti, C. D. Klaassen, Tissue distribution and ontogeny of sulfotransferase enzymes in mice. *Toxicological sciences : an official journal of the Society of Toxicology* **93**, 242-255 (2006).
56. X. Wu *et al.*, Structural and functional characteristics and tissue distribution pattern of rat OCTN1, an organic cation transporter, cloned from placenta. *Biochimica et Biophysica Acta (BBA) - Biomembranes* **1466**, 315-327 (2000).
57. H. Yabuuchi *et al.*, Novel membrane transporter OCTN1 mediates multispecific, bidirectional, and pH-dependent transport of organic cations. *The Journal of pharmacology and experimental therapeutics* **289**, 768-773 (1999).
58. Y. Alnouti, J. S. Petrick, C. D. Klaassen, Tissue distribution and ontogeny of organic cation transporters in mice. *Drug Metab Dispos* **34**, 477-482 (2006).
59. R. Agu *et al.*, Differential expression of organic cation transporters in normal and polyps human nasal epithelium: implications for in vitro drug delivery studies. *Int J Pharm* **406**, 49-54 (2011).
60. G. Horvath *et al.*, Epithelial organic cation transporters ensure pH-dependent drug absorption in the airway. *Am J Respir Cell Mol Biol* **36**, 53-60 (2007).
61. J. X. Mo *et al.*, Synthesis, transport and mechanism of a type I prodrug: L-carnitine ester of prednisolone. *Molecular pharmaceutics* **8**, 1629-1640 (2011).
62. M. Zeng *et al.*, Local and systemic oxidative stress status in chronic obstructive pulmonary disease patients. *Canadian respiratory journal : journal of the Canadian Thoracic Society* **20**, 35-41 (2013).
63. C. Pfeiffer, T. Bauer, B. Surek, E. Schömig, D. Gründemann, Cyanobacteria produce high levels of ergothioneine. *Food Chemistry* **129**, 1766-1769 (2011).
64. D. B. Melville, Ergothioneine. *Vitamins & Hormones* **17**, 155-204 (1959).
65. T. K. Shires, ERGOTHIONEINE DISTRIBUTION IN BOVINE AND PORCINE OCULAR-TISSUES. *Comparative biochemistry and physiology* **Part C, Pharmacology toxicology & endocrinology**, 117-120
(1997).
66. I. K. Cheah, B. Halliwell, Ergothioneine; antioxidant potential, physiological function and role in disease. *Biochim Biophys Acta* **1822**, 784-793 (2012).
67. I. Rahman *et al.*, Ergothioneine inhibits oxidative stress- and TNF-alpha-induced NF-kappa B activation and interleukin-8 release in alveolar epithelial cells. *Biochemical and biophysical research communications* **302**, 860-864 (2003).
68. J. E. Repine, N. D. Elkins, Effect of ergothioneine on acute lung injury and inflammation in cytokine insufflated rats. *Prev Med* **54 Suppl**, S79-82 (2012).
69. M. Rincon, C. G. Irvin, Role of IL-6 in Asthma and Other Inflammatory Pulmonary Diseases. *International Journal of Biological Sciences* **8**, 1281-1290 (2012).
70. S. H. Jeong *et al.*, Up-regulation of TNF-alpha secretion by cigarette smoke is mediated by Egr-1 in HaCaT human keratinocytes. *Experimental dermatology* **19**, e206-212 (2010).
71. H. G. Moon *et al.*, Lung epithelial cell-derived extracellular vesicles activate macrophage-mediated inflammatory responses via ROCK1 pathway. *Cell Death Dis* **6**, e2016 (2015).
72. X. K. Zhao *et al.*, Tristetraprolin Down-Regulation Contributes to Persistent TNF-Alpha Expression Induced by Cigarette Smoke Extract through a Post-Transcriptional Mechanism. *PloS one* **11**, e0167451 (2016).

73. J. J. Salomon *et al.*, The cell line NCl-H441 is a useful in vitro model for transport studies of human distal lung epithelial barrier. *Molecular pharmaceutics* **11**, 995-1006 (2014).
74. D. Nikodemus *et al.*, Paramount levels of ergothioneine transporter SLC22A4 mRNA in boar seminal vesicles and cross-species analysis of ergothioneine and glutathione in seminal plasma. *J Physiol Pharmacol* **62**, 411-419 (2011).
75. T. J. Urban *et al.*, Effects of genetic variation in the novel organic cation transporter, OCTN1, on the renal clearance of gabapentin. *Clinical pharmacology and therapeutics* **83**, 416-421 (2008).
76. D. S. Toh *et al.*, Functional analysis of novel variants in the organic cation/ergothioneine transporter 1 identified in Singapore populations. *Mol Pharm* **10**, 2509-2516 (2013).
77. D. S. Toh *et al.*, Genetic variations of the SLC22A4 gene in Chinese and Indian populations of Singapore. *Drug metabolism and pharmacokinetics* **24**, 475-481 (2009).
78. S. Sotgia *et al.*, Quantification of L-ergothioneine in whole blood by hydrophilic interaction ultra-performance liquid chromatography and UV-detection. *J Sep Sci* **36**, 1002-1006 (2013).
79. S. Sotgia *et al.*, Ultra-performance liquid chromatographic determination of L-ergothioneine in commercially available classes of cow milk. *J Food Sci* **79**, 1750-3841 (2014).
80. L. Z. Wang *et al.*, Quantification of L-ergothioneine in human plasma and erythrocytes by liquid chromatography-tandem mass spectrometry. *J Mass Spectrom* **48**, 406-412 (2013).
81. T. W. Sedlak *et al.*, Bilirubin and glutathione have complementary antioxidant and cytoprotective roles. *Proc Natl Acad Sci U S A* **106**, 5171-5176 (2009).
82. W. H. H. DONALD B. MELVILLE, AND ROSE LUBSCHEZ, TISSUE ERGOTHIONEINE. *Department of Biochemistry, Cornell University Medical College,New York.* , (1953).
83. P. E. Hartman, Ergothioneine as antioxidant. *Methods Enzymol* **186**, 310-318 (1990).
84. B. D. Paul, S. H. Snyder, The unusual amino acid L-ergothioneine is a physiologic cytoprotectant. *Cell death and differentiation* **17**, 1134-1140 (2010).
85. N. Demling *et al.*, Promotion of cell adherence and spreading: a novel function of RAGE, the highly selective differentiation marker of human alveolar epithelial type I cells. *Cell and tissue research* **323**, 475-488 (2006).
86. G. f. I.-B. M. V. Available:, http://www.fda.gov/downloads/Drugs/GuidanceComplianceRegulatoryInformation/, Guidances/ucm070107.pdf.
87. I. C. o. Harmonization, I. V. o. A. M. Methodology., I. Q. B. 1996.
88. C. Ehrhardt *et al.*, Influence of apical fluid volume on the development of functional intercellular junctions in the human epithelial cell line 16HBE14o-: implications for the use of this cell line as an in vitro model for bronchial drug absorption studies. *Cell and tissue research* **308**, 391-400 (2002).
89. R. A. Myers *et al.*, Genome-wide interaction studies reveal sex-specific asthma risk alleles. *Human Molecular Genetics* **23**, 5251-5259 (2014).

90. C. L. Noble *et al.*, The contribution of OCTN1/2 variants within the IBD5 locus to disease susceptibility and severity in Crohn's disease. *Gastroenterology* **129**, 1854-1864 (2005).
91. S. Waller *et al.*, Evidence for association of OCTN genes and IBD5 with ulcerative colitis. *Gut* **55**, 809-814 (2006).
92. J. Suchy *et al.*, Inflammatory response gene polymorphisms and their relationship with colorectal cancer risk. *BMC Cancer* **8**, 112 (2008).
93. H. Maegawa, M. Kato, K. Inui, R. Hori, pH sensitivity of H+/organic cation antiport system in rat renal brush-border membranes. *Journal of Biological Chemistry* **263**, 11150-11154 (1988).
94. H. Ren, N. P. Birch, V. Suresh, An Optimised Human Cell Culture Model for Alveolar Epithelial Transport. *PloS one* **11**, e0165225 (2016).
95. A. Stentebjerg-Andersen, I. V. Notlevsen, B. Brodin, C. U. Nielsen, Calu-3 cells grown under AIC and LCC conditions: implications for dipeptide uptake and transepithelial transport of substances. *European journal of pharmaceutics and biopharmaceutics : official journal of Arbeitsgemeinschaft fur Pharmazeutische Verfahrenstechnik e.V* **78**, 19-26 (2011).
96. B. Forbes, A. Shah, G. P. Martin, A. B. Lansley, The human bronchial epithelial cell line 16HBE14o- as a model system of the airways for studying drug transport. *International journal of pharmaceutics* **257**, 161-167 (2003).
97. C. Ehrhardt *et al.*, Towards an in vitro model of cystic fibrosis small airway epithelium: characterisation of the human bronchial epithelial cell line CFBE41o. *Cell and tissue research* **323**, 405-415 (2006).
98. R. Busche *et al.*, Permeability properties of apical and basolateral membranes of the guinea pig caecal and colonic epithelia for short-chain fatty acids. *Biochimica et Biophysica Acta (BBA) - Biomembranes* **1565**, 55-63 (2002).
99. O. I. Aruoma, J. P. Spencer, N. Mahmood, Protection against oxidative damage and cell death by the natural antioxidant ergothioneine. *Food and chemical toxicology : an international journal published for the British Industrial Biological Research Association* **37**, 1043-1053 (1999).
100. A. Kode, S. R. Yang, I. Rahman, Differential effects of cigarette smoke on oxidative stress and proinflammatory cytokine release in primary human airway epithelial cells and in a variety of transformed alveolar epithelial cells. *Respiratory Research* **7**, 132 (2006).
101. R. Colognato *et al.*, Modulation of hydrogen peroxide-induced DNA damage, MAPKs activation and cell death in PC12 by ergothioneine. *Clinical Nutrition* **25**, 135-145 (2006).
102. D. Hoffmann, E. L. Wynder, Chemical constituents and bioactivity of tobacco smoke. *IARC Sci Publ*, 145-165 (1986).
103. M. van der Toorn *et al.*, Lipid-soluble components in cigarette smoke induce mitochondrial production of reactive oxygen species in lung epithelial cells. *American journal of physiology. Lung cellular and molecular physiology* **297**, L109-114 (2009).
104. R. W. Li *et al.*, Uptake and protective effects of ergothioneine in human endothelial cells. *The Journal of pharmacology and experimental therapeutics* **350**, 691-700 (2014).
105. B. Kuźnar-Kamińska, J. Mikuła-Pietrasik, P. Sosińska, K. Książek, H. Batura-Gabryel, COPD promotes migration of A549 lung cancer cells: the role of chemokine CCL21.

International Journal of Chronic Obstructive Pulmonary Disease **11**, 1061-1066 (2016).
106. J. K. Bentley, M. B. Hershenson, Airway Smooth Muscle Growth in Asthma. *Proceedings of the American Thoracic Society* **5**, 89-96 (2008).
107. S. Yoshiyama *et al.*, Effect of cigarette smoke components on vascular smooth muscle cell migration toward platelet-derived growth factor BB. *Journal of pharmacological sciences* **115**, 532-535 (2011).
108. E. A. Wahl, T. L. Schenck, H. G. Machens, J. T. Egana, Acute stimulation of mesenchymal stem cells with cigarette smoke extract affects their migration, differentiation, and paracrine potential. *Sci Rep* **6**, 22957 (2016).
109. C. H. Yoon *et al.*, Cigarette Smoke Extract-induced Reduction in Migration and Contraction in Normal Human Bronchial Smooth Muscle Cells. *Korean J Physiol Pharmacol* **15**, 397-403 (2011).
110. S. Luanpitpong *et al.*, Regulation of lung cancer cell migration and invasion by reactive oxygen species and caveolin-1. *The Journal of biological chemistry* **285**, 38832-38840 (2010).
111. D. Gianni, B. Bohl, S. A. Courtneidge, G. M. Bokoch, The involvement of the tyrosine kinase c-Src in the regulation of reactive oxygen species generation mediated by NADPH oxidase-1. *Molecular biology of the cell* **19**, 2984-2994 (2008).
112. C. R. Kruse *et al.*, The effect of pH on cell viability, cell migration, cell proliferation, wound closure, and wound reepithelialization: In vitro and in vivo study. *Wound repair and regeneration : official publication of the Wound Healing Society [and] the European Tissue Repair Society* **25**, 260-269 (2017).
113. L. Magyari *et al.*, Prevalence of SLC22A4 1672T and SLC22A5 -207C combination defined TC haplotype in Hungarian ulcerative colitis patients. *Pathology oncology research : POR* **13**, 53-56 (2007).
114. J. Glas *et al.*, rs1004819 Is the Main Disease-Associated IL23R Variant in German Crohn's Disease Patients: Combined Analysis of IL23R, CARD15, and OCTN1/2 Variants. *PloS one* **2**, (2007).
115. L. Törkvist *et al.*, Contribution of the IBD5 locus to Crohn's disease in the Swedish population. *Scandinavian Journal of Gastroenterology* **42**, 200-206 (2007).
116. Y. Feng, P. Zheng, H. Zhao, K. Wu, SLC22A4 and SLC22A5 gene polymorphisms and Crohn's disease in the Chinese Han population. *Journal of digestive diseases* **10**, 181-187 (2009).
117. Y. Watanabe *et al.*, Two-stage case–control association study of polymorphisms in rheumatoid arthritis susceptibility genes with schizophrenia. *Journal of Human Genetics* **54**, 62-65 (2009).
118. T. H. Karlsen *et al.*, Genetic polymorphisms associated with inflammatory bowel disease do not confer risk for primary sclerosing cholangitis. *The American journal of gastroenterology* **102**, 115-121 (2007).
119. M. Li *et al.*, OCTN and CARD15 gene polymorphism in Chinese patients with inflammatory bowel disease. *World J Gastroenterol* **14**, 4923-4927 (2008).
120. L. Lakner *et al.*, [Possible role of selected IGR and SLC22A4/SLC22A5 loci in development of inflammatory bowel diseases]. *Orvosi hetilap* **150**, 1375-1380 (2009).

121. S. Vermeire *et al.*, Association of organic cation transporter risk haplotype with perianal penetrating Crohn's disease but not with susceptibility to IBD. *Gastroenterology* **129**, 1845-1853 (2005).
122. C. L. Noble *et al.*, DLG5 variants do not influence susceptibility to inflammatory bowel disease in the Scottish population. *Gut* **54**, 1416-1420 (2005).
123. T. Berg, T. Hegelund-Myrbäck, M. Nord, L. Gustavsson, in *C71. YOU ARE WHAT YOU BREATHE: AIRWAY CELL BIOLOGY IN COPD*. pp. A5849-A5849.
124. H. Tahara *et al.*, Functional genetic variation in the basal promoter of the organic cation/carnitine transporters OCTN1 (SLC22A4) and OCTN2 (SLC22A5). *The Journal of pharmacology and experimental therapeutics* **329**, 262-271 (2009).
125. V. D. Peltekova *et al.*, Functional variants of OCTN cation transporter genes are associated with Crohn disease. *Nat Genet* **36**, (2004).
126. N. Jarad, Chronic obstructive pulmonary disease (COPD) and old age? *Chronic respiratory disease* **8**, 143-151 (2011).
127. E. M. Lowery, A. L. Brubaker, E. Kuhlmann, E. J. Kovacs, The aging lung. *Clinical interventions in aging* **8**, 1489-1496 (2013).
128. Y. Fukuchi, The aging lung and chronic obstructive pulmonary disease: similarity and difference. *Proceedings of the American Thoracic Society* **6**, 570-572 (2009).
129. M. L. K. Han *et al.*, Gender and Chronic Obstructive Pulmonary Disease: Why It Matters. *Am J Respir Crit Care Med* **176**, 1179-1184 (2007).
130. M. T. Dransfield *et al.*, Gender differences in the severity of CT emphysema in COPD. *Chest* **132**, 464-470 (2007).
131. E. K. Silverman *et al.*, Gender-related differences in severe, early-onset chronic obstructive pulmonary disease. *Am J Respir Crit Care Med* **162**, 2152-2158 (2000).
132. Y. Liu *et al.*, Smoking duration, respiratory symptoms, and COPD in adults aged >/=45 years with a smoking history. *International Journal of Chronic Obstructive Pulmonary Disease* **10**, 1409-1416 (2015).
133. N. K. Jain, M. S. Thakkar, N. Jain, K. A. Rohan, M. Sharma, Chronic obstructive pulmonary disease: Does gender really matter? *Lung India : official organ of Indian Chest Society* **28**, 258-262 (2011).
134. M. J. Divo *et al.*, COPD comorbidities network. *The European respiratory journal* **46**, 640-650 (2015).
135. M. N. Movahed M, Association between amount of smoking with chronic cough and sputum production. *Internet J Pulm Med. 2006;7:1–3.*, (2006).
136. A. Langhammer, R. Johnsen, J. Holmen, A. Gulsvik, L. Bjermer, Cigarette smoking gives more respiratory symptoms among women than among men. The Nord-Trondelag Health Study (HUNT). *Journal of epidemiology and community health* **54**, 917-922 (2000).
137. A. Langhammer, R. Johnsen, A. Gulsvik, T. L. Holmen, L. Bjermer, Sex differences in lung vulnerability to tobacco smoking. *The European respiratory journal* **21**, 1017-1023 (2003).
138. M. J. Joo, D. H. Au, M. L. Fitzgibbon, J. McKell, T. A. Lee, Determinants of Spirometry Use and Accuracy of COPD Diagnosis in Primary Care. *Journal of General Internal Medicine* **26**, 1272-1277 (2011).
139. A. Sakamoto *et al.*, Quantitative expression of human drug transporter proteins in lung tissues: Analysis of regional, gender, and interindividual differences by liquid

chromatography–tandem mass spectrometry. *Journal of Pharmaceutical Sciences* **102**, 3395-3406 (2013).
140. M. Girardin *et al.*, Expression and functional analysis of intestinal organic cation/L-carnitine transporter (OCTN) in Crohn's disease. *Journal of Crohn's & colitis* **6**, 189-197 (2012).
141. K. A. Wojtal *et al.*, Changes in mRNA expression levels of solute carrier transporters in inflammatory bowel disease patients. *Drug metabolism and disposition: the biological fate of chemicals* **37**, 1871-1877 (2009).
142. I. K. Cheah, B. Halliwell, Ergothioneine; antioxidant potential, physiological function and role in disease. *Biochimica et Biophysica Acta (BBA) - Molecular Basis of Disease* **1822**, 784-793 (2012).
143. A. Temellini *et al.*, Glutathione conjugation with 1-chloro-2,4-dinitrobenzene (CDNB): interindividual variability in human liver, lung, kidney and intestine. *International journal of clinical pharmacology and therapeutics* **33**, 498-503 (1995).
144. B. Mannervik, The isoenzymes of glutathione transferase. *Advances in enzymology and related areas of molecular biology* **57**, 357-417 (1985).
145. D. J. Meyer *et al.*, Theta, a new class of glutathione transferases purified from rat and man. *The Biochemical journal* **274 (Pt 2)**, 409-414 (1991).
146. M. Widersten, B. Mannervik, Glutathione Transferases with Novel Active Sites Isolated by Phage Display from a Library of Random Mutants. *Journal of Molecular Biology* **250**, 115-122 (1995).
147. B. Coles, B. Ketterer, The role of glutathione and glutathione transferases in chemical carcinogenesis. *Critical reviews in biochemistry and molecular biology* **25**, 47-70 (1990).
148. h. p. n. n. n. g. c. a. M. National Center for Biotechnology Information. PubChem Compound Database; CID=3083620, 2018).
149. L. Servillo *et al.*, Ergothioneine products derived by superoxide oxidation in endothelial cells exposed to high-glucose. *Free Radic Biol Med* **108**, 8-18 (2017).
150. M. Deponte, Glutathione catalysis and the reaction mechanisms of glutathione-dependent enzymes. *Biochimica et biophysica acta* **1830**, 3217-3266 (2013).
151. S. S. Tang, C. C. Lin, G. G. Chang, Isolation and characterization of octopus hepatopancreatic glutathione S-transferase. Comparison of digestive gland enzyme with lens S-crystallin. *Journal of protein chemistry* **13**, 609-618 (1994).
152. N. E. Labrou, L. V. Mello, Y. D. Clonis, Functional and structural roles of the glutathione-binding residues in maize (Zea mays) glutathione S-transferase I. *The Biochemical journal* **358**, 101-110 (2001).
153. Z. Wang, L. Jin, G. Węgrzyn, A. Węgrzyn, A novel method for screening the glutathione transferase inhibitors. *BMC Biochemistry* **10**, 6 (2009).
154. D. F. Mello, M. Arl, R. Trevisan, A. L. Dafre, How important are glutathione and thiol reductases to oyster hemocyte function? *Fish & shellfish immunology* **46**, 566-572 (2015).
155. H. S. Minhas, P. J. Thornalley, Reduced glutathione esters—antidotes to toxicity. Cytotoxicity induced by hydrogen peroxide, 1-chloro-2,4-dinitrobenzene, and menadione in murine P388D1 macrophages in vitro. *Journal of Biochemical Toxicology* **10**, 245-250 (1995).
156. E. Laborde, Glutathione transferases as mediators of signaling pathways involved in cell proliferation and cell death. *Cell death and differentiation* **17**, 1373-1380 (2010).

157. S. Gupta, S. Rathaur, Filarial glutathione S-transferase: its induction by xenobiotics and potential as drug target. *Acta Biochim Pol* **52**, 493-500 (2005).
158. S. A. Terlouw, R. Masereeuw, P. H. van den Broek, S. Notenboom, F. G. Russel, Role of multidrug resistance protein 2 (MRP2) in glutathione-bimane efflux from Caco-2 and rat renal proximal tubule cells. *British journal of pharmacology* **134**, 931-938 (2001).
159. J. Bai, L. Lai, H. C. Yeo, B. C. Goh, T. M. Tan, Multidrug resistance protein 4 (MRP4/ABCC4) mediates efflux of bimane-glutathione. *The international journal of biochemistry & cell biology* **36**, 247-257 (2004).
160. P. Wu *et al.*, Analysis of human multidrug resistance protein 1 (ABCC1) by matrix-assisted laser desorption ionization/time of flight mass spectrometry: toward identification of leukotriene C4 binding sites. *Molecular pharmacology* **68**, 1455-1465 (2005).
161. Y. Liang, S. Li, L. Chen, The physiological role of drug transporters. *Protein & cell* **6**, 334-350 (2015).
162. S. Broer, Xenopus laevis Oocytes. *Methods in molecular biology (Clifton, N.J.)* **637**, 295-310 (2010).
163. T. Kvist, K. B. Hansen, H. Brauner-Osborne, The use of Xenopus oocytes in drug screening. *Expert opinion on drug discovery* **6**, 141-153 (2011).
164. I. J. Hidalgo, T. J. Raub, R. T. Borchardt, Characterization of the human colon carcinoma cell line (Caco-2) as a model system for intestinal epithelial permeability. *Gastroenterology* **96**, 736-749 (1989).
165. L. Svensson, B. B. Finlay, D. Bass, C. H. von Bonsdorff, H. B. Greenberg, Symmetric infection of rotavirus on polarized human intestinal epithelial (Caco-2) cells. *Journal of virology* **65**, 4190-4197 (1991).
166. T. Gaj, C. A. Gersbach, C. F. Barbas, 3rd, ZFN, TALEN, and CRISPR/Cas-based methods for genome engineering. *Trends in biotechnology* **31**, 397-405 (2013).
167. M. Sakagami, In vivo, in vitro and ex vivo models to assess pulmonary absorption and disposition of inhaled therapeutics for systemic delivery. *Advanced drug delivery reviews* **58**, 1030-1060 (2006).
168. R. Franco, J. A. Cidlowski, Glutathione efflux and cell death. *Antioxidants & Redox Signaling* **17**, 1694-1713 (2012).
169. H. Blokzijl *et al.*, Up-regulation and cytoprotective role of epithelial multidrug resistance-associated protein 1 in inflammatory bowel disease. *J Biol Chem* **283**, 35630-35637 (2008).
170. J. M. Brechot, I. Hurbain, A. Fajac, N. Daty, J. F. Bernaudin, Different pattern of MRP localization in ciliated and basal cells from human bronchial epithelium. *The journal of histochemistry and cytochemistry : official journal of the Histochemistry Society* **46**, 513-517 (1998).
171. M. van der Deen *et al.*, ATP-binding cassette (ABC) transporters in normal and pathological lung. *Respiratory Research* **6**, 59 (2005).
172. M. D. Nyquist, B. Prasad, E. A. Mostaghel, Harnessing Solute Carrier Transporters for Precision Oncology. *Molecules (Basel, Switzerland)* **22**, (2017).
173. T. Nakanishi, I. Tamai, Solute Carrier Transporters as Targets for Drug Delivery and Pharmacological Intervention for Chemotherapy. *Journal of Pharmaceutical Sciences* **100**, 3731-3750 (2011).

174. S. Nielsen *et al.*, Aquaporin-1 water channels in short and long loop descending thin limbs and in descending vasa recta in rat kidney. *The American journal of physiology* **268**, F1023-1037 (1995).
175. A. S. Verkman, Dissecting the roles of aquaporins in renal pathophysiology using transgenic mice. *Seminars in nephrology* **28**, 217-226 (2008).
176. M. J. Tait, S. Saadoun, B. A. Bell, M. C. Papadopoulos, Water movements in the brain: role of aquaporins. *Trends in neurosciences* **31**, 37-43 (2008).
177. A. Dvorak, A. E. Tilley, R. Shaykhiev, R. Wang, R. G. Crystal, Do Airway Epithelium Air–Liquid Cultures Represent the In Vivo Airway Epithelium Transcriptome? *American Journal of Respiratory Cell and Molecular Biology* **44**, 465-473 (2011).
178. C. Ehrhardt, K.-J. Kim, C.-M. Lehr. (2004), vol. 107, pp. 207-216.
179. C. I. Grainger, L. L. Greenwell, D. J. Lockley, G. P. Martin, B. Forbes, Culture of Calu-3 cells at the air interface provides a representative model of the airway epithelial barrier. *Pharmaceutical research* **23**, 1482-1490 (2006).
180. M. M. Gottesman, T. Fojo, S. E. Bates, Multidrug resistance in cancer: role of ATP-dependent transporters. *Nature reviews. Cancer* **2**, 48-58 (2002).
181. E. Lechapt-Zalcman *et al.*, MDR1-Pgp 170 expression in human bronchus. *The European respiratory journal* **10**, 1837-1843 (1997).
182. M. A. Wioland *et al.*, CFTR, MDR1, and MRP1 immunolocalization in normal human nasal respiratory mucosa. *The journal of histochemistry and cytochemistry : official journal of the Histochemistry Society* **48**, 1215-1222 (2000).
183. S. Endter, D. Francombe, C. Ehrhardt, M. Gumbleton, RT-PCR analysis of ABC, SLC and SLCO drug transporters in human lung epithelial cell models. *The Journal of pharmacy and pharmacology* **61**, 583-591 (2009).
184. K. Bleasby *et al.*, Expression profiles of 50 xenobiotic transporter genes in humans and pre-clinical species: a resource for investigations into drug disposition. *Xenobiotica; the fate of foreign compounds in biological systems* **36**, 963-988 (2006).
185. A. Sakamoto *et al.*, Drug Transporter Protein Quantification of Immortalized Human Lung Cell Lines Derived from Tracheobronchial Epithelial Cells (Calu-3 and BEAS2-B), Bronchiolar-Alveolar Cells (NCI-H292 and NCI-H441), and Alveolar Type II-like Cells (A549) by Liquid Chromatography-Tandem Mass Spectrometry. *J Pharm Sci* **104**, 3029-3038 (2015).
186. G. L. Scheffer *et al.*, Tissue distribution and induction of human multidrug resistant protein 3. *Laboratory investigation; a journal of technical methods and pathology* **82**, 193-201 (2002).
187. K. O. Hamilton *et al.*, Multidrug resistance-associated protein-1 functional activity in Calu-3 cells. *The Journal of pharmacology and experimental therapeutics* **298**, 1199-1205 (2001).
188. E. Courcot *et al.*, Xenobiotic metabolism and disposition in human lung cell models: comparison with in vivo expression profiles. *Drug metabolism and disposition: the biological fate of chemicals* **40**, 1953-1965 (2012).
189. N. W. Lutz *et al.*, Expression of Cell-Surface Marker ABCB5 Causes Characteristic Modifications of Glucose, Amino Acid and Phospholipid Metabolism in the G3361 Melanoma-Initiating Cell Line. *PloS one* **11**, e0161803 (2016).
190. O. K. Vatamaniuk, E. A. Bucher, M. V. Sundaram, P. A. Rea, CeHMT-1, a putative phytochelatin transporter, is required for cadmium tolerance in Caenorhabditis elegans. *The Journal of biological chemistry* **280**, 23684-23690 (2005).

191. S. M. Wilcox *et al.*, The role of the innate immune response regulatory gene ABCF1 in mammalian embryogenesis and development. *PloS one* **12**, e0175918 (2017).
192. S. Paytubi, N. A. Morrice, J. Boudeau, C. G. Proud, The N-terminal region of ABC50 interacts with eukaryotic initiation factor eIF2 and is a target for regulatory phosphorylation by CK2. *The Biochemical journal* **409**, 223-231 (2008).
193. J. W. Jonker *et al.*, Breast cancer resistance protein (Bcrp1/Abcg2) is expressed in the harderian gland and mediates transport of conjugated protoporphyrin IX. *American journal of physiology. Cell physiology* **292**, C2204-2212 (2007).
194. S. Nickel *et al.*, Expression and Activity of Breast Cancer Resistance Protein (BCRP/ABCG2) in Human Distal Lung Epithelial Cells In Vitro. *Pharmaceutical research*, (2017).
195. M. Toei, R. Saum, M. Forgac, Regulation and Isoform Function of the V-ATPases. *Biochemistry* **49**, 4715-4723 (2010).
196. J. Alimonti *et al.*, TAP expression provides a general method for improving the recognition of malignant cells in vivo. *Nature biotechnology* **18**, 515-520 (2000).
197. L. Zhang, Y. Zhang, P. Zhao, S. M. Huang, Predicting Drug–Drug Interactions: An FDA Perspective. *The AAPS Journal* **11**, 300-306 (2009).
198. T. Mikkaichi *et al.*, Isolation and characterization of a digoxin transporter and its rat homologue expressed in the kidney. *Proceedings of the National Academy of Sciences of the United States of America* **101**, 3569-3574 (2004).
199. M. Mueckler, B. Thorens, The SLC2 (GLUT) family of membrane transporters. *Molecular aspects of medicine* **34**, 121-138 (2013).
200. A. Carruthers, J. DeZutter, A. Ganguly, S. U. Devaskar, Will the original glucose transporter isoform please stand up! *American Journal of Physiology - Endocrinology and Metabolism* **297**, E836-848 (2009).
201. S. U. Devaskar, D. E. deMello, Cell-specific localization of glucose transporter proteins in mammalian lung. *The Journal of clinical endocrinology and metabolism* **81**, 4373-4378 (1996).
202. M. Uldry, M. Ibberson, M. Hosokawa, B. Thorens, GLUT2 is a high affinity glucosamine transporter. *FEBS letters* **524**, 199-203 (2002).
203. M. A. Hediger, M. J. Coady, T. S. Ikeda, E. M. Wright, Expression cloning and cDNA sequencing of the Na+/glucose co-transporter. *Nature* **330**, 379-381 (1987).
204. M. T. Guillam *et al.*, Early diabetes and abnormal postnatal pancreatic islet development in mice lacking Glut-2. *Nature genetics* **17**, 327-330 (1997).
205. A. R. Manolescu, R. Augustin, K. Moley, C. Cheeseman, A highly conserved hydrophobic motif in the exofacial vestibule of fructose transporting SLC2A proteins acts as a critical determinant of their substrate selectivity. *Molecular membrane biology* **24**, 455-463 (2007).
206. D. Fotiadis, Y. Kanai, M. Palacin, The SLC3 and SLC7 families of amino acid transporters. *Molecular aspects of medicine* **34**, 139-158 (2013).
207. G. Rudnick, R. Kramer, R. D. Blakely, D. L. Murphy, F. Verrey, The SLC6 transporters: perspectives on structure, functions, regulation, and models for transporter dysfunction. *Pflugers Archiv : European journal of physiology* **466**, 25-42 (2014).
208. X. T. Jin, A. Galvan, T. Wichmann, Y. Smith, Localization and Function of GABA Transporters GAT-1 and GAT-3 in the Basal Ganglia. *Frontiers in systems neuroscience* **5**, 63 (2011).

209. K. Wakayama, S. Ohtsuki, H. Takanaga, K. Hosoya, T. Terasaki, Localization of norepinephrine and serotonin transporter in mouse brain capillary endothelial cells. *Neuroscience research* **44**, 173-180 (2002).
210. K. A. Streby, N. Shah, M. A. Ranalli, A. Kunkler, T. P. Cripe, Nothing but NET: a review of norepinephrine transporter expression and efficacy of 131I-mIBG therapy. *Pediatric blood & cancer* **62**, 5-11 (2015).
211. Y. Tada *et al.*, Downregulation of serotonin reuptake transporter gene expression in healing colonic mucosa in presence of remaining low-grade inflammation in ulcerative colitis. *Journal of gastroenterology and hepatology* **31**, 1443-1452 (2016).
212. T. Claro da Silva, J. E. Polli, P. W. Swaan, The solute carrier family 10 (SLC10): beyond bile acid transport. *Molecular aspects of medicine* **34**, 252-269 (2013).
213. D. A. Groneberg, F. Doring, P. R. Eynott, A. Fischer, H. Daniel, Intestinal peptide transport: ex vivo uptake studies and localization of peptide carrier PEPT1. *American journal of physiology. Gastrointestinal and liver physiology* **281**, G697-704 (2001).
214. M. Nosworthy, R. Bertolo, J. Brunton, *Ontogeny of dipeptide uptake and peptide transporter 1 (PepT1) expression along the gastrointestinal tract in the neonatal Yucatan miniature pig*. (2012), vol. 110, pp. 1-7.
215. Y. Lai, in *Transporters in Drug Discovery and Development*. (Woodhead Publishing, 2013), pp. 633-674.
216. K. K. Wolf, M. F. Paine, P. B. Watkins, in *Comprehensive Toxicology (Second Edition)*. (Elsevier, Oxford, 2010), pp. 53-75.
217. R. Zhao, N. Diop-Bove, M. Visentin, I. D. Goldman, Mechanisms of membrane transport of folates into cells and across epithelia. *Annual review of nutrition* **31**, 177-201 (2011).
218. M. Kawami, M. Miyamoto, R. Yumoto, M. Takano, Methotrexate influx via folate transporters into alveolar epithelial cell line A549. *Drug metabolism and pharmacokinetics* **30**, 276-281 (2015).
219. R. Zhao, I. D. Goldman, Folate and thiamine transporters mediated by facilitative carriers (SLC19A1-3 and SLC46A1) and folate receptors. *Molecular aspects of medicine* **34**, 373-385 (2013).
220. F. Ingoglia *et al.*, Functional characterization of the organic cation transporters (OCTs) in human airway pulmonary epithelial cells. *Biochimica et biophysica acta* **1848**, 1563-1572 (2015).
221. J. S. Hwang, E. Y. Park, W. Y. Kim, C. W. Yang, J. Kim, Expression of OAT1 and OAT3 in differentiating proximal tubules of the mouse kidney. *Histology and histopathology* **25**, 33-44 (2010).
222. S. A. Eraly *et al.*, Decreased renal organic anion secretion and plasma accumulation of endogenous organic anions in OAT1 knock-out mice. *The Journal of biological chemistry* **281**, 5072-5083 (2006).
223. W. R. Wikoff, M. A. Nagle, V. L. Kouznetsova, I. F. Tsigelny, S. K. Nigam, Untargeted metabolomics identifies enterobiome metabolites and putative uremic toxins as substrates of organic anion transporter 1 (Oat1). *Journal of proteome research* **10**, 2842-2851 (2011).
224. C. D. Cropp *et al.*, Organic anion transporter 2 (SLC22A7) is a facilitative transporter of cGMP. *Molecular pharmacology* **73**, 1151-1158 (2008).

225. W. Sun, R. R. Wu, P. D. van Poelje, M. D. Erion, Isolation of a family of organic anion transporters from human liver and kidney. *Biochemical and biophysical research communications* **283**, 417-422 (2001).
226. R. M. Pelis, S. H. Wright, SLC22, SLC44, and SLC47 transporters--organic anion and cation transporters: molecular and cellular properties. *Current topics in membranes* **73**, 233-261 (2014).
227. E. Traiffort, S. O'Regan, M. Ruat, The choline transporter-like family SLC44: properties and roles in human diseases. *Molecular aspects of medicine* **34**, 646-654 (2013).
228. H. Meyer zu Schwabedissen, C. Verstuyft, H. Kroemer, L. Becquemont, R. B Kim, *Human Multidrug and Toxin Extrusion 1 (MATE1/SLC47A1) Transporter: Functional Characterization, Interaction with OCT2 (SLC22A2), and Single Nucleotide Polymorphisms*. (2010), vol. 298, pp. F997-F1005.
229. A. J. Lickteig, X. Cheng, L. M. Augustine, C. D. Klaassen, N. J. Cherrington, Tissue distribution, ontogeny and induction of the transporters Multidrug and toxin extrusion (MATE) 1 and MATE2 mRNA expression levels in mice. *Life sciences* **83**, 59-64 (2008).
230. R. Boggavarapu *et al.*, Expression, purification and low-resolution structure of human vitamin C transporter SVCT1 (SLC23A1). *PloS one* **8**, e76427 (2013).
231. B. Mackenzie, A. C. Illing, M. A. Hediger, Transport model of the human Na+-coupled L-ascorbic acid (vitamin C) transporter SVCT1. *American journal of physiology. Cell physiology* **294**, C451-459 (2008).
232. M. Burzle *et al.*, The sodium-dependent ascorbic acid transporter family SLC23. *Molecular aspects of medicine* **34**, 436-454 (2013).
233. A. del Arco *et al.*, Expression of the aspartate/glutamate mitochondrial carriers aralar1 and citrin during development and in adult rat tissues. *European journal of biochemistry* **269**, 3313-3320 (2002).
234. H. Lu, C. Chen, C. Klaassen, Tissue distribution of concentrative and equilibrative nucleoside transporters in male and female rats and mice. *Drug metabolism and disposition: the biological fate of chemicals* **32**, 1455-1461 (2004).
235. J. H. Gray, R. P. Owen, K. M. Giacomini, The concentrative nucleoside transporter family, SLC28. *Pflugers Archiv : European journal of physiology* **447**, 728-734 (2004).
236. S. A. Baldwin *et al.*, The equilibrative nucleoside transporter family, SLC29. *Pflugers Archiv : European journal of physiology* **447**, 735-743 (2004).
237. H. Kim, X. Wu, J. Lee, SLC31 (CTR) family of copper transporters in health and disease. *Molecular aspects of medicine* **34**, 561-570 (2013).
238. B. Mackenzie, J. D. Erickson, Sodium-coupled neutral amino acid (System N/A) transporters of the SLC38 gene family. *Pflugers Archiv : European journal of physiology* **447**, 784-795 (2004).
239. A. E. Klomp, B. B. Tops, I. E. Van Denberg, R. Berger, L. W. Klomp, Biochemical characterization and subcellular localization of human copper transporter 1 (hCTR1). *The Biochemical journal* **364**, 497-505 (2002).
240. S. Grewal *et al.*, SNAT2 Amino Acid Transporter Is Regulated by Amino Acids of the SLC6 γ-Aminobutyric Acid Transporter Subfamily in Neocortical Neurons and May Play No Role in Delivering Glutamine for Glutamatergic Transmission. *Journal of Biological Chemistry* **284**, 11224-11236 (2009).

241. A. Rodriguez *et al.*, Expression of the System N transporter (SNAT5/SN2) during development indicates its plausible role in glutamatergic neurotransmission. *Neurochemistry international* **73**, 166-171 (2014).
242. H. D. C. Smyth, *Molecular Pharmaceutics*.
243. B. Hagenbuch, B. Stieger, THE SLCO (FORMER SLC21) SUPERFAMILY OF TRANSPORTERS. *Molecular aspects of medicine* **34**, 396-412 (2013).
244. G. A. Kullak-Ublick *et al.*, Molecular and functional characterization of an organic anion transporting polypeptide cloned from human liver. *Gastroenterology* **109**, 1274-1282 (1995).
245. A. Obaidat, M. Roth, B. Hagenbuch, The expression and function of organic anion transporting polypeptides in normal tissues and in cancer. *Annual review of pharmacology and toxicology* **52**, 135-151 (2012).
246. K. Fujiwara *et al.*, Identification of thyroid hormone transporters in humans: different molecules are involved in a tissue-specific manner. *Endocrinology* **142**, 2005-2012 (2001).
247. A. S. Verkman, Role of aquaporins in lung liquid physiology. *Respiratory physiology & neurobiology* **159**, 324-330 (2007).
248. R. E. Day *et al.*, Human aquaporins: regulators of transcellular water flow. *Biochimica et biophysica acta* **1840**, 1492-1506 (2014).
249. J. Lebeck, Metabolic impact of the glycerol channels AQP7 and AQP9 in adipose tissue and liver. *Journal of molecular endocrinology* **52**, R165-178 (2014).